Dissertation

Combustion Process Improvement for a Wood Gas Internal Combustion Engine of a Biomass Power Plant

carried out for the purpose of obtaining the degree of
Doctor technicae (Dr. techn.),

submitted at TU Wien
Faculty of Mechanical and Industrial Engineering
by
Jure GALOVIĆ
Mat.No.: 01328725

under the supervision of
Assoc. Prof. Dipl.-Ing. Dr.techn. Peter Hofmann
Institute of Powertrains and Automotive Technology, TU Wien

Reviewed by
Univ.Prof. Dr.techn. Dipl.-Ing. Bernhard Geringer
Institute of Powertrains and Automotive Technology, TU Wien
and
Univ.-Prof. Dipl.-Ing. Dr.techn. Helmut Eichlseder
Institute of Thermodynamics and Sustainable Propulsion Systems, TU Graz

Vienna, June 29, 2023

Signature

Eidesstattliche Erklärung

Ich habe zur Kenntnis genommen, dass ich zur Drucklegung meiner Arbeit unter der Bezeichnung

„Combustion Process Improvement for a Wood Gas Internal Combustion Engine of a Biomass Power Plant"

nur mit Bewilligung der Prüfungskommission berechtigt bin. Ich erkläre weiters an Eides statt, dass ich meine Dissertation nach den anerkannten Grundsätzen für wissenschaftliche Arbeiten selbständig ausgeführt habe und alle verwendeten Hilfsmittel, insbesondere die zugrunde gelegte Literatur genannt habe.

Weiters erkläre ich, dass ich dieses Dissertationsthema bisher weder im In- noch im Ausland (einer Beurteilerin/ einem Beurteiler zur Begutachtung) in irgendeiner Form als Prüfungsarbeit vorgelegt habe und dass diese Arbeit mit der vom Begutachter beurteilten Arbeit übereinstimmt.

Ich nehme zur Kenntnis, dass die vorgelegte Arbeit mit geeigneten und dem derzeitigen Stand der Technik entsprechenden Mitteln (Plagiat-Erkennungssoftware) elektronisch-technisch überprüft wird. Dies stellt einerseits sicher, dass bei der Erstellung der vorgelegten Arbeit die Qualitätsvorgaben im Rahmen der geltenden Regeln zur Sicherung guter wissenschaftlicher Praxis „Code of Conduct" an der TU Wien eingehalten wurden. Zum anderen werden durch einen Abgleich mit anderen studentischen Abschlussarbeiten Verletzungen meines persönlichen Urheberrechts vermieden.

Vienna, June 29, 2023

Signature

Preface

The present doctoral thesis was carried out on Institute of Powertrains and Automotive Technology (IFA) TU Wien within the projects funded by GLOCK Private Foundation and Austrian Research Promotion Agency. The simulation results were obtained by using the commercial code *Converge CFD* with free academic license provided by Convergent Science.

I acknowledge, in full gratitude, Associate Prof. Dipl.-Ing. Dr.techn. Peter Hofmann, primary supervisor of this doctoral thesis, Head of Institute Univ.Prof. Dr.techn. Dipl.-Ing. Bernhard Geringer, and Dr. Johannes Konrad for their guidance, encouragement and the scientific and technical advices they provided during my research work. Particular gratitude to Univ.Prof. Dr.techn. Dipl.-Ing. Bernhard Geringer and Univ.-Prof. Dipl.-Ing. Dr.techn. Helmut Eichlseder for reviewing this thesis, and the chairperson of examination board, Univ.-Prof. i.R. Dipl.-Ing. Dr.techn. Hermann Hofbauer.

Special thanks to colleges from IFA, Institute of Chemical, Environmental and Bioscience Engineering TU Wien, GLOCK Technology, GLOCK ecotech and GLOCK Ökoenergie for cooperation and support during my research work.

I dedicate this doctoral thesis to my family.

Vienna, June, 29th 2023

Jure Galović

Abstract

On the path toward carbon neutrality, decentral small-scale biomass power plants with a power output lower than 50 kW_{el} can play a crucial role in heat and electricity supply and grid stability in areas with rich wood resources. The biomass, such as wood chips, is gasified, and the wood gas is utilized by an internal combustion engine that drives a generator. The state-of-the-art small high-speed SI wood gas engines are usually converted from compression ignition (diesel) engines fitted with spark plugs, and operate on the naturally aspirated stoichiometric mixture. Efficient engine operation is challenging due to specific operating conditions imposed by the wood gasification and wood gas properties. Hence, the present doctoral thesis aims to investigate and improve the combustion process for efficient and low-emissions operation of small high-speed wood gas engines. The potential for efficiency improvement and emissions reduction is determined by applying selective optimization measures. 3D CFD simulation is applied for investigations regarding in-cylinder flow motion. The experimental investigations of the combustion process are performed on a developed single-cylinder engine test bench with a fully flexible gas composition mixer. In addition, the efficiency loss analysis is performed by a 0D/1D simulation.

A stable lean combustion process is realized by adjusting a combustion chamber shape for intensive charge motion and increasing the compression ratio. Boosting intake pressure prevents significant engine efficiency losses related to the low-pressure gas supply and gas exchange process resulting in an efficiency improvement. Adjusting the engine operating parameters by a combustion control can compensate for the composition fluctuations and avoid efficiency losses of more than 1%. An efficiency breakthrough is achieved by applying spark-assisted compression ignition on the naturally aspirated wood gas engine. A holistic implementation of optimization measures on the research engine results in an efficiency improvement of 5,55 percentage points compared to the basic engine. Thereby, the raw NO_X emissions are reduced by 52% to the level below the limitation according to Austrian legislation. With increasing λ, *"Near-Zero NO$_X$ Emissions"* are achieved, whereby an exhaust gas aftertreatment system can reduce CO effectively.

Kurzfassung

Auf dem Weg zur Klimaneutralität können kleine dezentrale Biomasse-Blockheizkraftwerke (BHKW) mit Leistungen von bis zu 50 kW_{el} eine wichtige Rolle für die Wärme- und Strombereitstellung sowie die Netzstabilität in Gebieten mit ausreichenden Holzressourcen spielen. Holzgas wird in einem Gaserzeuger im BHKW aus Hackschnitzel und dem Oxidationsmittel Luft gewonnen, dann gereinigt und in einem Holzgasmotor für den Stromgeneratorantrieb umgesetzt. Da das Holzgas einen hohen Anteil an Inertgasen und dementsprechend einen geringen Heizwert hat, und die Zusammensetzung stark fluktuiert, ist ein effizienter Motorbetrieb herausfordernd. Ziel der vorliegenden Dissertation ist die Untersuchung und Optimierung des Brennverfahrens für einen effizienten und emissionsarmen Motorbetrieb. Durch gezielte Motoroptimierungsmaßnahmen wird das Potenzial zur Wirkungsgraderhöhung und Emissionsminimierung ermittelt. Mittels der 3D-CFD-Simulation wird die Brennraumgeometrie analysiert. Die experimentellen Untersuchungen des Brennverfahrens erfolgen an einem dafür entwickelten Einzylinder-Forschungsmotor am Motorprüfstand mit einem vollflexiblen Gasmischer. Die Wirkungsgradanalysen resultieren aus der 0D/1D Motorprozessrechnung.

Ein stabiler Verbrennungsprozess wird durch die Anpassung der Brennraumgeometrie zur Intensivierung der Ladungsbewegung sowie durch die Verdichtungsanhebung erreicht. Die durch die Gaserzeugungs- und Gasreinigungsprozesse bedingten Gaswechselverluste werden durch Aufladung minimiert. Die Anpassung der Motorbetriebsparameter mittels einer adaptiven Verbrennungsregelung kann die negativen Effekte einer fluktuierenden Holzgaszusammensetzung reduzieren und Wirkungsgradverluste von mehr als 1% vermeiden. Durch die Anwendung der SACI „Spark-Assisted Compression Ignition" wird eine weitere signifikante Wirkungsgraderhöhung des Holzgas-Saugmotors realisiert. Eine holistische Umsetzung der vielversprechendsten Optimierungsmaßnahmen am Forschungsmotor führt zu einer Wirkungsgraderhöhung von 5,55 Prozentpunkten im Vergleich zum Basis-Holzgasmotor. Dabei werden die NO_X-Emissionen um 52% reduziert und entsprechen der diesbezüglichen aktuellen österreichischen Gesetzgebung. Mit zunehmender Abmagerung werden „Near-Zero-NO_X-Emissions" erreicht, wobei ein Abgasnachbehandlungssystem die CO-Emissionen effektiv reduziert.

Contents

Abbreviations

0D	Zero Dimensional
1D	One Dimensional
3D	Three Dimensional
A_{min}	Stoichiometric Air-fuel Ratio
AHRR	Apparent Heat Release Rate
AMR	Adaptive Mesh Refinement
BMEP	Break Mean Effective Pressure
CAD	Crank Angle Degree
CFD	Computational Fluid Dynamics
CHP	Combined Heat and Power
CI	Compression Ignition
CNG	Compressed Natural Gas
COV_{IMEP}	coefficient of variance in IMEP
EGR	Exhaust Gas Recirculation
GHG	Green House Gas
HC_1	Hydrocarbon emissions (Methane)
HCCI	Homogenous Charge Compression Ignition
ICE	Internal Combustion Engine
ICEBE	Institute of Chemical, Environmental, and Bioscience Engineering
IMEP	Indicated Mean Effective Pressure
IPCC	Intergovernmental Panel on Climate Change
IT	Ignition Timing
L	Liter

LHV	Lower Heating Value
LNG	Liquified Natural Gas
LPG	Liquified Petroleum Gas
MFB	Mass Fraction Burned
MN	Methane Number
NG	Natural Gas
NO_X	Nitrogen Oxides
OP	Operating Point
RANS	Reynolds-Averaged Navier–Stokes
SACI	Spark-Assisted Compression Ignition
SCR	Selective Catalytic Reduction
SI	Spark Ignition
TDC	Top Dead Center
TDCf	Top Dead Center firing
THC	Total Hydrocarbons
TKE	Turbulent Kinetic Energy
TWC	Three-Way Catalyst
V	Volume
WG	Wood Gas

Nomenclature

Greek Symbols

γ	-	Heat capacity ration
ε	-	Geometric compression ratio
Φ	-	Fuel/Air equivalence ratio
η_i	-	Indicated efficiency
η_{th}	-	Theoretical efficiency
λ	-	Relative air-fuel ratio
λ_m	-	Total charge mass-based relative air-fuel ratio

Symbols

A	kg/h	Air mass flow
A_C	mm²	Cylinder area
B	mm	Bore
C	kg/h	Total intake mass flow
$CO_{2\ Fresh\ charge}$	%	Molar percentage of CO_2 in the dry fresh charge
$CO_{2\ Intake}$	%	Molar percentage of CO_2 in the dry intake gas
$CO_{2\ Exhaust}$	%	Molar percentage of CO_2 in the dry exhaust gas
D_B	mm	Inner diameter of the piston crown
$d^2AHRR/dCAD^2$	J/CAD²	Second derivative of apparent heat release rate
F	kg/h	Fuel mass flow
MFB5-90%	CAD	Combustion duration defined by 5% and 90% mass fraction burned

MFB50%	CADaTDCf	50% of mass fraction burned
$\dot{m}_{Air}$	kg/h	Air mass flow
$\dot{m}_{Fuel}$	kg/h	Fuel mass flow
$\dot{m}_{EGR}$	kg/h	EGR mass flow
$\dot{m}_{Intake}$	kg/h	Total intake mass flow
$\dot{m}_{Fresh\ charge}$	kg/h	Mass flow of fresh charge
$\dot{m}_{Residual}$	kg/h	Mass flow of residual gas
n	rpm	Engine speed
S_P	m/s	Instantaneous piston speed
V_B	m³	Volume of the piston crown
V_{Sq}	m/s	Theoretical squish velocity
Z	mm	Distance between the top piston edge and the cylinder head at TDC

1 Introduction

Energy from fossil fuels empowered the development of technology and the shift to modern life. However, the harmful environmental effects escalated due to the intensive exploitation of resources during the past century. Fossil fuels burning, deforestation, and agriculture increase greenhouse gas (GHG) emissions in the atmosphere, which are associated with anthropogenic global warming. Among the GHG related to human activities, carbon dioxide (CO_2) is the most important for its relatively long lifetime and growing atmospheric concentrations [1], [2]. Figure 1 shows the atmospheric CO_2 concentrations over the past 800 thousand years determined from the air trapped in ice cores and a daily record for more recent times. The atmospheric CO_2 concentration constantly fluctuated over geological epochs and has sharply increased in the past 250 years. The observed increment correlates with anthropogenic activities such as fossil fuel burning.
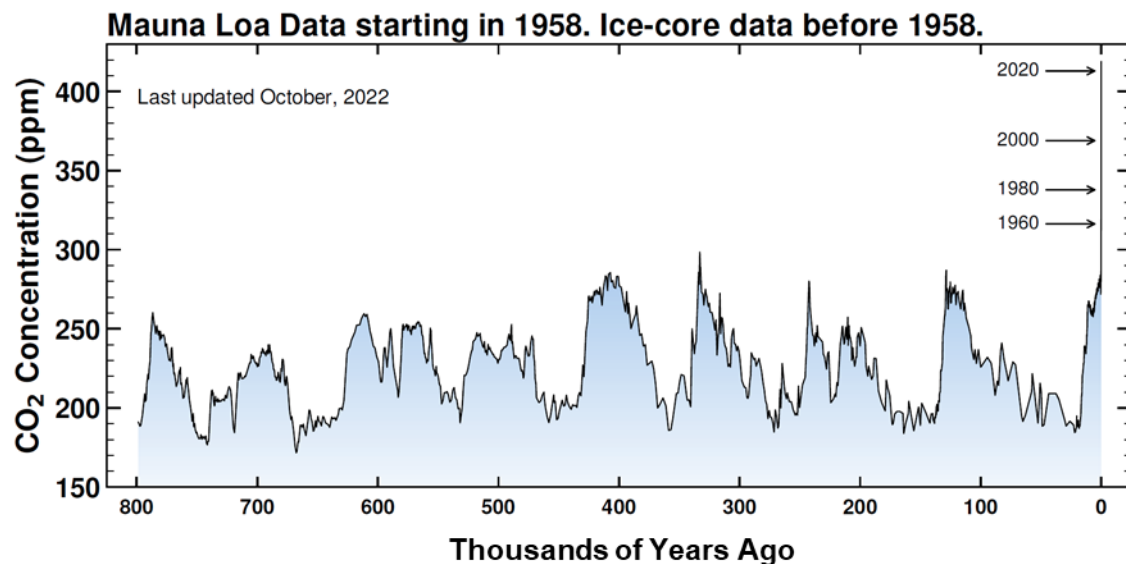
Figure 1: Atmospheric CO_2 concentration: a composite record of atmospheric CO_2 levels over the past 800 thousand years determined from the air trapped in ice cores from Antarctica [3], [4]; and a daily record of global atmospheric CO_2 concentration at Mauna Loa Observatory in the USA (the Keeling Curve) starting in 1958. [5]

The "global warming" affects directly or indirectly almost every segment of life on Earth. Among others, it is manifested in environmental changes (e.g., temperature rising, ice melting, increasing sea level, and changing sea composition) and extreme weather conditions (e.g., the intensity of heat waves, storms, and floods). The process of the climate changes associated with introducing GHG into the atmosphere and the consequences are described in more detail in [2], [6], [7], [8], [9].

According to scientific assessments on climate change provided by the Intergovernmental Panel on Climate Change (IPCC) [9], cutting CO_2 emissions is the most attractive approach for mitigating climate change since atmospheric CO_2 has a dominant influence on global warming. This approach can be applied in various sectors – electric energy supply, transportation, energy use in buildings, industry, agriculture, and waste management. The highest potential for reducing CO_2 emissions is in the power industry (public electricity and heat generation plants), which accounts for 36,51% of global CO_2 emissions [10]. Therefore, supplying electricity and heat from renewable energy sources is crucial for reducing CO_2 emissions from fossil fuels.

On the path towards carbon neutrality, transforming energy systems from centralized to decentralized structures coupled with smart grids shall strive. Decentralized energy systems based on the cogeneration principle (simultaneous supply of heat and electrical energy) are resource efficient due to high overall process efficiency and low energy transport losses between the supply and consumption site. In addition to volatile renewable energy sources such as wind and sun, decentral biomass power plants can play a crucial role in electricity supply and grid stability. They offer flexibility in scale-up and ownership management. The nominal power output is adjusted to the energy demand of the supplied facility. For example, small biomass power plants can supply heat and electricity for small industries, homes, hotels, or heating- and electricity grids in areas with high wood resources. They usually provide a nominal power output below 50 kW$_{el}$ and are considered small-scale in the present thesis.

The main advantages of biomass power plants are high overall process efficiency and a low carbon footprint. The biomass stores atmospheric CO_2 by photosynthetic absorption during its growth. The absorbed CO_2 is returned to the atmosphere through combustion or as the dead biomass decays. Using sustainable biomass feedstock (e.g., wood chips) as fuel for combined heat and power (CHP) plants, CO_2 emissions are balanced because no CO_2 from fossil fuels is introduced into the atmosphere. Figure 2 shows the CO_2 cycle during the utilization of wood chips in biomass power plants.

The life cycle assessments of various biomass power plants (different nominal power ranges) report a low carbon footprint below 70 g-CO_2eq/kWh compared to the coal (~900 g-CO_2eq/kWh) or natural gas (~500 g-CO_2eq/kWh) power plants [11], [12]. The low carbon footprint makes the biomass power plant an attractive solution that contributes to mitigating climate change by defossilizing heat and electricity supply, which is the primary motivation for its application and further development, also embraced in the present thesis.
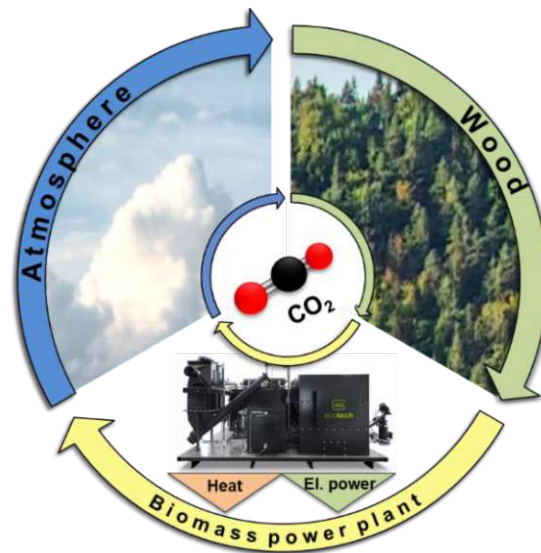
Figure 2: CO_2 Cycle during the utilization of wood chips in biomass power plant

Key components of an engine-based biomass power plant are a gasifier, where the conversion of wood chips to combustible wood gas occurs, and an internal combustion gas engine (ICE) which utilizes the produced wood gas and drives the generator. The exhaust gas and wood gas are cooled in heat exchangers, and the heat is supplied to the heating grid. The wood gasifier and gas engine operate in an interplay whereby each affects the operation of the other. Therefore, this system represents a specific environment for ICE operation. However, efficient engine operation is challenging due to gas composition fluctuations and high contents of inert gases which affect combustion. Hence, the present doctoral thesis focuses on investigating the combustion process for the wood gas engine of a small biomass power plant.

After introducing the motivation for developing biomass power plants in the first part of the present doctoral thesis, the second part briefly overviews the operating principle, gasification, and energy conversion technologies applied in a small wood gas power plant. The third part reports the state of technical development of wood gas engines from the literature and assesses the engines' design parameters and technology relevant for combustion process improvement. The methodological approach for combustion process investigation and improvement of wood gas engines is defined in the fourth part. The last part presents the investigations and announces the potential for improving engine efficiency and reducing exhaust gas emissions by holistically applying selective optimization measures on the basic wood gas engine.

2 Biomass Power Plant

Applied technologies, operating principles, and conditions of the engine-based biomass power plant investigated in the scope of the research projects are briefly described in this chapter.

Depending on the required power output, fuel characteristics, and operating regime, different gasification and energy conversion technologies can be applied in biomass power plants. The gasifiers can be classified based on the scale of operation, oxidation agent (e.g., oxygen, air, or steam), heating principle (e.g., direct heating – autothermal, or indirect heating – allothermal), system pressure (e.g., pressurized or atmospheric), and reactor type (e.g., fixed bed, fluidized bed or plasma). Each gasification principle affects the quality of the product gas and is more or less suitable with the specific energy conversion device [13]. Among the energy conversion devices such as steam turbines, gas turbines, and ICE, the latter is usually applied in a lower power range due to techno-economic reasons. According to [14], it offers significantly higher reliability and ensures high cost-effectiveness in the power range below 600 kW_{el}. Energy conversion technologies such as Stirling engines, Brayton or Rankine cycle engines, and thermoelectric or thermionic generators are not considered for application in biomass power plants due to their complexity and high costs at the time.

A fixed bed gasifier is usually combined with an internal combustion gas engine in small biomass power plants due to its simple design, relatively pure product gas without needing an extensive gas cleaning system, and flexibility in the operation with the ICE.

2.1   Configuration

The configuration of the state-of-the-art engine-based small-scale biomass power plant is schematically presented in Figure 3. It is fuelled with wood chips or pellets. Throughout the process, the wood chips are fed to the gasifier, where they undergo gasification. The wood gas flows from the gasifier and then passes a dry gas filter where ash and dust are separated. Before entering the engine, the wood gas is cooled in a heat exchanger, filtered through an additional safety wet filter, and mixed within a venturi nozzle with air. Thereby, a throttle valve controls the airflow. The engine drives the generator at a constant speed, converting mechanical energy into electrical energy. A three-way catalyst (TWC) reduces exhaust pollutant emissions. Before releasing the engine exhaust gas into the atmosphere, it is cooled in an exhaust gas cooler. The exhaust gas, and wood gas heat exchangers, and the engine coolant circuit are connected to the heating grid. The nominal power output of the presented biomass power plant is 18 kW_{el} and 44 $kW_{th,}$ and it is designed to operate 8000 hours annually.
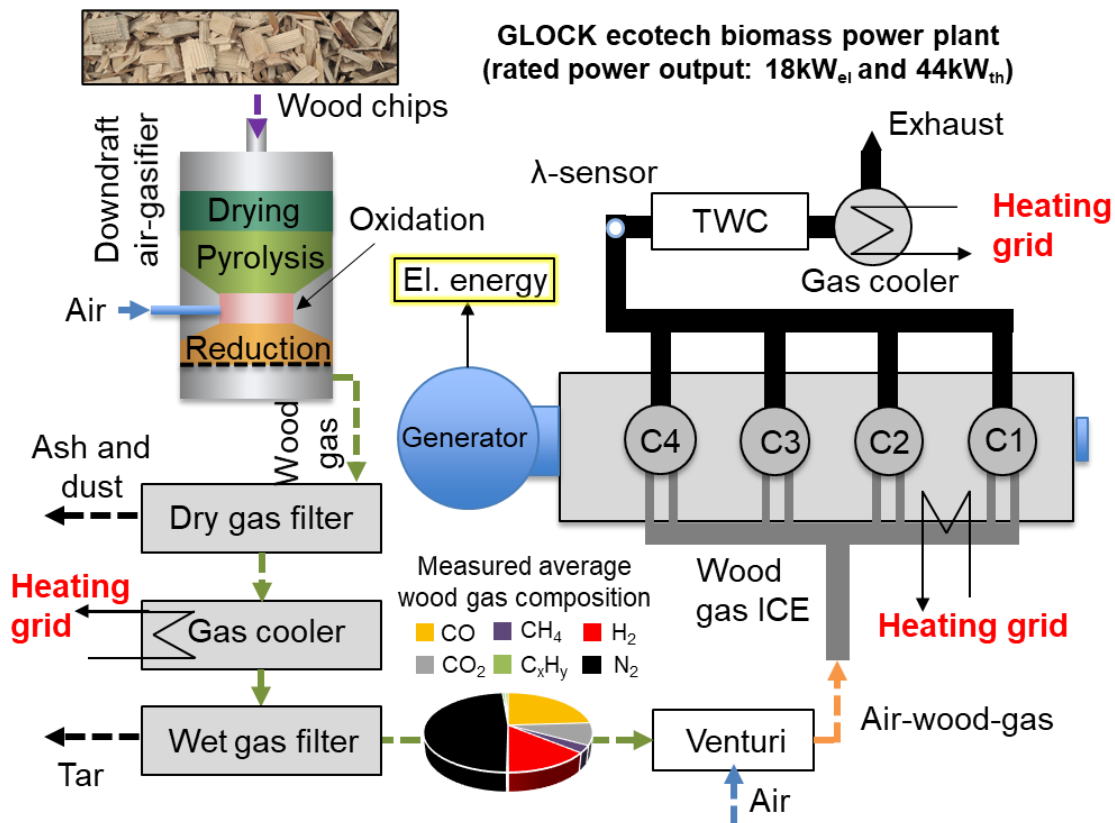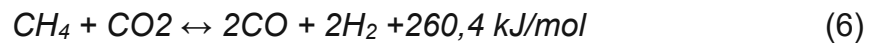
Figure 3: Schematic view of the investigated biomass power plant and streams of the operating process (process flow)

2.2 Gasification of Wood Chips

An overview of gasification technologies, comprehensive descriptions of operating principles, and ranking of gasifiers according to performance indicators are given in [15] and [16]. Here, a fixed-bed downdraft gasifier is briefly described – see Figure 3. The wood chips are fed on the top, and the gasification agent air is introduced on the gasifier's side. They move in the same downward direction inside the gasifier, forming four different reaction zones. At the first stage in the **drying zone**, the wood chips are heated up without oxygen, water is vaporized, and the chips are dried. At higher temperatures (above 150°C), **pyrolysis** takes place. During this process, large molecules (e.g., cellulose, hemicellulose, and lignin) are broken down into medium-sized molecules and carbon (char), and the volatile organic compounds go into the gas phase. The gasification agent air is introduced in the combustion or **oxidation zone**, where the products from the pyrolysis are partially burned. The oxidation reactions are exothermic (release heat) and cause the increase of the temperature up to 1500°C, defining the autothermal gasification character of this type of gasifier. The released heat is required for the drying process, the pyrolysis, and the **reduction zone**, whereby endothermic reactions occur. In the final step, the reduction reactions of the products from the oxidation zone (hot gases and glowing charcoal) occur as stated in [16] and [17] and given in Equation 1 – 6:

$$C + H_2O \rightarrow CO + H_2 +135,7 \ kJ/mol \tag{1}$$
$$C + CO_2 \rightarrow 2CO +169,4 \ kJ/mol \tag{2}$$
$$C + 2H_2 \rightarrow CH_4 -89,8 \ kJ/mol \tag{3}$$
$$CO + H_2O \leftrightarrow CO_2 + H_2 -33,6 \ kJ/mol \tag{4}$$
$$CH_4 + H_2O \leftrightarrow CO + 3H_2 +226,8 \ kJ/mol \tag{5}$$
$$CH_4 + CO2 \leftrightarrow 2CO + 2H_2 +260,4 \ kJ/mol \tag{6}$$

After the reduction zone, wood gas and solid particles (dust and ash) leave the gasifier and flow to the filters. The product of biomass gasification – wood gas (or product gas) – is a gas mixture consisting of combustible gases carbon monoxide (CO), hydrogen (H_2), methane (CH_4), as well as high molecular hydrocarbon compounds (C_xH_y). It also contains specific incombustible gases, carbon dioxide (CO_2), water vapor (H_2O), and, when air is used as a gasification agent, high amounts of nitrogen (N_2). These gases reduce the mixture's lower heating value (LHV) and act as a thermal buffer, reducing the combustion temperature due to their heat capacity. Among combustible components, CO and H_2 have the highest contribution to the LHV. However, the wood gas LHV of 4-6 MJ/kg is low compared to the LHV of conventional fuels. CO exerts high resistance to engine knocking, whereby H_2 has low ignition energy, high laminar flame speed, and is knock-willing. However, H_2 extends the dilution limits of the combustion mixture, improves its ignitability, and increases its laminar flame velocity gaining the overall mixture knocking resistance.

The composition of the gas mixture can fluctuate over time due to the operating mode of the gasifier (see Chapter 5.1) or wood quality and affects the combustion process and engine operation. Besides, wood gas contains tar compounds, S-compounds, N-compounds, Cl-compounds, and dust, which adversely affect engine operation and exhaust gas aftertreatment, as reported in [18]. For example, tars condense at a temperature below the dew point and cause clogging of engine components such as turbochargers and heat exchangers. However, they do not significantly influence the combustion process due to their low fraction. The advantage of downdraft gasifiers is the potentially low tar content in the wood gas, allowing the extensive gas cleaning systems to be omitted. The particulate matter is separated from the gas stream in the dry gas filter – "candle filter" – which consists of a porous ceramic or metallic structure. Air flushing periodically regenerates the filter (see Chapter 5.1). The wet safety filter is an oil gas scrubber that can remove tars by occurrence.

The gasifiers that apply air and steam as gasification agents produce higher amounts of hydrogen (H_2) in product gas [15]. Using only steam as a gasification agent in allothermal gasification can obtain a hydrogen-rich (H_2-rich) and nitrogen-free (N_2-free) product gas. This concept is used in dual-fluidized-bed gasifiers to gasify a wide range of feedstocks [19], [20]. The "heat pipe reformer" concept reported in [21] also supplies

a gas mixture with a high fraction of H_2 and a low fraction of inert gases. However, these concepts are not considered for small-scale biomass power plants (power range below 50 kW_{el}) due to complexity and high costs.

2.3 Wood Gas Engine for Small Biomass Power Plant

In small-scale biomass power plants, robust high-speed engines for agricultural, maritime, or mainly stationary applications are typically applied due to their durability. They are mainly based on compression ignition (CI) engine geometry (for diesel operation) and converted for SI operation on conventional fuels such as compressed natural gas (CNG) or liquid petroleum gas (LPG) by the engine manufacturers. The spark ignition combustion concept is usually applied due to gaseous fuel properties, which ensure mixture ignitability and flame propagation, flexible combustion control, and simple engine retrofitting from CI to SI operating mode. Also, the SI combustion concept enables an autonomous operation without requiring additional fuels for dual-fuel combustion. Adaptations of the fuelling system and adjustments of engine parameters are made individually, depending on the utilized gaseous fuel. Using wood gas (or similar gases with low LHV), feasible engine power is accomplished with a large displacement volume and stoichiometric operation. Light-duty automotive gas engines are inappropriate for this application due to limited durability (~8000 working hours) and displacement volume. In the power range below 50 kW_{el}, the engines are usually naturally aspirated and operate on a stoichiometric mixture [22], [23]. A TWC reduces NO_X, CO, and total hydrocarbon emissions (THC). Due to engine simplicity and low power density, long maintenance intervals are possible. Turbocharged and lean burn engines are generally applied in a higher power range [24], [25]. Despite the advancement of conventional modern gas engines, these converted naturally aspirated and stoichiometric gas engines represent the state-of-the-art for small-scale biomass power plants.

Figure 4 depicts the geometry of the basic wood gas engine integrated into the investigated biomass power plant – it has CI-characteristic intake ports for producing swirl charge motion. Moreover, the basic engine design is not adjusted to the gas quality, its fluctuations, and the operating conditions of a biomass power plant. The combustion chamber is shaped between the piston crown and the flat cylinder head. The spark plug is fitted at the edge of the combustion chamber due to the narrow space in the cylinder head, and the compression ratio ε is adjusted for SI operation on wood gas.
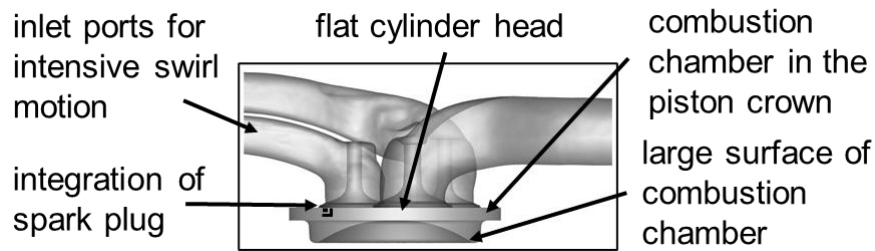
Figure 4: The geometry of the wood gas engine: CI-characteristic swirl generating inlet ports (helical port up and directed port down), piston crown combustion chamber, and integrated spark plug

The engine is operated at full load and constant speed maintained by the generator and the grid frequency. Typical for small-scale biomass power plants is that the wood gas flow, and thus the air for the gasifier are driven by the engine. Therefore, the engine is continuously operated at a lower intake pressure than atmospheric, similar to the throttled operation of conventional SI engines (see operating conditions in Chapter 5.1). The additional gas exchange work needed for fresh charge aspiration through the gasifier results in efficiency loss. The wood gas and air are mixed within a venturi mixer in the intake manifold. The central mixture formation (venturi) is usually used in stationary gas engines when the gas source has low upstream pressure, such as wood gas, biogas, sewage gas, or landfill gas. It ensures a homogeneous mixture and allows the mixing of large gas quantities (e.g., when gas exerts a low stoichiometric air-fuel ratio). The relative air-fuel ratio λ is set by adjusting the wood gas flow and the throttle valve for air. Thus, total mass flow and intake pressure[1] remain unchanged, but the engine load is reduced as λ increases (quality control). The main specifications of the basic engine are given in Table 1. According to the current Austrian legislation, engine exhaust gas emissions are limited to 1 g/m^3_n of NO_X, and 1,5 g/m^3_n of CO [26].

Table 1: Main specifications of the wood gas basic engine

Modell of basic engine	*Kubota*, V3600-E3B
Type of basic engine	CI converted to SI, four strokes
Number of cylinders	4
Engine load regulation	Quality control
Intake / Exhaust valve	2 / 1, fixed valve timing
Aspiration	Naturally aspirated
Bore	98 mm
Stroke	120 mm
Compression ratio ε	11:1
Engine speed (constant)	1500 rpm
λ (constant)	1

---

[1] At the constant intake pressure and engine speed, the pumping work remains unchanged as λ gains.

3 Gas Internal Combustion Engines – State of the Art

This chapter briefly overviews the technical development of wood gas engines and related combustion processes from the literature. The content is limited primarily to aspects important for understanding this thesis.

Due to limited crude oil resources, increasing fuel price trends, and mild adverse environmental impact, gas engines play an essential role in stationary power generation, marine and vehicle propulsion. The diversity of modern gas engines results from constant engine development and optimization for various types of stationary (off-road) or mobile (on-highway) applications, fuel types, and operating conditions [27]. Most heavy-duty gas engines are initially designed as compression ignition engines for operation on diesel and upgraded to operate on gas as dual fuel (mainly large slow-speed engines) or spark ignition gas engines. The engines initially designed for gas operation benefit avoiding compromises regarding the adaption of both versions on the same basis. Modern large gas engines achieve up to 50% efficiency and break mean effective pressure (BMEP) higher than 24 bar operating on conventional fuels [28]. High break engine efficiency of over 41% and low pollutant emissions are achieved even in operation on special gases [24]. Large gas engines cover a wide power range and have high durability.

On the other hand, the efficiency of small engines is limited by high heat losses due to large surface-to-volume ratios compared to large engines. Increasing the surface-to-volume ratio results in cooling effects, i.e., higher wall heat transfer. Additionally, the importance of incomplete combustion increases in small engines since a higher proportion of the flame front is in contact with the combustion chamber wall, and subsequent flame quenching and crevice flow increase [29].

In light-duty on-road applications, vehicles and SI gasoline engines are usually upgraded with a gas storage and gas supply system for monovalent (only on gaseous fuel) or bivalent operation on gasoline or gaseous fuels [30]. In gas operating mode (e.g., CNG direct injection [31]), they achieve performances comparable to the operation on liquid fuels. Gas engines usually operate on compressed natural gas, liquified natural gas (LNG), or liquified petroleum gas. Applying CNG, LNG, or LPG instead of gasoline or diesel results in lower CO_2 emissions due to a lower carbon-to-hydrogen ratio, thus bridging the transition from carbon-based fossil fuels to renewable hydrogen or carbon-neutral fuels [27], [30], [32]. Hence, a great potential to reduce CO_2 emissions is also demonstrated by a vehicle engine operation on biogas instead of CNG and gasoline [33]. Stationary gas engines run even on low calorific fuels such as sewage gas, biogas, wood gas, or others. Among the low calorific gases, wood gas

also contains carbon components. However, it is considered a carbon-neutral fuel since the carbon emissions are balanced, as described in Chapter 1.

3.1 Overview of Gaseous Fuels

Gaseous fuels for gas engines can be divided into fossil, biologically, and technically produced gases, according to [30]. They have different compositions and, thus, combustion properties such as methane number (MN), LHV, and stoichiometric air-fuel ratio (A_{min}). An overview of different gaseous fuels composition is given in Table 2 according to [30] and [34].

Table 2: Composition of gaseous fuels (composition can vary due to different sources of fuel)

		CH_4	C_2H_6	C_xH_y	H_2	CO_2	CO	N_2	O_2	MN	LHV	A_{min}
		% Vol.dry								[-]	kWh/m³$_N$	m³$_N$/m³$_N$
Fossil gases	Natural Gas	65-99	0-25	0-18	-	0-3	-	0-15	0	60-99	8,5-10,5	9,5-10,5
	Mine gas	25-50	0-1	-	-	0-3	-	30-65	9-12	100-120	2,5-5	1,7-4,5
	Flare gas	35-90	2-20	5-25	0-0,5	15-45	-	0-45	0-0,5	40-80	5-13	5-12
	LPG	-	-	100	-	-	-	-	-	<40	26-35	33-24
Biological gases	Biogas	45-70	-	-	-	25-40	-	1-12	0-3	117-142	4,5-6,5	4,3-6,2
	Landfill gas	40-60	-	-	-	30-40	-	5-20	0-4	123-154	4-6	3,8-5,7
	Sewage gas	55-70	-	-	-	30-40	-	-	0-2	130-140	5,5-7	5,2-6,7
Technical gases	Blast furnace gas	-	-	-	2-4	20-25	20-30	45-60	-	120-130	0,8-1,1	0,55-0,8
	Wood gas	0-12	0-4	0-6	12-45	0-25	12-45	0-60	0-3	40-90	1,4-4,8	1,1-4,1
	Coke Gas	20-30	-	1	50-65	1-5	5-8	4-6	1	40-50	4-5	3,4-4,4
	Hydrogen	-	-	-	-	-	-	-	-	0	3	2,38
Gas for investigations	Wood gas[2]	2,7	-	1,2	14	9,3	24,2	48,6	-	-	4,9	1,3

By utilization of fossil or biologically produced gases such as LPG, flare gas, biogas, landfill gas, or sewage gas, engine load and efficiency comparable to natural gas engine operation are achievable due to high LHV [18], [30], [32], [33]. Technically

---

[2] Average wood gas composition measured on the operating biomass power plant in the field in the framework of the present doctoral research (see Chapter 5.1); MN is not determined.

produced gases (i.e., gas mixtures) such as wood gas are more challenging fuels for gas engines. Low heating value, amount of inert gases, composition fluctuations, impurities such as tar, dust, moisture, or high tendency for engine knocking[3] convolute the engine design and limit the achievable engine power and efficiency [30], [35], [36]. Every engine has to be adjusted for specific fuel properties and operating conditions of the system to fulfil fundamental requirements such as durability, high efficiency, and low pollutant emissions. Thus, the combustion process development has decisive importance for specific applications such as engine operation on wood gas.

3.2 Key Technologies for Combustion Process Improvement

Modern gas engine technologies such as lean engine operation, high-energy ignition systems, turbocharging, and advanced combustion concepts are state-of-the-art in large gas engines. Because of the current state of development (see Chapter 2.3), SI wood gas engines for small-scale biomass power plants exhibit considerable improvement potential by implementing modern gas engine technologies. However, this challenges development, design, and engine operation. An optimal setup of relevant development parameters is necessary to achieve high engine efficiency and low pollutant emissions simultaneously. Thereby, the fuel properties have to be considered. The most critical parameters in combustion process development, according to [12] and [37], are:

- Ignition parameters and fresh charge composition and state (associated with lean combustion or exhaust gas recirculation (EGR))
- Combustion chamber geometry (shape and spark plug location)
- In-cylinder charge motion (e.g., mean velocity, tumble, swirl, and squish)
- Compression ratio ε
- Intake pressure boosting strategy (e.g., supercharging, turbocharging)
- Mixture formation and ignition concept
- High-energy ignition system
- Valve timing (Miller or Atkinson concepts).

Due to the differences in engine size, in-cylinder thermodynamic conditions, fuel characteristics, and specific operating conditions (appearing in the power plant, which are significantly different compared to conventional engine applications), the implementation of modern gas engine technologies on the related small high-speed SI

---

[3] The knock resistance is an important property of engine fuels quantified by the MN for gases and assumes values between zero for high knocking tendency (H_2) and 100 for low knocking tendency (CH_4) [28].

wood gas engine can produce different impacts on performance efficiency and emissions. The following subchapters review the gas engine optimization measures from the literature and asseses them for application on the small high-speed wood gas engine.

3.2.1   Fresh Charge Composition and Combustion Process

The charge composition affects the combustion process, engine performance, efficiency, and emissions. The fresh charge can be diluted with excess air (lean engine operation, $\lambda > 1$) or exhaust gas (by EGR). The exhaust gas can be mixed with the fresh charge in the intake manifold (externally EGR) or within the cylinder (internally EGR) by controlling the residual burned gases from the previous cycle.

The advantages of fresh charge dilution are the potential improvement of indicated efficiency, lower NO_X emissions, and reduced engine-knocking [4] tendency. The temperature and the composition of the cylinder charge affect the heat capacity ratio (γ) and, therefore, the theoretical efficiency of the ideal cycle (constant-volume, see Chapter 5.4.1) according to the ideal cycle analysis. As γ increases, a higher peak pressure (temperature and energy release) is achieved at the start of the expansion. Consequently, the charge expands through a larger temperature ratio during expansion, thus transferring a larger fraction of its energy at the start of expansion to the piston as work [37].

For example, during the lean engine operation, the combustion products are at a lower temperature, less dissociation of the triatomic molecules CO_2 and H_2O occurs, and the mixture contains an excess of oxygen and nitrogen (both diatomic molecules). A higher portion of fuel's chemical energy is released as sensible energy near TDC and transferred as work to the piston during expansion resulting in higher fuel conversion efficiency [37]. In addition, low temperatures reduce the wall heat transfer but prolong the fresh mixture's reaction time and ignition delay. However, lower charge peak temperatures during lean operation decrease the tendency to knock. The dilution of fresh charge with exhaust gas affects the efficiency similar to the dilution with excess air [37]. It is usually applied at $\lambda \sim 1$ and enables TWC application for exhaust gas aftertreatment.

Moreover, the most important engine parameters affecting NO_X emissions are the mixture composition (λ and burned mass fraction of the total in-cylinder unburned gas

---

[4] Engine knocking is spontaneous and uncontrolled autoignition of fresh charge not captured by the flame front occurring due to excided autoignition temperature. A rapid energy release generates high-frequency and high-amplitude pressure oscillations which can damage the engine components. Occurrence of engine knocking depends on different parameters such as the thermodynamic conditions (e.g., temperature and pressure) fuel (e.g., Methane number – see Chapter 3.1), fresh charge properties (e.g., dilution) and engine speed.

mixture – i.e., residual gas and EGR) and the spark timing [37]. They rule the main factors which drive the thermal NO_X formation – the mixture temperature (unburned and burned) and the concentration of atomic oxygen and nitrogen in the burned mixture within the combustion chamber [38]. For example, decreased peak combustion temperature during engine operation with diluted fresh charge inhibits nitrogen oxide formation and reduces engine NO_X emissions.

The disadvantages of fresh charge dilution are worse combustion quality and reduced naturally aspirated engine performance due to lower mixture LHV. The reduced engine performance can be compensated by intake pressure boosting in turbocharged or supercharged engines. Further, increasing the dilution affects the combustion process through the dependence of the laminar flame speed on the fresh charge composition, pressure, and temperature. As the laminar flame speed decreases with increasing dilution extent, the combustion duration increases, and combustion stability deteriorates, adversely affecting the efficiency [39]. The variance of indicated mean effective pressure (IMEP) is used as a comparative value i.e., measure for combustion stability. Usually, the operating points with a coefficient of variance in IMEP (COV_{IMEP}) of more than 5% are classified as unstable. The importance of this adverse effect is reduced by ensuring a fast combustion system through the design of the combustion chamber. However, as the dilution limit approaches, pollutant emissions from unburned fuel increase due to flame quenching, partial burning cycles, and misfires. They can be minimized by an oxidation catalyst in lean engine operation or a TWC in stoichiometric operation (with EGR).

During the stoichiometric engine operation without mixture dilution, the threat of engine-knocking increases, and high nitrogen oxides (NO_X) emissions occur. The occurrence of engine-knocking limits load and increment of compression ratio. Its avoidance is an essential constraint for the combustion process development. Therefore, gas engines with high power densities (especially low- and medium-speed large gas engines) usually operate leaner than stoichiometric as the knocking tendency decreases. Simultaneously, the efficiency increases and NO_X emissions sink, whereby higher rates of unburned fuel emissions occur, as discussed above. Nonetheless, the combustion process depends on the engine speed. It occurs faster with growing engine speed, reducing the engine knocking. Small high-speed engines (applied for vehicle propulsion systems or stationary engines for generator drive) also operate stoichiometric and apply the TWC for emission reduction [28], [34], [37], [40].

3.2.2 Charge Motion and Combustion Chamber

The start of combustion, and thus the ignition and early phase of flame development, are of essential importance for combustion stability. In SI engines, the spark released

by the spark plug induces local heating, forming radicals and igniting the fresh charge [37], [38]. The required ignition energy depends on the spark plug area's mixture composition, temperature, pressure, and charge motion. It increases with the increasing extent of mixture dilution, pressure, and flow velocities [37], [41]. The charge motion can deflect the spark forming an arc between two electrodes, which enlarges the activated volume when the spark plug has a large electrode gap, and sufficient ignition energy is supplied. A combustion concept that focuses on intensive charge motion and comprises an appropriately stretched spark channel ensures the combustion of the diluted mixture at a high compression ratio [42]. The small-scale turbulences also significantly affect the spark and favor its extinction if sufficient ignition energy is not supplied. Since the flame kernel initially propagates with laminar flame velocity, the ignition initiation and flame development are aggravated due to mixture dilution (e.g., with excess air) and reduced laminar flame velocity [37], [38], [43].

In addition to the ignition and early flame development phases, the turbulence intensity also significantly affects the following flame propagation through flame front folding and increasing its surface area and thickness, leading to a higher conversion rate [37], [38]. Turbulent flame propagation occurs significantly faster than laminar flame propagation in the early combustion phase, and its velocity depends on turbulence intensity and structure. Thus, the intensive charge motion reduces the combustion duration and improves combustion stability even in operation with diluted mixtures. However, when the charge motion is too intensive, the turbulent flow results in an over-accelerated exchange of reactants and products in the flame zone, and insufficient time is available for the chemical reaction. Consequently, flame quenching occurs [37], [41], resulting in aggravated engine efficiency and high emissions associated with unburned fuel.

Moreover, stable and fast combustion of a sufficiently diluted mixture is a prerequisite for achieving the highest possible efficiency and low NO_x emissions simultaneously, avoiding the usage of complex exhaust aftertreatment. According to [37], accelerating the combustion rate from moderate to fast at constant operating conditions and mixture composition improves efficiency modestly. The fast combustion process enables utilizing more diluted mixtures (lean or EGR) without significant deterioration in combustion stability and thus gains the efficiency sizeable due to the benefits associated with mixture dilution.

Types of In-Cylinder Charge Motion

An intensive in-cylinder charge motion essential for fast and stable combustion is ensured by appropriately designing the intake system, valves, valve timing, and combustion chamber geometry. The intake flow can be adjusted by different approaches, such as adjusting the valves lift, valve masking, or flaps in the intake

manifold, as demonstrated in automotive gasoline engines [44], [45], [46]. Appropriate modifications of inlet valve seats also increase in-cylinder motion intensity [25]. However, the valve masking or flaps are unsuitable for a wood gas engine since they increase the intake flow resistance and result in engine throttling. In gas engines based on the CI platform with swirl-generating ports and flat cylinder heads (see Chapter 2.3), an excellent path to generate intensive charge motion is by adjusting the combustion chamber's design, defined by the piston crown shape. Tumble, swirl, and squish represent the possible charge motion that makes turbulence within the combustion chamber. High turbulence intensity increases the flame development and propagation rate, and the occurring small turbulence scale shortens combustion time. Withal, higher in-cylinder velocities increase heat transfer limiting the efficiency improvement.

Figure 5 shows three types of in-cylinder global charge motion.
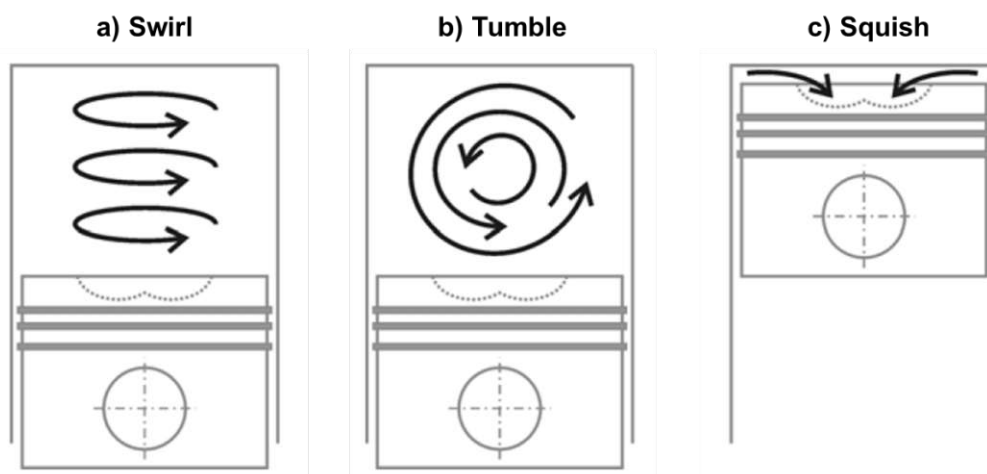
Figure 5: Schematic of basic in-cylinder charge motion: swirl a), tumble b), and squish c) – adopted from [47] and modified

A charge rotation about the cylinder axes is called a **swirl**, and it occurs when the intake flow with an angular momentum enters the cylinder – see Figure 5 a). The specially designed intake ports generate the swirl during the intake stroke, and a suitably designed combustion chamber (e.g., pistons crown shape) intensifies the rotational motion during the compression stroke by piercing most of the air into a piston crown as the piston approaches the top dead center (TDC) [37]. A rotation of the charge motion about an axis orthogonal to the cylinder axis is named **tumble** – see Figure 5 b). It is usually generated through a specially designed "pent-roof" combustion chamber and valves with inclined valve steam (not shown in the figure). The flow enters the cylinder through the upper portion of the opened valve area, streams down the liner, and moves across the piston and upward along the liner to complete rotation. At the end of the compression, the tumble disperses into small eddies, increasing turbulent kinetic energy (TKE) and accelerating the combustion. Different tumble

motions within the cylinder can occur, such as "normal," "reverse," and "cross" tumble (combined with swirl) [37]. Toward the end of the compression stroke, gas is displaced into the piston crown when the piston approaches the cylinder head. The occurring radial or transverse charge motion is called **squish** – see Figure 5 c). It positively affects flame development and propagation at the beginning of combustion. Its intensity depends on the size of the squish area (i.e., the percentage of the piston area which closely approaches the cylinder head) [37].

The presented types of basic charge motion can interact depending on the combustion chamber design. In engines with a flat cylinder head and helical swirl port (e.g., the related wood gas engine), an intensive charge motion can be generated by modifying the piston crown for squish motion. Swirl can be intensified during compression stroke within the piston crown, while squish can be generated by the piston crown with a large squish area when the piston approaches closely to the cylinder head.

Combustion Chamber Geometry

Moreover, combustion chamber geometry and the spark plug location form the flame front surface area affecting the combustion rate and heat transfer. According to [37], the highest flame surface area is achieved in compact open chambers with a "pent-roof" cylinder head or piston crown, where flame captures the highest possible mixture bulk and rubs the lowest possible chamber surface. Positioning the spark plug centrally to the mixture bulk increases the flame surface significantly, resulting in faster combustion and the lowest heat transfer. The heat transfer intensity depends on the combustion chamber surface area, the magnitude of in-cylinder gas velocities during combustion and expansion, and the gas and wall temperatures. Therefore, efficiency improvement is limited by the higher heat transfer rates accompanying the higher in-cylinder velocities. For a spark plug located at the combustion chamber's edge (see Figure 4), an appropriate positioning of the piston crown (relative to the cylinder axis and spark plug location) and optimal piston crown shape can ensure the highest possible flame-front surface area.

Various designs of piston crown shapes were simulatively and experimentally investigated regarding enhancing the charge motion and efficiency improvement of lean gas engines in recent years – see Figure 6, [43]. Simple piston crown geometries a) to e) result in modest turbulence intensity and thus in moderate combustion speed. The geometry f) leads to the fastest combustion speed due to high turbulent intensity [48], [49]. Simple piston crown geometries were also applied on wood gas engines such as b) in [23], e), and f) in [22]. Thereby the lean operation is limited by deterioration in combustion stability.
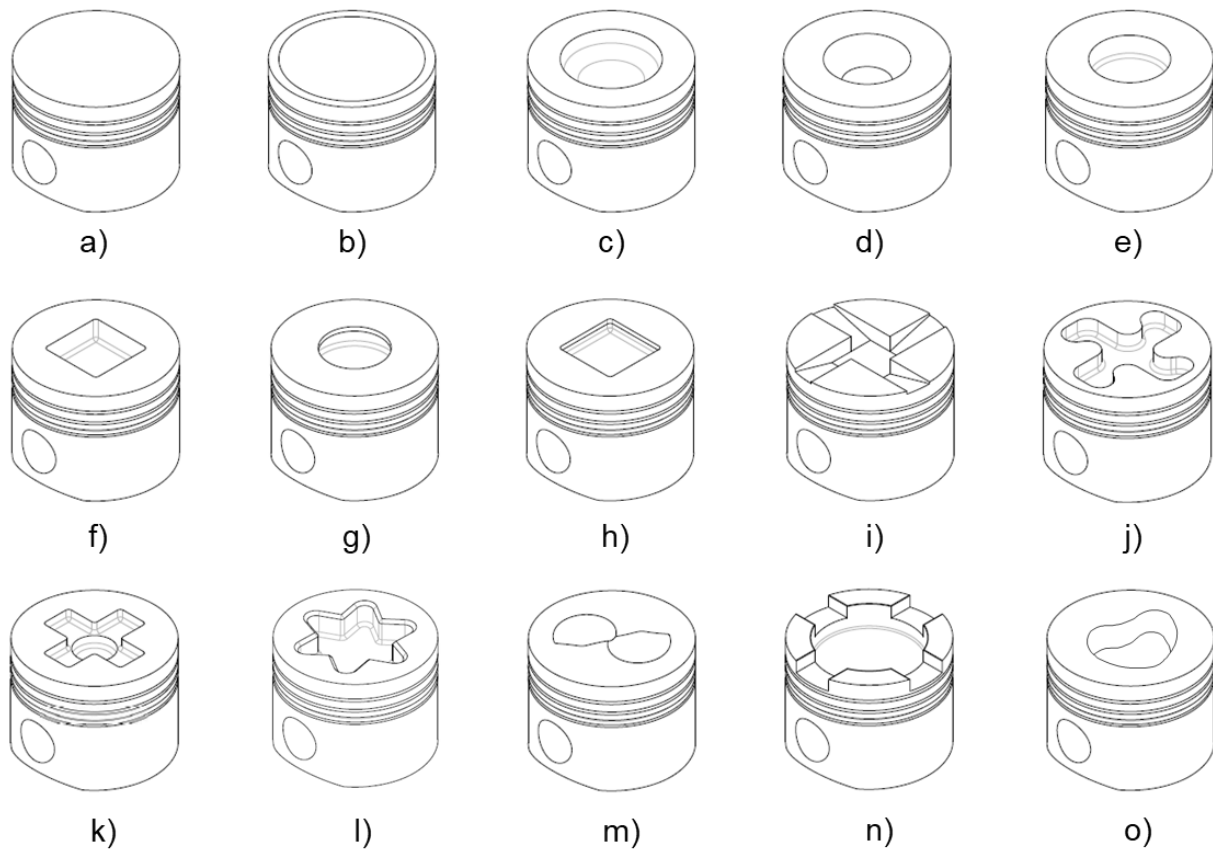
Figure 6: Schematic view of the investigated piston crown geometries adopted from [43] and modified:

  a) "Flat" – in NG engines [48], [49];

  b) "Hemi" – in NG engines [48], [49] and in WG engines [23];

  c) "Turbine" – in NG engines [48], [49];

  d) "Cone" – in NG engines [48], [49];

  e) "Cylinder" – in NG engines [48], [49] and in WG engines [22];

  f) "Square" – in NG engines [48], [49] and in WG engines [22];

  g) "Reentrant Cylinder" – in NG engines [50], [51], [52];

  h) "Reentrant Square" – in NG engines [50];

  i) "Fair Top" – in NG engines [50];

  j) "Quartette" – in NG engines [50], and in WG engines [53];

  k) "Cross" – in NG engines [48], [49];

  l) "Star-shaped G1" – in NG engines [43];

  m) "Nebula" – [48], [49], [51] in NG engines;

  n) "Swirl groove" [54] or "ATAC piston" [55] – in NG and LPG engines;

  o) "Asymmetric heart-shaped" – for large gas engines [56], [57].

Piston crowns g) and h) represent the "Reentrant" design. It increases the squish area at a constant compression ratio promoting the squish flow [50] and enhancing the swirl flow [51]. Investigations on the piston crown g) stated that as the "Reentrant level"

increases, the resulting substantial squish motion increases turbulence intensity and accelerates the flame propagation. The efficiency improvement is limited by a high wall heat transfer and increased knock tendency [52]. Complex and rugged geometries with protruded edges and corners such as i) to m) aim to break up the swirl and thus generate small-scale turbulences. The geometries j) and k) achieve intensive charge motion [48], [49]. A stable lean wood gas engine operation is ensured with geometry j) in [53]. The piston crown l) is based on star shape and shows maximum turbulence before TDC, positively affecting early flame propagation. The piston crown is positioned eccentrically and is thus concentric with the spark plug in the related engine [43]. Piston crown n) is derived from simple cylindrical piston crown geometry (CI engine platform) and has milled recesses, which break up the swirl flow and increases the turbulence level, thus reducing the combustion duration [54], [55]. An asymmetrical piston crown shape o), which enhances in-cylinder flow, is developed in [56] and applied in large SI gas engines [57]. It ensures optimal flow velocity at the ignition point and fast combustion of the fuel-air mixture in the entire combustion chamber.

In summary, a suitable piston crown design can enhance the turbulence level in engines with a flat cylinder head and swirl intake port, which is essential for fast combustion. A low chamber surface area and optimal spark plug positioning can also ensure minimal wall heat transfer and flame quenching. Based on reviewed approaches, the most suitable geometries can be adapted and modified for the application on small wood gas engines.

3.2.3　Compression Ratio

According to the ideal cycle analysis, the fuel conversion efficiency gains with increasing γ and as compression ratio ε increases (see Chapter 5.4.1). In the constant-volume cycle, the cylinder pressure at the start of the expansion and the volume ratio through which the charge expands during the expansion stroke increase as the compression ratio increases (at constant γ) [37]. These two effects increase the indicated work per cycle and overcome a slight increase in the negative compression work.

Although the indicated efficiency of a real engine follows the increasing efficiency trend (with growing ε) of the ideal cycle, it is significantly lower due to factors depending on compression ratio such as temperature-dependent gas properties (e.g., γ), combustion efficiency (related to the unburned fuel), combustion duration, heat losses, reduced expansion work due to gas exchange, the importance of crevices volume and others. The importance of these factors increases at a higher compression ratio limiting the efficiency improvement. In addition to the geometrically set compression ratio ε, the actual compression and expansion ratios depend on valve timing and flow, which is

also affected by the engine speed. The extent of efficiency improvement by increasing the compression ratio also depends on cylinder size and engine load [37]. According to [37] and [58], as ε is increased until the highest efficiency is reached in a real engine, the gas temperature during the expansion and exhaust stroke and the wall heat losses as a portion of fuel's chemical energy decline. The emissions of unburned fuel (HC in gasoline engines) increase due to the higher importance of crevices volume and related flame quenching, especially in premixed engines at high ε. Additionally, a modest effect on NO emissions is reported.

The increase of ε is limited by the tendency to engine knocking, pre-ignition, and high thermal load. The occurrence of irregular combustion phenomena depends on the fuel properties (i.e., laminar flame velocity), engine design parameters (i.e., ε, charge motion, and spark plug location), and operating parameters (i.e., engine load and speed). The operating parameters influence the fresh mixture temperature, pressure, and the time the mixture is exposed to these high state values before being captured by the flame. The latter is also affected by the chamber design and spark plug position [37].

Research work [59] examines the effect of the compression ratio on the combustion process and efficiency of natural gas lean SI engine. As the ε is gradually increased from 13 to 16, the ignition delay is modestly reduced (~3 CAD), the combustion duration and the cyclic variations of IMEP (COV_{IMEP}) remain in the same range, and the efficiency gains for more than 2%. [60] investigated the effect of wall heat transfer on homogenous charge compression ignition (HCCI) natural gas engine efficiency by reducing the surface-to-volume ratio at a constant compression ratio (ε=26). Changing the engine layout decreased the wall heat transfer by 25% and improved the indicated efficiency by 5,3%.

Several studies reported the effects of compression ratio on wood gas engine efficiency and performance investigated on the engine test bench. [23] and [61] investigated the operation of a small, naturally aspirated wood gas engine (3,3 L displacement volume and power of 20 kW) integrated into the biomass power plant. The compression ratio increase from 11,5 up to 17 resulted in break efficiency improvement of 3,2% in slightly rich operation (fuel-air equivalence ratio (Φ)~1,1). No irregular combustion phenomena occurred at the highest investigated compression ratio while operating on particular wood gas. [22] reported the engine knocking during the slightly rich engine operation on wood gas with ε=16; by decreasing ε to 12, knocking was avoided. The compression ratio of a small single-cylinder wood gas engine (0,6 L displacement volume) was gradually increased from 9,7 to 17, and the effects on the operation were investigated in [62]. This investigation occurred on the wood gas engine integrated into the biomass power plant. The efficiency increased by

more than 3% as the ε increased, and the engine operated stable and without knocking. Additionally, a high potential for engine break efficiency improvement of 3,8% by increasing ε from 9,3 to 15 and operating on biogas is reported in [63]. Thereby, the NO emissions increase due to higher peak combustion temperatures.

The above-reviewed research studies demonstrate the stable operation of wood gas engines of different sizes with a high compression ratio (up to ε=17). Due to wood gas' ability to tolerate high dilution and increased knocking resistance of fresh mixture, applying a higher compression ratio results in a remarkable efficiency improvement. Hence, further investigating the limit to which ε can be increased, the effects on the combustion process, and emissions can define the full potential for efficiency improvement of the wood gas engine.

In addition to the compression ratio, technologies such as the Miller and Atkinson cycles influence the cylinder's thermodynamic state and thus affect the engine efficiency, the knock behavior, and nitrogen oxide emissions. The potential for efficiency improvement of small SI engines by applying the Miller or Atkinson cycle is demonstrated in [64] and [65]. However, in the scope of the present research, Miller or Atkinson cycles are not evaluated for application on the related small wood gas engine due to the current state of engine development.

3.2.4   Intake Pressure Boosting

Modern gas engines are typically fitted with turbochargers. This way, the density of the fresh charge is increased, and higher engine power and efficiency can be achieved compared to the same-sized naturally aspirated engine. Feasible power release is achieved even in lean engine operation without increasing the engine displacement volume. However, technical challenges usually arise from the fuel gas composition in engines operating on special gases such as wood gas. The biogases and technical gases may contain components that can clog the turbocharger and intercooler if an extensive gas cleaning system is not integrated. Further, operating conditions such as pressure and temperature of supplied fuel gas, exhaust gas temperature, and back pressure can limit its application.

Limited literature is available about the strategies for intake pressure boosting in wood gas engines of small biomass power plant systems (power range below 50 kW$_{el}$). [66] reported the investigations of a turbocharged wood gas engine (power range of 20 kW$_{el}$) connected directly to the wood gasifier. The turbocharger increases the intake pressure for more than 100 mbar from under-pressure (negative) to over-pressure level (positive pumping work). As a result, the power increases, but the efficiency improvement is not achieved due to high back pressure and an unsuitable turbocharger in the cited study. A comparison of a single-cylinder research engine

operating on wood gas and natural gas (power range above 150 kW$_{el}$) with a supercharger is reported in [53]. The engine reached high loads at absolute intake pressures up to 2 bar$_a$ using both fuels, whereas stable engine operation is possible in a wider lean operating range using wood gas due to its properties. [67] reported an application of a turbocharged gas engine (power range above 200 kW$_{el}$) in a biomass power plant with a wood gas supply slightly above the atmospheric pressure. The turbocharger is designed according to the operating conditions and has achieved the desired pressure ratio during wood gas and dual fuel operation. The study [68] investigated different-sized wood gas engines (power output of 90 – 500 kW$_{el}$) and addressed the importance of turbocharger matching for operation with low calorific gases.

In small-scale biomass power plants (power range below 50 kW$_{el}$), the engine intake pressure is below the atmospheric (see Chapter 5.1). In that case, energy transfer occurs from the piston to the working fluid during the gas exchange phase (negative pumping work), negatively affecting the engine's efficiency. Therefore, intake pressure boosting represents a high potential for engine efficiency improvement.

3.2.5 Adaptive Combustion Control

Wood gas properties directly affect the combustion process – different heating values, octane numbers, and molecular composition strongly influence energy output, knocking tendency, and emissions. For example, volatile H$_2$ content affects the combustion duration and can cause sporadic combustion engine knocking. The wood gas composition can vary significantly (see Chapter 5.1). Gas buffer tanks can reduce these fluctuations [30]. On the engine side, the combustion parameters, such as ignition timing or air-fuel ratio, has to be adjusted for efficient and low-emission operation.

Small high-speed engines usually apply conventional combustion control based on an open-loop approach. Important combustion parameters are stored in characteristic maps for the possible operating points. In that case, it is necessary to incorporate tolerances to achieve stable combustion considering volatile gas compositions and changed conditions at the expense of efficiency and emissions. In contrast, an adaptive combustion control applies a closed-loop approach, offering the possibility to minimize the tolerances and react automatically to changed boundary conditions. It can be realized as cylinder-pressure-based combustion control. The combustion process is measured directly with the cylinder pressure sensors, and essential variables such as IMEP and the center of combustion (i.e., 50% of mass fraction burned (MFB50%)) are determined. Based on these operating data, combustion can be optimized for each cylinder individually (cylinder balancing) and adjusted to

changing fuel composition, environmental influences, or components aging within a few operating cycles [69], [70].

In the field of large gas engines, the combustion process is usually monitored and adjusted by a cylinder-pressure-based control system [71], [72], [73]. A functional mixture formation control based on an in-cylinder pressure sensor for each cylinder is realized on a large wood gas engine and reported in [21]. The system adjusts the gas dosing and compensates for gas quality fluctuations. An applied NO_X controller ensures low NO_X emissions by adjusting the air-fuel ratio and ignition timing. Further, a cylinder-pressure-based SI engine combustion control with acceptable costs for serial production is developed and tested for automotive applications [74]. The ignition timing control is based on MFB50% and knock detection. The engine fuel economy is improved by up to 3% in steady and transient conditions.

A suitable adaptive combustion control for a wood gas engine can rest on a cylinder-pressure-based control system. It can enable efficient engine operation by adjusting the engine parameters during changes in operating conditions. The center of combustion and the NO_X emissions are possible controlling variables, which can be determined from the measured cylinder pressure. The changes in wood gas composition, λ, and intake manifold pressure represent possible variable boundary conditions to which engine operation must be adapted. Among the possible manipulated variables, the ignition timing affects the combustion process essentially. For the realization of cylinder-pressure-based combustion control, an appropriate cylinder pressure sensor and capable engine control unit are needed. Although high costs limited the application of adaptive combustion control on small high-speed wood gas engines in the past, it can ensure efficient operation despite permanent fluctuations in wood gas composition. Additionally, possible irregular combustion and engine knocking can be avoided. It can also enable applying alternative combustion concepts on wood gas engines that need precise cycle-to-cycle control for adjusting ignition timing.

3.2.6   Advanced Combustion Concepts for Wood Gas Engines

Depending on the engine size, gaseous fuel, and application, different combustion concepts are applied to gas engines to achieve the highest efficiency, emissions, and engine performance. They can be divided by the type of gas mixture formation and ignition.

Mixture Formation

The mixture formation can occur within the cylinder through direct fuel injection, port fuel injection, or externally upstream of the cylinders in a venturi mixer, depending on

gas supply, engine load, and safety requirements. Central mixture formation in a venturi mixer ensures a homogeneous mixture and allows the mixing of large gas quantities (e.g., when gas exerts a low stoichiometric air-fuel ratio) [30]. It is usually used in stationary gas engines when the gas source has low upstream pressure, such as wood gas in a biomass power plant. The application of an injection system on small high-speed wood gas engines in a biomass power plant is, at the time, unreliable due to the need for complex gas supply (compressing of wood gas) and thorough purification (separation of condensates and dust) systems.

Spark Ignition Concepts

Depending on the engine size, three different approaches for spark ignition are usually applied on gas engines and schematically presented in Figure 7.
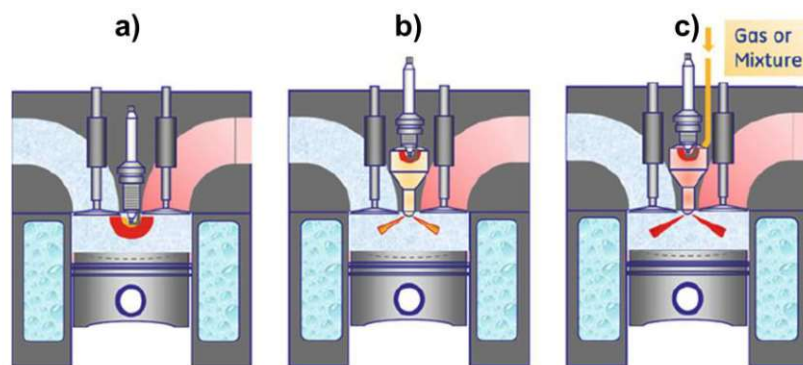
Figure 7: Ignition concepts of SI gas engines: open combustion chamber, chamber spark plug (unscavenged pre-chamber), and scavenged pre-chamber; adopted from [30]

In small gas engines, sufficient ignition energy is usually provided when the spark plug is placed directly in an open combustion chamber (Figure 7 a). This combustion concept is also applied in the related wood gas engines – see Chapter 2.3. The unscavenged pre-chamber or chamber spark plug (Figure 7 b) is used when the cylinder displacement volume is higher than 3 L for boosting the ignition process. The fresh charge is ignited within the spark plug chamber, and flame jets ignite the mixture in the main combustion chamber, improving the combustion process. A scavenged pre-chamber is required in large gas engines (6 L/cylinder) – Figure 7 b). The pre-chamber is placed in the cylinder head, linked to the main combustion chamber by orifices, and demands a separated fuel supply. The ignition of stoichiometric fresh charge occurs by a spark plug and generates a flame front within the pre-chamber, which ignites the lean fresh charge in the main combustion chamber in multiple places. Among the three solutions, the scavenged pre-chamber exerts the highest investment costs, especially for application on small engines [28], [30], [34].

[43] gives a comprehensive literature review on the investigations of chamber spark plugs and pre-chambers combustion concepts for automotive gas engines (bore to 125 mm). The reviewed studies reported the different potentials for reducing emissions, and combustion duration, increasing combustion stability, and extending lean combustion capability. The factors affecting the combustion process are the pre-chamber geometry, volume, and the number, diameter, and arrangement of the orifices. The applications of a chamber spark plug, unscavenged pre-chamber, and scavenged pre-chamber on an automotive 2-cylinder research engine (1 L displacement volume) operated on NG are also experimentally investigated [43]. Due to the increased ignition energy of the large-volume pre-chamber (unscavenged), a significant reduction of combustion delay is achieved compared to conventional and chamber spark plugs. A shorter combustion duration and higher stability result in a 2% efficiency improvement over the open chamber and chamber spark plug concepts in the investigated operating point. However, the highest dilution is achieved with a conventional spark plug due to residual gases within the chamber. The combustion concept with scavenged pre-chamber (NG injection) ensures a rapid combustion duration and extended lean operation resulting in efficiency improvement by 4% and a reduction of NO_X emissions by 46% in the investigated operating point. [75] investigated biogas (laboratory gas mixture) and natural gas operation of an unscavenged pre-chamber gas engine (10 L displacement volume) and reported the engine operation on biogas with no disadvantage regarding the combustion process.

Despite the proven advantages of the combustion concept with scavenged pre-chamber for conventional gas engines, the high investment costs and the need for a separated fuel supply (e.g., compressed wood gas for scavenged pre-chamber) make this approach complex and limit its application on related small high-speed wood gas engines. The unscavenged pre-chamber and pre-chamber spark plugs can potentially improve the combustion process of the wood gas engine.

To extend the limits of conventional spark plug ignition systems for open combustion chambers regarding the operation with a highly diluted mixture (lean or exhaust gas), advanced high-energy concepts such as Double-Coil-, Multi-Charge-, Corona-, Microwave- and Laser-ignition systems are investigated for automotive engines in [76]. Although the concepts such as Corona- and Laser-ignition show potential for engine efficiency improvement, their application is not proven successful due to high costs at the time and thus is not further considered for application on wood gas engines.

Compression Ignition Concepts

Compression ignition gas engines operate in dual fuel mode. A **dual fuel combustion concept** involves two different fuels (e.g., usually natural gas and Diesel or even combinations such as hydrogen/Diesel [77], gasoline/Diesel [78], or NG/gasoline [79] in the research phase) introduced into the combustion chamber at the same time which form a combustible mixture with the air. [80] gives a comprehensive overview of the dual fuel combustion concepts and their applications in engine scales, from passenger cars to large engines in the marine sector or for stationary power generation. Also, small high-speed dual fuel gas engines operating on wood gas and pilot diesel are realized and applied in biomass power plants – see [30] and [81]. However, the dual fuel combustion concept is not well established in biomass power plants with small high-speed engines because the demand for additional fuel (e.g., fossil or biodiesel) can limit its self-sufficiency.

Alternative combustion strategies that combine the aspects of SI and autoignition can achieve advancements in internal combustion engines [82]. For example, the **HCCI** combustion concept relies on the autoignition of the premixed homogeneous charge, simultaneously reducing fuel consumption and emissions. Modest changes in the fresh charge's temperature, pressure, and composition significantly affect the combustion process and allow only a narrow operating range potentially suitable for electricity generation at the constant operating point. Due to low combustion temperatures, the HCCI engines can achieve high thermal efficiency and low NO_X emissions in a lean operation. For example, a small natural gas HCCI engine with a high compression ratio ($\varepsilon=26$) and modified combustion chamber (small surface-to-volume ratio) achieves an efficiency improvement of 6% compared to SI operation with $\varepsilon=12$ [60]. A significant advantage of the HCCI concept regarding small wood gas engines is the ability to utilize the unprocessed hot wood gas (at a charge temperature above the tar dew point), thereby avoiding tar condensation [67]. However, the high sensitivity of the autoignition process to wood gas composition fluctuations is reported in [83]. The lack of controlling the local thermodynamic variables and the wood gas fluctuations limit efficient engine operation with low emissions. High mechanical stress in undesired early autoignition can also lead to engine failure [84]. Effects of wood gas composition on HCCI combustion are investigated on a small gas engine (1,6 L) in [85]. It is reported that the combustion speed increases significantly with increasing H_2/CO_2 ratio and yields engine knocking. Research [86] reported comparable HCCI engine performance on particular wood gas and natural gas compositions. In addition, a comparison between the HCCI and SI engine operation on wood gas [53] reported the increased lean range as the main benefit of the HCCI concept since the efficiency and emissions remained similar.

Applying external triggers which influence the autoignition can avoid the main drawback of HCCI combustion regarding the lack of control. Different triggering strategies such as intake pressure boosting, variable compression ratio, or variation of the residual gas fraction are potentially suitable for HCCI depending on the engine design and operating conditions [84]. A possible approach for precisely triggering the autoignition represents the spark assistance. The combustion concept that can overcome the difficulties of HCCI regarding combustion control and stability is **spark-assisted compression ignition (SACI)** combustion. It employs a controlled spark ignition of a small portion of the fresh charge, which triggers the autoignition by compression heating from an expanding flame front [87], [88]. The principle is schematically presented in Figure 8. Compared to the conventional HCCI, where the autoignition timing results from various not easy controlled in-cylinder conditions, the spark assistance influences the beginning of the bulk autoignition and extends the operating conditions under which the autoignition is usable [84]. As a result of SACI, a fast heat release, which nears the combustion to the ideal cycle, the possibility to operate on lean mixtures, and an applied high compression ratio represent the potential for engine efficiency improvement and pollutant emissions reduction.
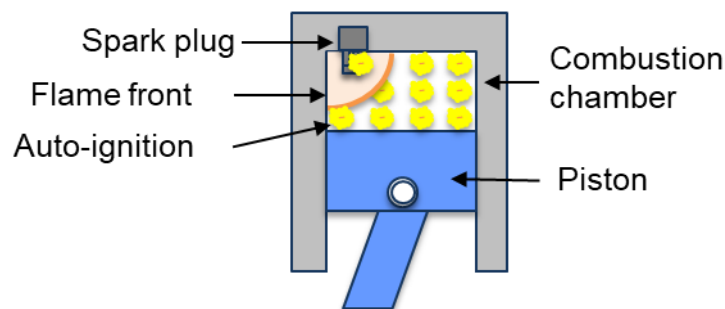
Figure 8: Schematic of SACI combustion – expanding flame front of SI (orange) provides heat and pressure, ensuring controlled autoignition of the fresh charge (yellow)

The principle for achieving SACI in an SI engine is schematically depicted in Figure 9 and described in the following. Without external triggers, the autoignition threshold is not reached during the motored cycle (solid line) under defined conditions (intake pressure, temperature, and composition). The autoignition threshold depends mainly on the charge pressure, temperature, and composition. Introducing a specific quantity of energy and radicals that exceeds what only a spark plug could supply for SI combustion mode makes it possible to push the fuel mixture into a bulk autoignition process (dashed line). Thus, an additional aid is necessary for achieving the autoignition threshold besides the conventional spark plug for the transition from SI to SACI combustion in an engine.
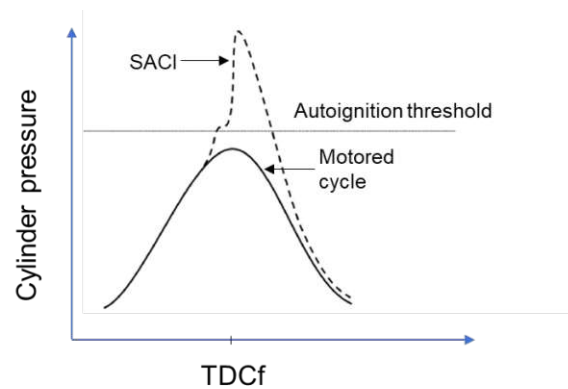
Figure 9: Schematic for achieving SACI principle: motored pressure curve (solid line) and SACI combustion (dashed line); adopted from [84] and modified

SACI can be achieved in an SI engine by different methods and modest modifications – heating of fresh charge, adjusting compression ratio ε, trapping hot burned gases in the cylinder (internal EGR), utilization of auto-ignitable fuels, amplifying the spark ignition in a pre-chamber or combining different methods. Thereby, the spark assistance initiates the ignition and enhances the combustion control. In gasoline SI engines for automotive applications, SACI is usually achieved by trapping the exhaust gases in the cylinder during the valve overlap. These residual gases increase the charge temperature and supply the radicals supporting the autoignition [88]. Several experimental studies reviewed in [87], [88], and [89] reported diverse combustion behaviors depending on the residual gas fraction and the ignition timing. [86] proposes methods for amplifying the spark ignition by applying a pre-chamber spark plug, a piston cavity (as a subvolume), and a jet ignition concept for achieving SACI. The benefits for efficiency and emissions are achieved due to rapid combustion and lean operation, especially in partial load. Further, the development of a small natural gas "spark-assisted HCCI" engine (power output of 1kW) is reported in [90]. The engine operates on a stoichiometric charge diluted with EGR and employs a spark plug for initiating the autoignition. An automotive gasoline engine that applies a spark-controlled compression ignition is already released in serial production [91].

To sum up, the spark-assisted autoignition can overcome the drawbacks of flame propagation (SI) at extreme thermodynamic conditions and high sensitivity to the operating conditions of HCCI. Considering the operating conditions of biomass power plants, SACI can be applied on a wood gas engine by sufficiently increasing the compression ratio or intake temperature in combination with spark assistance.

4 Research Objectives

Wood gas utilization in internal combustion engines is challenging due to specific wood gas properties such as high content of inert gases, volatile composition, and pressure fluctuations imposed by wood gasification and gas purification processes. Conventional gas engines demand combustion process optimization and an optimal set of relevant development parameters to achieve high efficiency and low pollutant emissions operating on wood gas. Thus, the main objective of this thesis is to investigate and improve the combustion process for efficient and low-emissions operation of small high-speed wood gas engines.

Based on the state of development, selective optimization measures and engine technologies will be assessed for implementation on the wood gas engine by applying a joint simulative and experimental approach. The sequence of optimization measures is depicted in Figure 10. The combustion concept must apply a lean or EGR combustion strategy and a high compression ratio to improve thermal efficiency and reduce NO_X formation. Essential for a stable combustion process of the diluted mixture is an intensive charge motion, which can be ensured by precisely adjusting the combustion chamber geometry. Moreover, alternative combustion concept, such as spark-assisted compression ignition, enables omitting the efficiency losses of the conventional SI concept. Boosting intake pressure can prevent significant engine efficiency losses related to the low-pressure gas supply and gas exchange process. Adjusting the engine operating parameters by a combustion control can compensate for the composition fluctuations and avoid related efficiency losses. Thus, applying a specific combination and interaction of the well-known engine optimization measures on a small high-speed wood gas engine represents the main contribution of this thesis.

An optimal wood gas engine setup is to be defined with a holistic implementation of the optimization measures and adjusting the engine parameters on the research wood gas engine. The potential for efficiency improvement and pollutant emissions reduction compared to the basic engine will be determined.
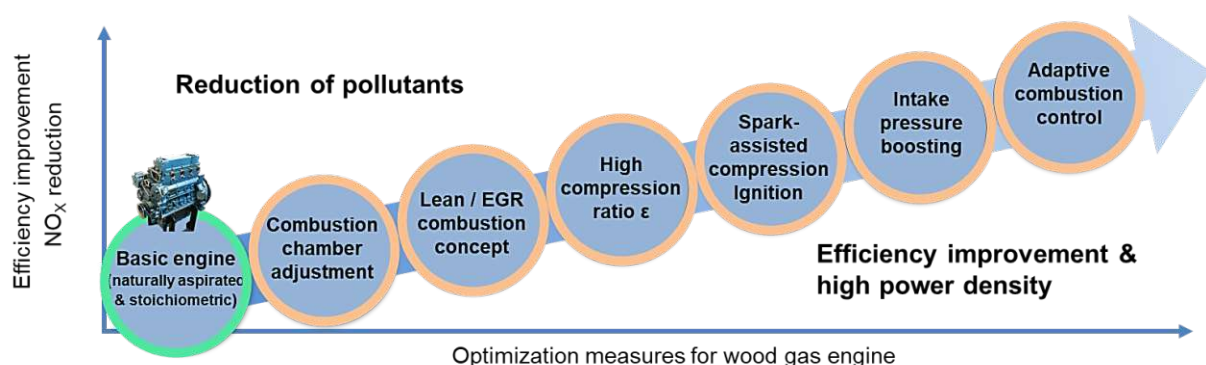

Figure 10: Selective optimization measures for wood gas engine

5 Methodology

The methodology for investigations of the combustion process is described in this chapter. A particular research approach is based on simulative and experimental investigations and is schematically depicted in Figure 11. It comprises assessing the specific operating conditions in the actual biomass power plant in the field, development and verification of a single-cylinder research engine and gas composition mixer on the test bench, development and verification of simulation models, simulative and experimental investigations, and evaluation of specific optimization measures.
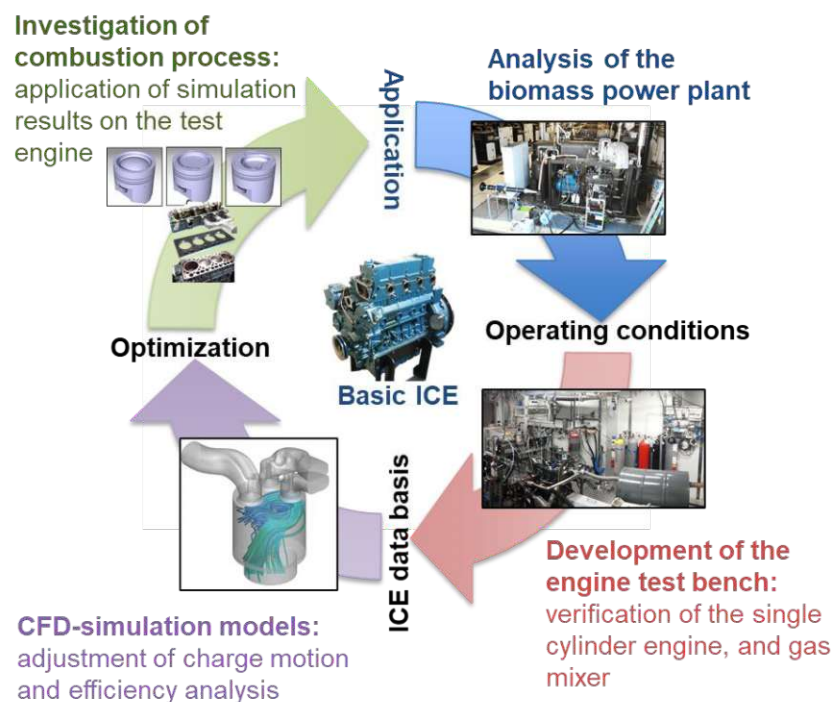
Figure 11: The research approach for the combustion process investigations and improving the wood gas engine

5.1 Analysis of Biomass Power Plant

The operation of the wood gas engine is analyzed on the biomass power plant in the field in the scope of the research projects. Here, the measuring procedure and the operating conditions are briefly reported. The biomass power plant is equipped with a gas filtering system and analyzers for offline and online gas analysis, air mass flow meter, pressure gauges, thermocouples, engine indicating instruments, λ-sensor, and data acquisition systems. A measuring spark plug with an integrated cylinder pressure sensor type 6113C *Kistler* is used to measure cylinder pressure. Figure 12 shows the biomass power plant with measurement instruments.
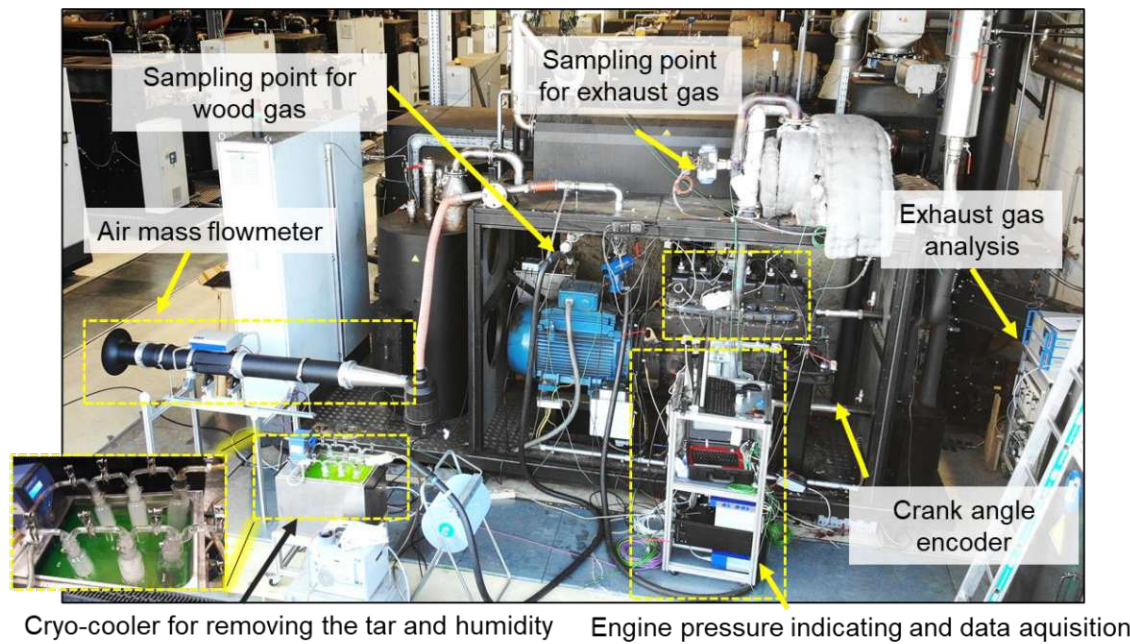
Figure 12: Biomass power plant with measurement instruments in the field

The relative air-fuel ratio (λ) is calculated from the measured exhaust gas and wood gas compositions according to *"Brettschneider"* [92]. It quantifies the mixture's stoichiometry and gives the excess air's extent.

The wood gas mass flow ($\dot{m}_{Fuel}$) is calculated according the Equation 7 [38] from the determined λ, measured air mass flow ($\dot{m}_{Air}$), and the air required for the complete combustion of wood gas (A_{min}):

$$\dot{m}_{Fuel} = \frac{\dot{m}_{Air}}{\lambda \cdot A_{min}}$$

(7)

$\dot{m}_{Fuel}$	fuel mass flow (wood gas) [kg/h]
$\dot{m}_{Air}$	air mass flow [kg/h]
A_{min}	air required for the complete combustion [kg$_{air}$/kg$_{fuel}$]
λ	relative air-fuel ratio [-]

A_{min} is determined by solving the elementary combustion reactions for each combustible component according to [93].

To analyze the operating conditions imposed by the biomass power plant, the wood gas engine operated in the nominal operating point, i.e., lightly leaner than stoichiometric, at the highest possible load and constant engine speed. The ignition timing variations are performed to assess the related effects on the combustion process. The gas analysis is conducted for 30 minutes. The engine cylinder pressure is indicated in 200 consecutive cycles several times during the gas analysis. Thereby

the measurements occurred in the middle engine cylinder. The operating parameters of the gasification process remained unchanged.

The results of the online wood gas analysis are presented in Figure 13 a). The average wood gas composition (dry), including the components measured by offline analysis (C_xH_y), is listed in Table 2. Figure 13 b) shows the measured intake engine pressure, which is below the atmospheric due to the engine aspiration of wood gas through the gasification system – see Chapter 2.3. The peaks indicate a periodical filter flashing.
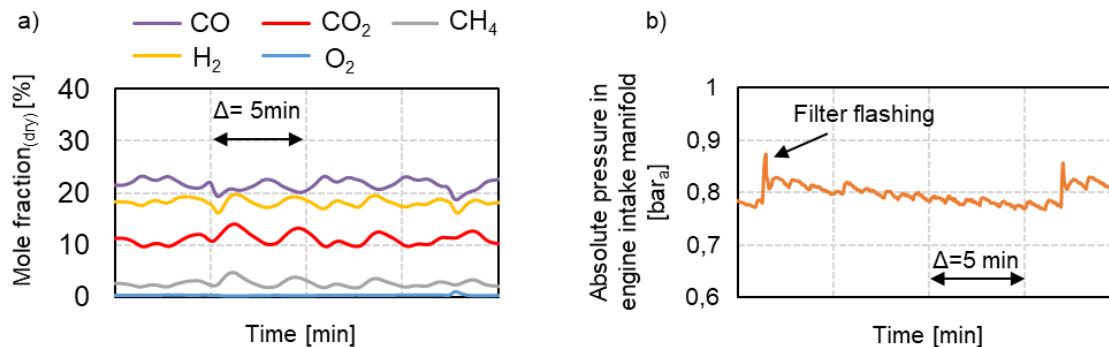
Figure 13: Operating conditions of biomass power plant: fluctuations of wood gas composition (dry) during online gas analysis at the position upstream of venturi (N_2 is not shown), a) and absolute pressure in the engine intake manifold, b)

In addition, the operating conditions determined on the biomass power plant are listed in Table 3. The engine measurements are presented in the next chapter.

Table 3: Operating conditions of biomass power plant

Parameter	Mean value	Parameter	Mean value
Ambient		Wood gas	
$T_{Ambient}$ [°C]	22	T [°C]	83
$p_{Ambient}$ [mbar]	954	p [mbar]	~875
Rel. humidity [%]	50	Tar [g/Nm³]	2,6
LHV_{Wood} [MJ/kg]	18,3	H_2O [Vol.-%]	2-6
Air-gas mixture (engine intake manifold)		Dust [mg/Nm³]	<5
T_{Engine_Intake} [°C]	30	HCl [ppm]	<1
p_{Engine_Intake} [mbar]	~875	NH_3 [ppm]	~450
Rel. humidity [%]	50	H_2S [ppm]	~19

The methodology for gas analysis of biomass power plant in the field is described in more detail in [94]. Based on the assessments of operating conditions (wood gas composition, volume flows, temperatures, pressures, exhaust gas composition, and engine operating behavior), a single-cylinder research engine and a wood gas composition mixer are developed on the test bench and verified, as described in the

next chapter. The described assessments serve as a foundation on which the approach for the ICE combustion process development is built.

5.2   Single-Cylinder Research Engine and Gas Mixer on the Test Bench

The test bench architecture with a single-cylinder research engine and a wood gas composition mixer developed for the investigations of the combustion process is schematically depicted in Figure 14. The in-line 4-cylinder wood gas engine is modified to a single-cylinder research engine and adapted to a test bench with a speed-controlled dynamometer and a fully flexible gas composition mixer. The fired cylinder is equipped with a cooled piezoresistive pressure transducer (quartz) for cylinder pressure measurements. The intake and exhaust pipes of the fired cylinder are equipped with thermocouples, pressure gauges, and piezoelectric pressure transducers. Further, intake air mass flow ($\dot{m}_{Air}$) is measured at the air supply pipe. For gas analysis, sampling points in exhaust pipes are adapted. The composition of raw exhaust gas is measured continuously based on the infra-red principle (CO and CO_2), paramagnetic principle (O_2), as well as by flame ionization detector (CH_4) and chemiluminescence analyzer for nitrogen oxides (NO_X). A pipe connecting the exhaust and intake manifold for low-pressure extern EGR is also designed. The EGR mass flow ($\dot{m}_{EGR}$) is controlled by an electrically adjustable EGR valve.
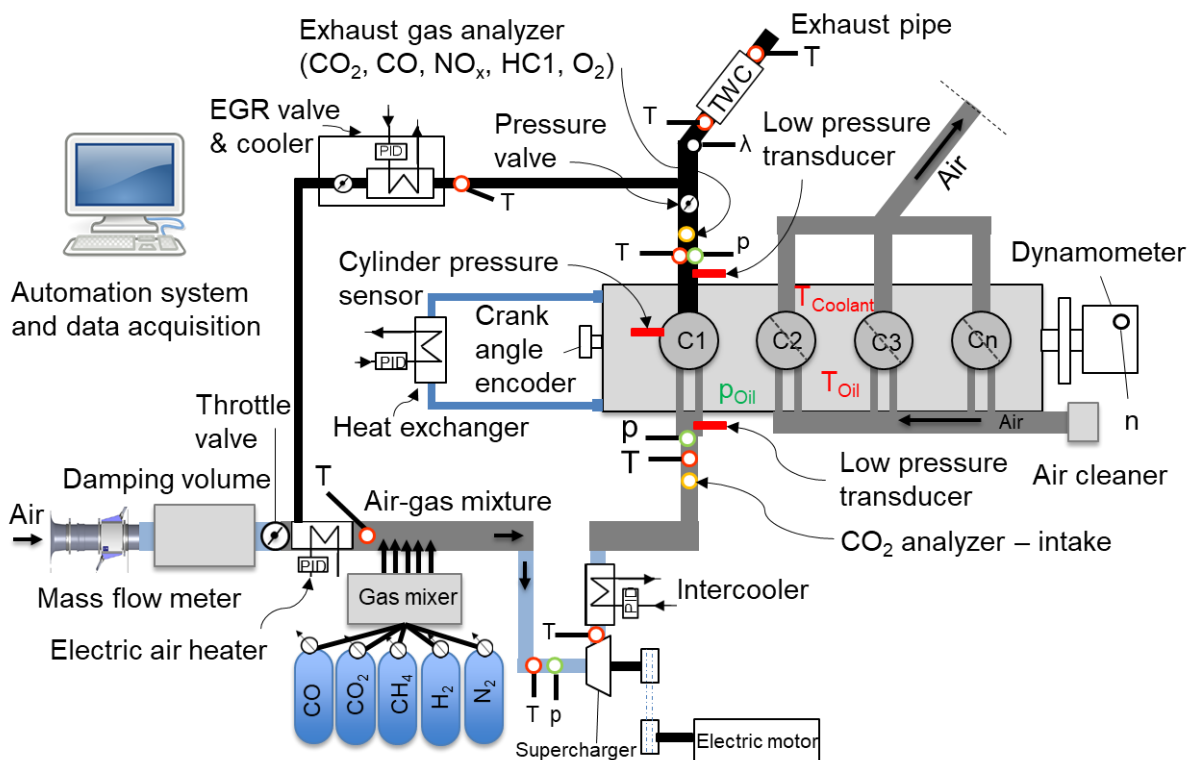
Figure 14: Schematic view of the adapted single-cylinder engine equipped with measurement instruments at the engine test bench

The rate of extern EGR is defined in <u>Equation 8</u> as the ratio of extern EGR mass flow and total intake mass flow according to [38]:

$$Rate\ of\ EGR = \frac{\dot{m}_{EGR}}{\dot{m}_{Intake}} = \frac{\dot{m}_{EGR}}{\dot{m}_{Fresh\ charge} + \dot{m}_{Residual} + \dot{m}_{EGR}}. \tag{8}$$

$\dot{m}_{EGR}$	Mass flow of extern EGR [kg/h]
$\dot{m}_{Intake}$	Total intake mass flow [kg/h]
$\dot{m}_{Fresh\ charge}$	Mass flow of fresh charge [kg/h]
$\dot{m}_{Residual}$	Mass flow of residual gases (includes internal EGR, if any) [kg/h].

The EGR rate on the wood gas engine test bench is determined according to [38] from the measured CO_2 content in the intake manifold ("CO_2 analyzer – intake" in Figure 14), exhaust pipe (Exhaust gas analyzer in Figure 14), and environmental CO_2 concentration (measured during air-cycle by "CO_2 Analyzer intake" in Figure 14). Since the wood gas contains CO_2, the CO_2 content in fresh charge (mixture consisting of ambient air and wood gas) is considered. <u>Equation 9</u> gives the rate of EGR on wood gas engine:

$$Rate\ of\ EGR = \frac{[CO_2]_{Intake} - [CO_2]_{Fresh\ charge}}{[CO_2]_{Exhaust} - [CO_2]_{Fresh\ charge}} \tag{9}$$

$[CO_2]_{Exhaust}$	molar percentage of CO_2 in the dry exhaust gas [mol%$_{dry}$]
$[CO_2]_{Fresh\ charge}$	molar percentage of CO_2 in the dry fresh charge [mol%$_{dry}$]
$[CO_2]_{Intake}$	molar percentage of CO_2 in the intake (including EGR) [mol%$_{dry}$]

The test bench automation system comprises engine control and data acquisition. It accurately adjusts engine parameters such as ignition timing, air-fuel ratio, charging pressure, and temperature. Engine indicating occurs by *AVL Indicom* with a resolution of 0,1 CAD. The average pressure curve of 200 consecutive cycles is used for thermodynamic analysis. All other signals are measured with a sampling rate of 20 Hz.

The gas composition mixer supplies the ICE with a gas mixture defined composition and reproduces the biomass power plant's wood gas supply, avoiding the sluggish behavior of real gasification and long start-up processes. It is developed in the framework of the research project and includes controlling software and hardware components – see <u>Figure 15</u>. The gas mixer´s software comprises gas mixing rules and controlling parameters written and executed in the environment of *Tornado* by *K&S Engineers*. The calculation and control of the mixing process are based on the required wood gas composition in terms of mass fractions and wood gas mass flow. The hardware involves air and gas mass flow sensors, solenoid valve coils, and a gas analyzer. The single gas components are supplied from the gas pressure cylinders. An air throttle valve controls the air mass flow and the intake pressure for naturally aspirated engine operating mode. The wood gas and air are centrally mixed,

reproducing the mixture formation process in biomass power plants. The central mixture formation is usually applied when the gas supply occurs under low pressure, such as for small high-speed wood gas engines.
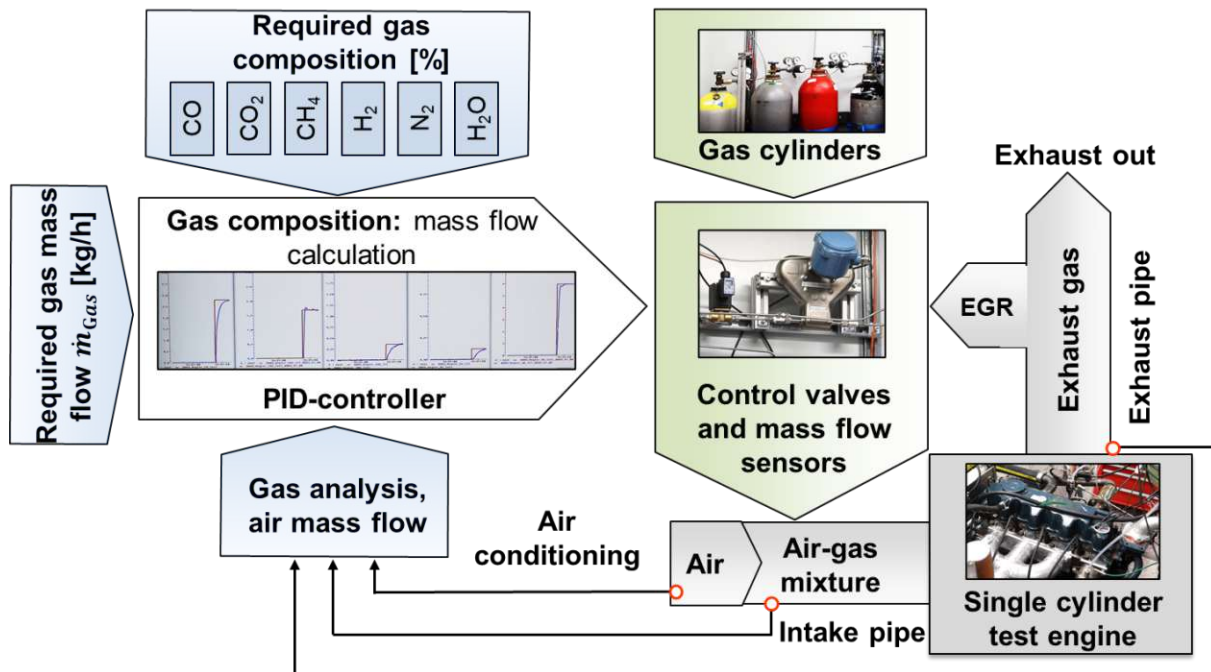

Figure 15: Schematic view of developed gas mixer for gas supply of test engine

To investigate the effects of lean and EGR engine operation on the test bench, the engine operating conditions and parameters are adjusted to reproduce the real biomass power plant operation. At the constant engine speed and intake pressure, the relative air-fuel ratio is set by adjusting the wood gas flow and the air throttle valve. When the mixture dilution occurs with EGR on the naturally aspirated premixed wood gas engine (λ=1), the mass flow of the aspirated fresh mixture linearly decreases with increasing EGR rate at the constant intake pressure. Thereby, the constant in-cylinder charge mass and in-cylinder residual mass are assumed.

The intake pressure boosting is realized with an external electrically driven supercharger for the investigations on the test bench – see Figure 14. The intake pressure is set by adjusting the charger's rotational speed, and the intake temperature is controlled by a heat exchanger positioned downstream of the supercharger. An electrically adjustable flap valve in the exhaust system is used to produce the necessary exhaust gas back pressure.

To simplify the mixed wood gas composition, volume fractions of higher C_XH_Y compounds are substituted by an additional volume fraction of CH_4. Since the components such as tar and dust do not significantly influence the combustion process due to their low fraction, they are not added to the mixed wood gas for the test bench

investigations. The simplified composition of the wood gas for test bench investigations is summarized in Table 4.

Table 4: Simplified wood gas composition for investigations on the test bench

Simplified wood gas composition for test bench	
Parameter	Value
CO [%vol.dry]	23,9
CO_2 [%vol. dry]	9,2
CH_4 [%vol.dry]	5,3
H_2 [%vol.dry]	14
N_2 [%vol.dry]	47,6
LHV [MJ/kg]	5,7
A_{min} [kg/kg]	1,6

The test bench architecture also allows the implementation of engine optimization measures such as modification of combustion chamber geometry and adjusting of ε. To investigate the effects of combustion chamber design and ε on the combustion process, the different piston crowns are milled on the specially designed piston blanks and implemented in the research engine. Due to the increased compression height of the piston blanks, the engine is modified with an adapter plate inserted between the cylinder head and the crankcase – see Figure 16. The adapter plate contains the cooling ducts, oil ducts, guides for the valve lifters, and holes for the cylinder head bolts. The main geometric engine parameters (e.g., stroke, bore, connecting rod length, displacement, and valve timing) remain unchanged. Due to the thin adapter plate and the slight increase in piston mass after modification, minor influences on heat transfer are neglected.
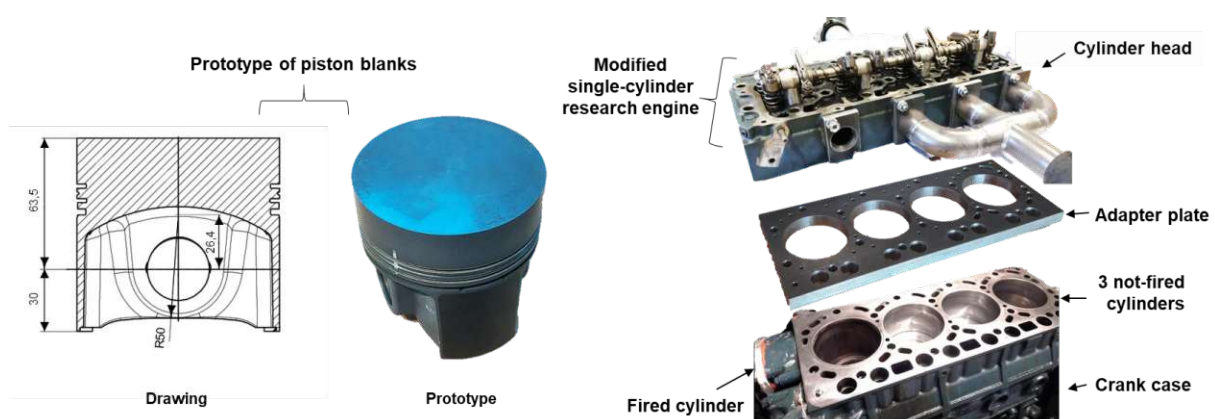
Figure 16: The prototype of piston blanks with high compression height allows designing different piston crown geometries (left) and modifications of single-cylinder engine for investigation of the combustion process (right)

5.3   Validation of the Research Engine

The same operating point analyzed on the wood gas engine integrated into the actual biomass power plant in the field is reproduced on the developed single-cylinder research engine at the test bench. The results are compared to validate the experimental approach for the investigations of the combustion process and to check the accordance between the engine integrated into the biomass power plant and the test engine. Both engines have the same basic layout and operate under the same conditions – constant intake manifold pressure and temperature, engine speed, and fresh charge composition. For combustion process comparison, variations of ignition timing are performed.

Figure 17 shows IMEP, COV$_{IMEP}$, combustion duration (MFB5-90%), ignition delay, and raw exhaust gas emissions (NO and CO) over the ignition timing. The data observed on the engine integrated into the actual biomass power plant, and the single-cylinder research engine on the test bench are in good agreement over the investigated operating points. The shaded area presents the ignition timing, which gives the maximum IMEP in the absence of irregular combustion phenomena. Since only indicated values are observed in the scope of the present research, the ignition timing that gives maximum IMEP is considered optimal and occurs when the center of combustion (50% of the mass burned fraction) meets 9° after TDC. Thus, the optimal ignition timing (IT) is referred to as IT=IT$_{IMEP=max}$ in the present work. The maximum of IMEP curve determined on the test engine is relatively flat (see Figure 17). As ignition timing is advanced or retarded from optimal settings, IMEP decreases. In advanced settings, engine knocking occurs. COV$_{IMEP}$ increases exponentially, and the combustion duration linearly as the ignition timing is retarded from initially advanced timing. The ignition delay remained constant over the variations. The raw exhaust gas emissions of CO and NO linearly increase as the ignition timing is advanced from initially retarded settings. The increase in CO is less intensive than in NO over investigated operating points for both engines. As the ignition timing is advanced, the combustion occurs earlier in the cycle, and higher peak cylinder pressure and burned gas temperatures increase NO formation rates. The modest variation in IT around the IT=IT$_{IMEP=max}$ (green shaded area) alters the NO emissions significantly. Therefore, careful adjustments of IT are essential to obtain accurate NO emissions. As the cylinder pressure increases with advanced ignition timing, a higher portion of the unburned mixture that does not participate in the combustion process is filled into the crevice volumes contributing to a slight increase in the CO emissions.

The same trends observed in both engines proved the accordance of the developed single-cylinder engine set up for the investigations of the combustion process. Minor discrepancies in results are attributed to fluctuations in wood gas composition supplied

by the gasifier during the measurements of the engine integrated into the actual power plant in the field. For example, an alteration of gas composition during the logging of 200 consecutive engine cycles significantly affects the cylinder pressure curve.
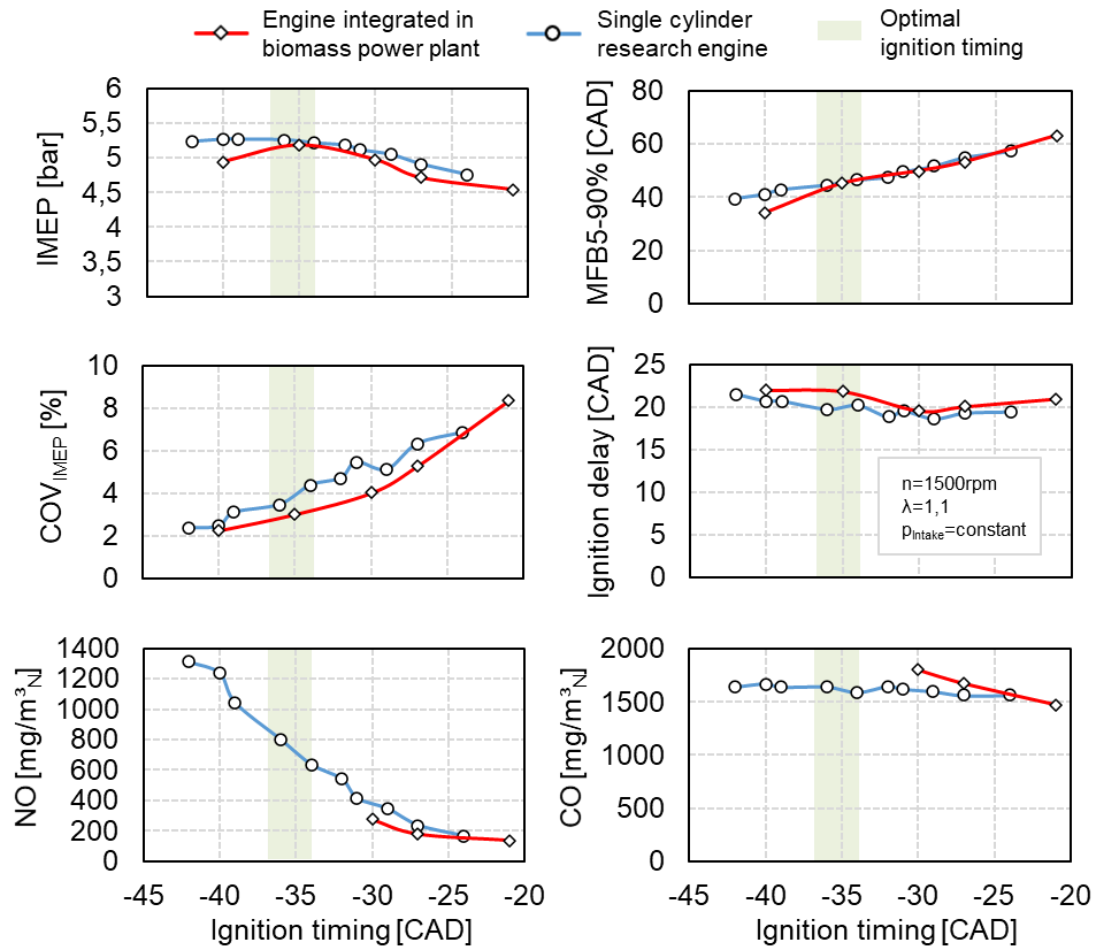

Figure 17: Verification of single-cylinder research engine for investigations of the combustion process: comparison of IMEP, coefficient of variance in IMEP (COV$_{IMEP}$ – as a measure of combustion stability), combustion duration (MFB5-90%), ignition delay and also raw exhaust gas emissions (NO and CO, measured at the integrated engine only in several operating points due to limitations of measurement instruments) at constant engine speed, λ and intake pressure (875 mbar$_{absolut}$)

5.4   Modeling and Simulation

For the detailed analysis of the wood gas combustion process, 0D/1D simulation is used. To analyze the effects of the piston crown geometry on the charge motion, a 3D CFD simulation of in-cylinder flow is performed.

5.4.1   Thermodynamical Combustion Analysis

The thermodynamic efficiency analysis of the combustion process is performed in the 0D/1D simulation software environment (*GT-Power*) to quantify efficiency losses

related to the specific mechanisms. The engine process simulation enables analysis of the test bench measurement data and determines in a "reverse run calculation" the combustion characteristics such as burn rate, scavenging losses, mass flows through the valves, and other quantities that cannot be measured directly on the engine test bench. During the iterative calculation, the fuel mass converted for each time step is adjusted stepwise until the calculated cylinder pressure equals the measured cylinder pressure signal. The results include a detailed efficiency loss analysis of the considered operating point. A 0D/1D-simulation model of the research engine is built for thermodynamic analysis of the engine operation – see Figure 18. The intake and exhaust area templates are specified with the inlet and outlet pressure curves, and the exact gas composition and temperature measured on the test bench for each operating point. The cylinder pressure signal is specified in the combustion chamber template. Additionally, the templates of the intake and exhaust systems, combustion chamber, and crankshaft are defined with engine geometry and parameters (e.g., engine speed, valve timing, valve lift, and flow coefficients). The wall heat transfer is modeled using the *Woschni* heat transfer submodel (*WoschniGT*), and the wall temperatures are defined as constant [95].
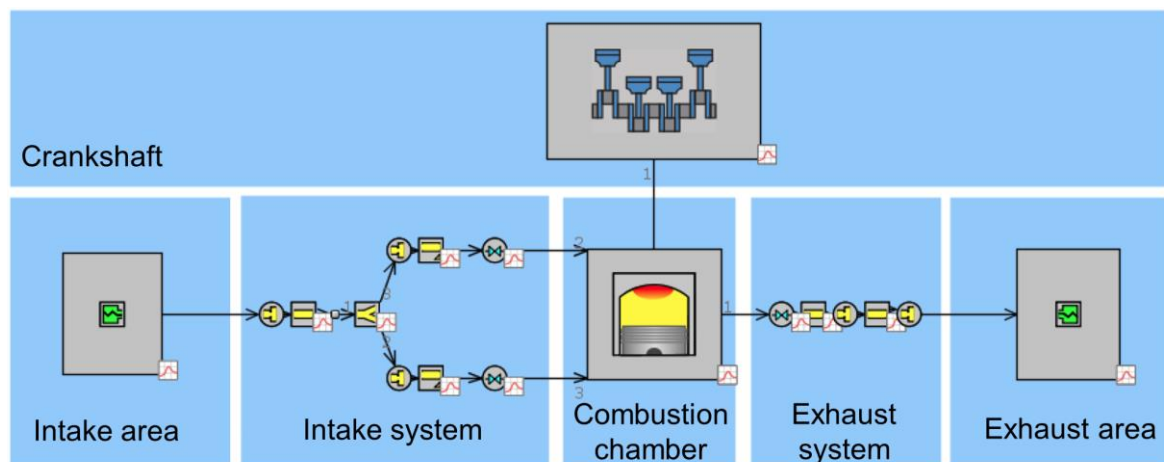
Figure 18: Simulation model of single-cylinder research engine for efficiency loss analysis

The efficiency analysis provides detailed insights into the combustion process and compares the effects of changing the engine design, fuel, combustion mode, and operating conditions. It quantifies the efficiency with which the fuel heat released by combustion can ideally be converted into useful work (ideal cycle) and theoretically avoidable losses of the real engine work process [38].

Simplified assumptions concerning the combustion process, heat transfer, gas exchange, and gas properties are necessary to analyze the engine process. Starting from the ideal constant-volume process (with ideal gas as working fluid and constant

specific heat ratio $\gamma = 1{,}4$), which represents the theoretical efficiency limit for the Otto engine (theoretical efficiency η_{th} increases with increasing compression ratio ε and specific heat ratio γ, see Equation 10, [37]), real conditions gradually replace ideal assumptions.

$$\eta_{th} = 1 - \frac{1}{\varepsilon^{\gamma-1}} \tag{10}$$

η_{th}	theoretical efficiency
ε	geometric compression ratio
γ	specific heat capacity ratio

The efficiency losses assigned to the individual real conditions are determined according to [95]. A succession of the losses is described below:

- Efficiency losses due to fluid properties occur because of temperature- and composition-depended changes of specific heat ratio (ideal gas is assumed).
- Efficiency losses due to unburned fuel occur because of incomplete combustion and result in energy lost to exhaust in the form of emissions (e.g., CO and HC_1).
- Efficiency losses due to real combustion are caused by finite combustion duration, sub-optimal location of the combustion center, and scavenging losses during valve overlap. Compared to the ideal cycle where the complete combustion occurs at TDC, the real finite combustion results in an efficiency loss since the proportion of energy converted into mechanical work is smaller the further the piston moves away from TDC.
- Efficiency loss due to heat transfer to the combustion chamber walls.
- Efficiency loss due to gas exchange considers the gas exchange determined with average intake and exhaust pressures of an ideal gas and with the real pressure signals.
- Indicated efficiency is determined by subtracting all the losses from the theoretical efficiency.

The efficiency loss analysis is performed in the selected operating points on the basic engine setup and by applying selective optimization measures such as adjustment of combustion chamber geometry, lean and EGR operation with different dilution rates, and adjustment of compression ratio. The operating points (OP) are selected to highlight the effect of optimization measures on engine efficiency improvement and are listed in Table 5. They give a representative comparison of optimization measures and the efficiency improvement potential.

Table 5: Investigated operating points on the single-cylinder engine test bench for efficiency loss analysis

OP Number	Feature	λ / EGR	ε
OP 1	Basic piston crown	λ=1,1 / EGR=0%	11
OP 2	Cylindric piston crown	λ=1,1 / EGR=0%	11
OP 3	Asymmetric piston crown	λ=1,1 / EGR=0%	11
OP 4	Asymmetric piston crown: Lean operation	λ=1,2 / EGR=0%	11
OP 5	Asymmetric piston crown: Lean operation	λ=1,5 / EGR=0%	11
OP 6	Asymmetric piston crown: EGR operation	λ=1 / EGR=10%	11
OP 7	Asymmetric piston crown: Lean operation	λ=1,5 / EGR=0%	12,5
OP 8	Asymmetric piston crown: Lean operation	λ=1,5 / EGR=0%	14,5
OP 9	Asymmetric piston crown: Lean operation	λ=1,5 / EGR=0%	16,4
OP 10	Asymmetric piston crown: Lean operation	λ=1,5 / EGR=0%	19,5
OP 11	Asymmetric piston crown: Lean operation	λ=1,5 / EGR=0%	22,2

The simulation results are compared with the measurements for every operating point to verify the quality of the simulation model. Figure 19 and Figure 20 compare the simulation and measurement results of two operating points: logp-logV diagrams and the intake, cylinder, and exhaust pressures. The results show good agreements between calculated and measured pressure traces.
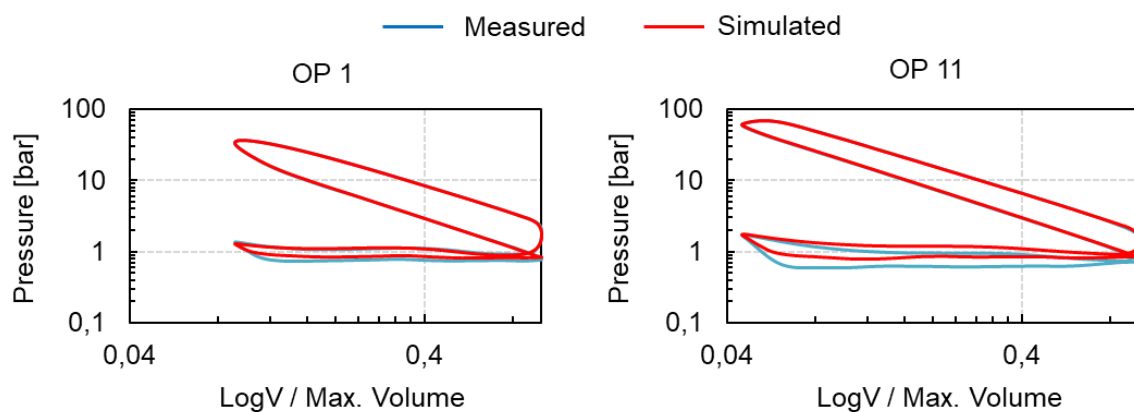
Figure 19: Comparison of measured and simulated Log p Log V – OP 1 (left) and OP 11 (right)
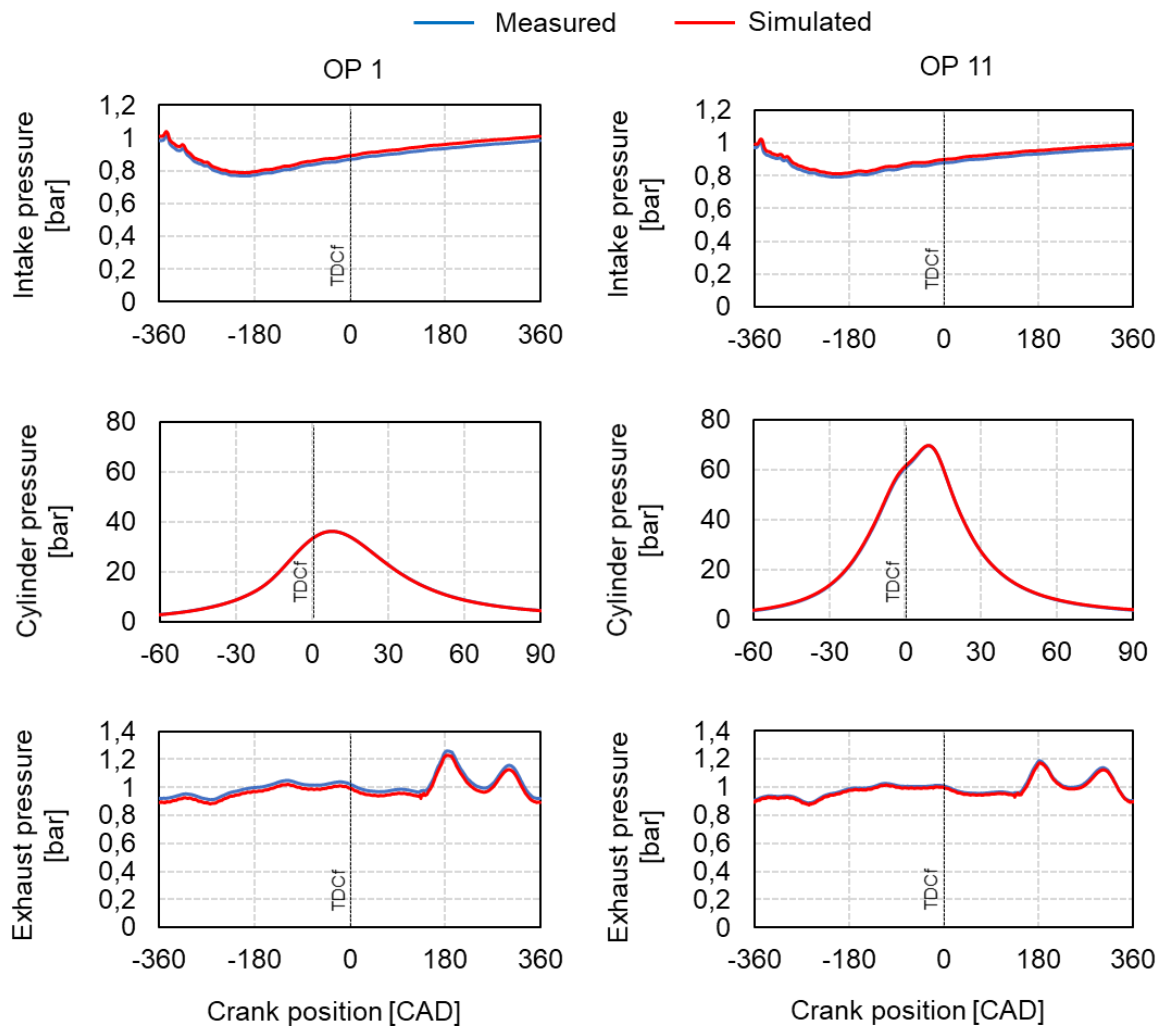
Figure 20: Comparison of measured and simulated low and high pressures – OP 1 (left) and OP 11 (right)

Figure 21 compares the simulation results with test bench measurements of total mass flow, peak cylinder pressure, and IMEP. The mass flow, peak cylinder pressure, and IMEP are accurately calculated. Slight deviations between simulation results and measurements of mass flow in OP 9 to 11 imply that less fresh charge flow is required in the model than measured on the test bench with increasing ε. The increasing emissions of unburned fuel with increasing ε can explain this trend. Although measured exhaust gas emissions are considered in the simulation model to account for the degree of incomplete combustion, this is only done for HC, CO, and NO emissions, while unburned hydrogen is not considered. Apart from those deviations, the simulation model accurately reproduces the engine operation in the analyzed operating points and provides reliable efficiency analyses.
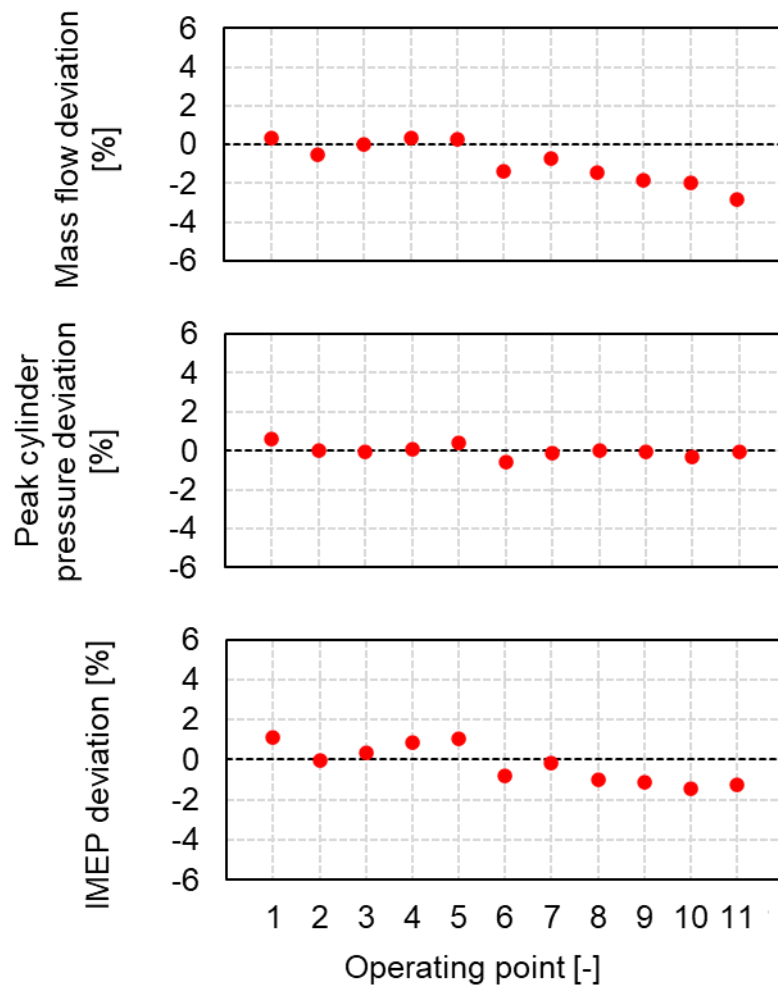
Figure 21: Comparison of the simulation results with the measurements on the single-cylinder research engine – total mass flow, peak cylinder pressure, and IMEP

5.4.2 CFD-Simulation

The commercial code *Converge CFD* (Version 3.0) is used to investigate the in-cylinder charge motion of different combustion chamber geometries. To create a simulation model for the 3D CFD analysis, the 3D geometry of the entire combustion chamber is required in digital data format (CAD formats or .stl). The combustion chamber geometry of the research engine is determined using a developed "reverse engineering" method schematically depicted in Figure 22. First, the intake and exhaust ports are cast with two-component silicone rubber (e.g., dental impression material – Figure 22 a). The casts replicate the flow domain of each port (Figure 22 b). They are scanned with high accuracy using a 3D scanner (*AICON-PrimeScan*) – Figure 22 c). Additionally, intake and exhaust valves are separately scanned to create the complete model geometry. In the further steps, the geometry needed for the 3D CFD simulation is generated and merged using the 3D processing software *GeomagicWrap* and imported into the *Converge Studio* for pre-processing – see Figure 22 d).
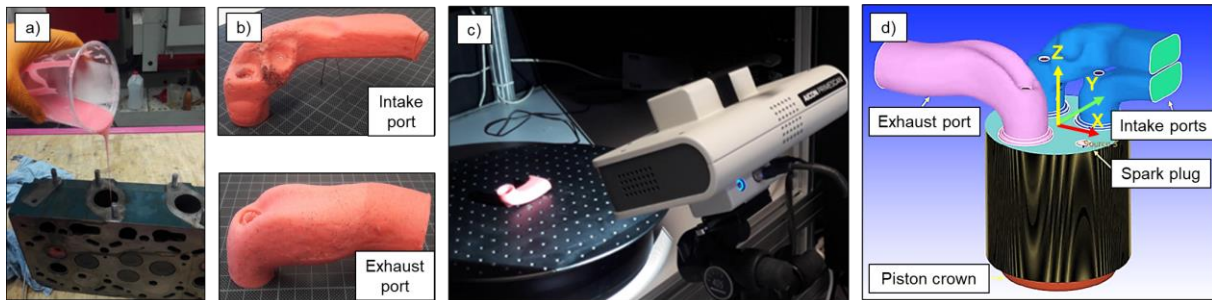
Figure 22: Reverse engineering method for determining the engine geometry for 3D CFD simulation: the casting of the intake and exhaust ports including valve seats – a), obtained casts (i.e., reproduction of the flow domain), – b), 3D scanning of casts – c), merged engine geometry for pre-processing – d)

During the pre-processing, the case setup is defined. The investigation of the charge motion is carried out on the mesh of the entire combustion chamber. The global Cartesian grid size is 4 mm. A method for adaptive mesh refinement (AMR) integrated with *Converge CFD* software refines the computational mesh according to the predefined settings in regions where large gradients of flow and thermodynamic quantities occur in each piston position [96]. For specific regions, such as valve gaps or spark plug, fixed embeddings with high and constant refinements of mesh minimize the effects of the computational mesh on the results. The grid size is reduced to 1 mm in fixed embeddings. The global mesh and applied mesh refinements resulted in up to 230000 computational cells for flow calculations.

The calculation of turbulent flow is based on Reynolds-Averaged Navier-Stokes equations (RANS) [97]. For turbulence modelling, the RNG k-ε model[5] is used. In contrast to the frequently applied k-ε -model, it accounts for the effects of different scales of motion, making it more accurate and reliable for the present investigation. The test bench measurement data are used to fit the simulation model. The boundary conditions determined in the experimental measurements on the basic research engine setup (e.g., intake and exhaust temperatures, composition, indicated intake and exhaust pressures) are imposed on the intake and exhaust side of the simulation model. Valve timing, valve lift, and flow coefficients are also integrated into the model. For the model validation, the simulation of the average motoring cycle is performed, and the simulation results are compared with the measurements. Table 6 lists the mean intake and exhaust pressures, the peak cylinder pressure, and the mass flow of

---

[5] RNG k-ε turbulence model renormalize the Navier-Stokes equations using a statistical technique called Re-Normalization Group (RNG) methods to account for the effects of different scales of motion such as effects of the velocity dilatation and changes in kinematic viscosity on turbulence dissipation rate [96] [97], [98], [99].

the average motoring cycle (200 consecutive cycles) at wide-open-throttle (1500 rpm) measured on the test bench and the simulation results with the basic piston variant.

Table 6: Comparison of the simulation results with the measurements on the single-cylinder research engine

Parameter	Mean intake pressure	Cylinder peak pressure	Mean exhaust pressure	Mass flow
Measured	0,9133 bar	24,842 bar	1,003 bar	34,28 kg/h
Simulation	0,9134 bar	24,886 bar	1,004 bar	34,31 kg/h

Figure 23 compares the measured and simulated cylinder pressure curves. The results show good agreements between calculated and measured values and pressure curves. Thus, the simulation model accurately reproduces the charge flow during the motored air cycle and provides a reliable tool for in-cylinder flow analysis.
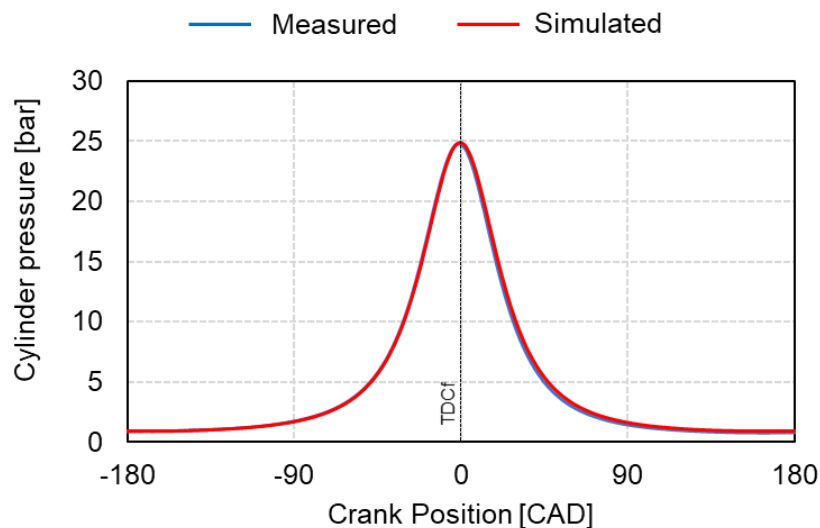
Figure 23: Comparison of the simulation results with the measurements on the single-cylinder research engine: measured and simulated cylinder pressure curves of average motored air cycle at wide-open-throttle and 1500 rpm (basic piston, ε=11)

Variants of the pistons with differently sized squish areas and different piston crown shapes are designed and incorporated into the simulation models. The in-cylinder charge motion of the motored air cycle is investigated with applied piston crown geometries. The evaluation criteria for the designed geometries are the intensity of in-cylinder flow velocity, swirl, and turbulent kinetic energy. The absolute values observed during flow investigations with different combustion chamber geometries can be compared because the calculations are all performed under the assumption of the same boundary conditions. Thus, the results reported in Chapter 6.2 compares the trends of the flow effects depending on the piston crown shape.

The following chapters present the numerical and experimental results.

6 Adjustment of Combustion Chamber Design

Effects of combustion chamber design on in-cylinder charge motion and combustion process are investigated in the following. The numerical investigations concern in-cylinder motion with different piston crown geometries. The lean and EGR engine operations are experimentally investigated on the research engine concerning efficiency and emissions.

6.1 Investigated Combustion Chamber Geometries

A compact combustion chamber design that provides unhindered flame propagation and intensive charge motion is a prerequisite for a fast and stable combustion process. The piston crown shape and squish area are essential adjusting parameters within the combustion chamber for affecting the in-cylinder charge motion in engines with a flat cylinder head. Based on the investigations of proven piston crown geometries reviewed in Chapter 3.2.2, a cylindrical (symmetrical) piston crown with a medium squish area and an asymmetrically-shaped piston crown with a large squish area are designed for the investigation. Figure 24 schematically depicts the basic, cylindrical, and asymmetrical piston crown variants.
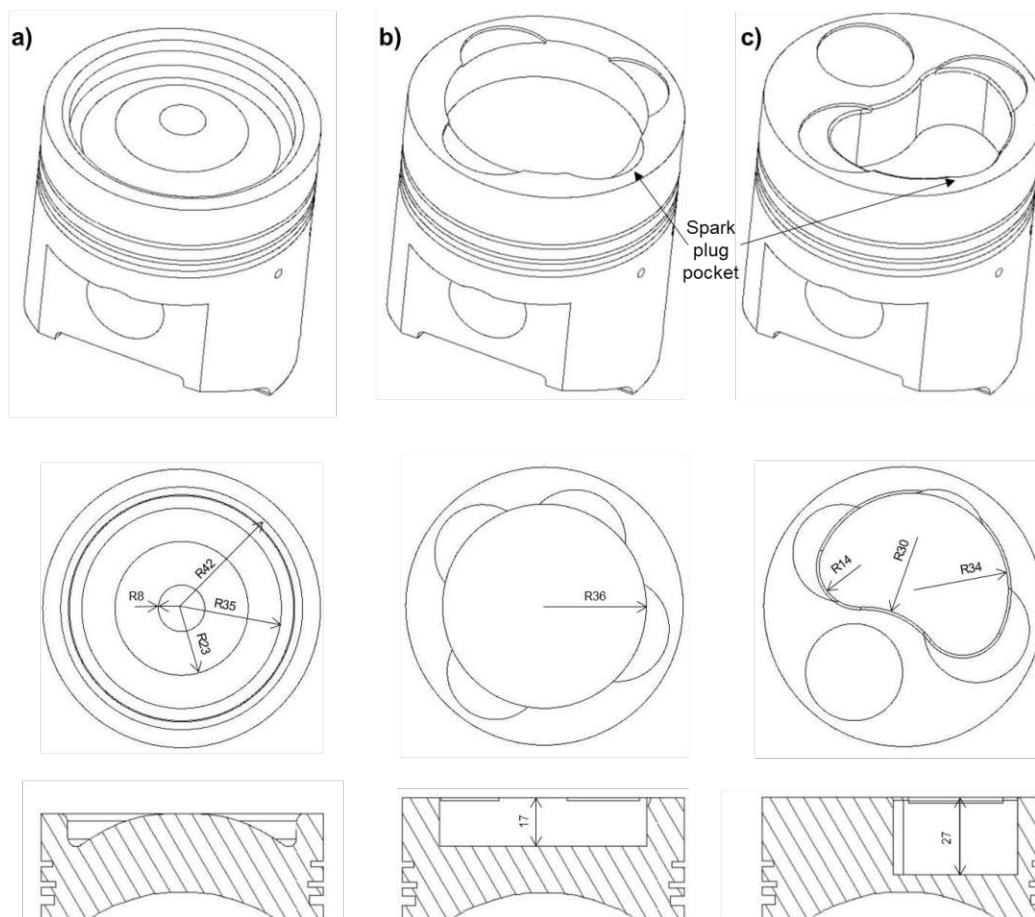
Figure 24: Investigated piston crown geometries: basic a), cylindrical b) and asymmetrical c)

The basic piston crown (see Figure 24 a) represents the starting point for the present optimization. It has an inner diameter at the upper end of 40 mm. The crown´s bottom has a convex shape. A high distance between the top edge of the piston and the cylinder head of 6,5 mm at the TDC exhibits a weak squish effect. Among the simplest geometries (reviewed in Chapter 3.2.2), a cylindrically shaped piston crown ensures a small surface-to-volume ratio within the combustion chamber. The designed prototype has an inner diameter of 72 mm and a depth of 17 mm – see Figure 24 b). The distance between the top edge of the piston and the cylinder head is minimized to 1,05 mm at TDC. In that way, the piston exhibits a medium-sized squish area. The asymmetrically-shaped piston crown has a heart-like shape and a single symmetry axis which does not coincide with any other axis – see Figure 24 c). It is also positioned on the spark plug side within the combustion chamber to ensure a maximal possible flame front area at the given spark plug position. The special design exhibits a large squish area (at a minimized distance between the top edge of the piston and the cylinder head of 1,05 mm). The heart-like shape remains the same over the full depth. The cylindrical and asymmetrical piston crown geometries have a cavity on the edge of the squish area (a spark plug pocket) to enlarge the space around the spark plug at TDC. The crevice volume of cylindrical and asymmetrical piston crowns is 33% larger compared to the basic variant. Figure 25 depicts the surface-to-volume ratio at TDC of the investigated piston crowns. The cylindrical and asymmetrically-shaped piston crowns exhibit a lower surface-to-volume ratio at TDC.
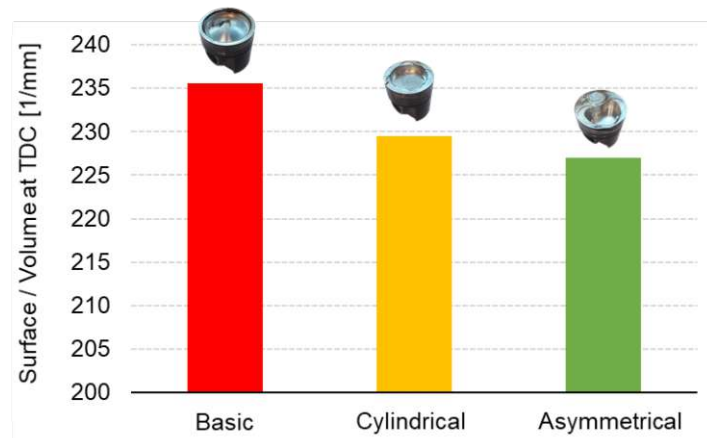

Figure 25: The surface-to-volume ratio at TDC of the investigated piston crowns

In order to compare the intensity of the squish, the size of the squish area[6] and the theoretical squish velocity normalized by the mean piston speed are presented for each geometry in Figure 26. According to [37], the theoretical squish velocity (v_{sq}) is calculated from the instantaneous displacement of gas across the inner edge of the

---

[6] The percentage of the piston area which closely approaches the cylinder head [37].

squish region for the bowl-in piston – see Equation 11. The effects of gas dynamics are neglected for simplification.

$$\frac{v_{sq}}{S_p} = \frac{D_B}{4Z}\left[\left(\frac{B}{D_B}\right)^2 - 1\right]\frac{V_B}{A_c Z + V_B} \tag{11}$$

Thereby, B stays for the bore, D_B for the inner diameter of the piston crown, V_B is the volume of the piston crown, A_c is the cylinder area, S_p is the instantaneous piston speed, and Z is the distance between the top piston edge and the cylinder head at TDC.

Figure 26 a) shows the squish area of the investigated piston crowns – the basic piston crown has no squish area, the cylindrical piston crown has a medium (40% of bore surface area), and the asymmetrical piston crown has a large squish area (65% bore surface area). Figure 26 b) shows that $\frac{v_{sq}}{S_p}$ increases as the piston approaches the TDC due to intensified gas flow from the squish region into the piston crown and reaches the maximum at about 10 CAD before TDC. As the size of the squish area increases, the peak $\frac{v_{sq}}{S_p}$ also increases, and the highest value is achieved with the asymmetrically shaped piston crown.
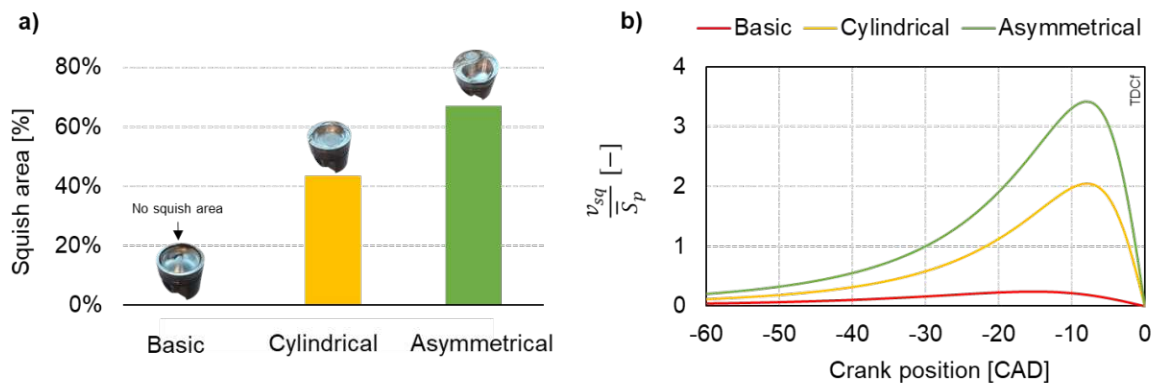
Figure 26: Comparison of the investigated piston crowns: squish area a) and theoretical squish velocity normalized by mean piston speed b)

6.2 Numerical Analysis of the In-Cylinder Flow

3D CFD simulation is applied to investigate the effects of the piston crown design on the charge motion. The in-cylinder flow is investigated during a simulated air cycle at a wide-open-throttle (1500rpm). Figure 27 shows the determined flow velocity in the combustion chamber of the piston variants at a crank angle position of 10 CAD before TDCf. The lowest flow velocity and, thus, light charge motion is generated with the basic geometry. A higher flow velocity occurs in the cylindrical piston crown in the squish area (light blue shade). Due to the piston movement in the TDC direction, the

charge is pushed out of the squish area, resulting in a squish flow. The larger squish area in the asymmetrically-shaped piston crown enhances this effect. High flow velocities (red shade) occurring within the squish area of asymmetrically shaped piston crown prove the intensive squish motion. The presented trend of flow velocities within basic, cylindrical, and asymmetrical pistons determined by CFD analysis correlate with the increasing trend of the calculated theoretical squish velocities normalized by the mean piston speed depicted in Figure 26 b).
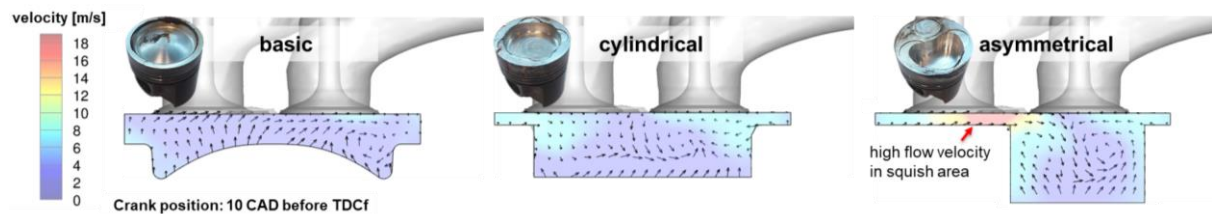
Figure 27: Flow velocity within the combustion chamber at a crank angle position of 10 CAD before TDCf – results of numerical analysis

Figure 28 shows the determined intensity of the swirl ratio and turbulent kinetic energy averaged over the combustion chamber. The swirl ratio presents the angular speed of flow about the center of mass in the z-direction (see Figure 22 d) normalized by the angular speed of the crankshaft [97]. It can be seen that a swirl-dominated charge motion occurs within the combustion chambers. It is generated by the intake port geometry (swirl port). The swirl ratio substantially increases during compression by forcing the charge into the cylindrical (yellow) and asymmetrically-shaped (green) piston crown as the piston approaches the TDC. The highest swirl ratio is achieved slightly before TDC. Due to the asymmetrical shape of the combustion chamber (green), which causes a light deflection of flow patterns, the swirl ratio is slightly lower than within the cylindrical piston crown. The swirl and intensive squish flow patterns interact and amplify the turbulences.
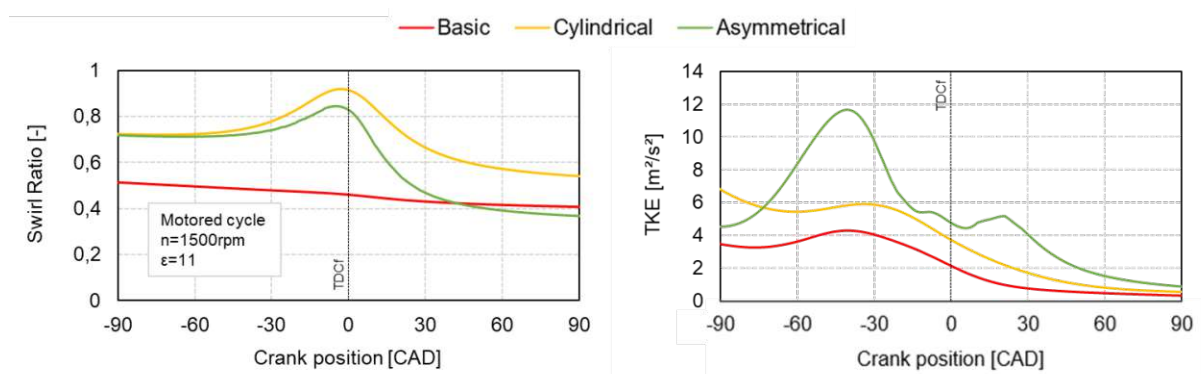

Figure 28: Results of the numerical analysis: Swirl ratio and turbulent kinetic energy within the combustion chamber (motored cycle simulation)

The asymmetrically shaped piston crown reaches the highest intensity of TKE among the investigated variants. The peak at the end of the compression phase (40 CAD before TDCf) is significantly higher compared to the cylindrical and basic variants and implies the intensive in-cylinder charge motion.

These trends can be observed in Figure 29. It visualizes the turbulent kinetic energy in a sectional plane within the combustion chamber at different crank positions between -40 and 0 CAD after TDCf. The TKE distribution is uniform in the middle of the basic piston crown and shows a decreasing trend towards the combustion chamber edges. As the piston approaches the TDC, the turbulence dissipates almost wholly. Similar trends occur at the cylindrical and asymmetrical piston crowns. However, the area in the center of the combustion chamber exhibits a higher turbulence level. Although the turbulent kinetic energy dissipates as the piston approaches the TDC, the highest level of the TKE among the investigated variants is achieved in the center of the combustion chamber with an asymmetrically shaped piston crown, making it suitable for accelerating the combustion process. Hence, the presented results demonstrate the significant effects of the investigated piston crown geometries on the in-cylinder flow.
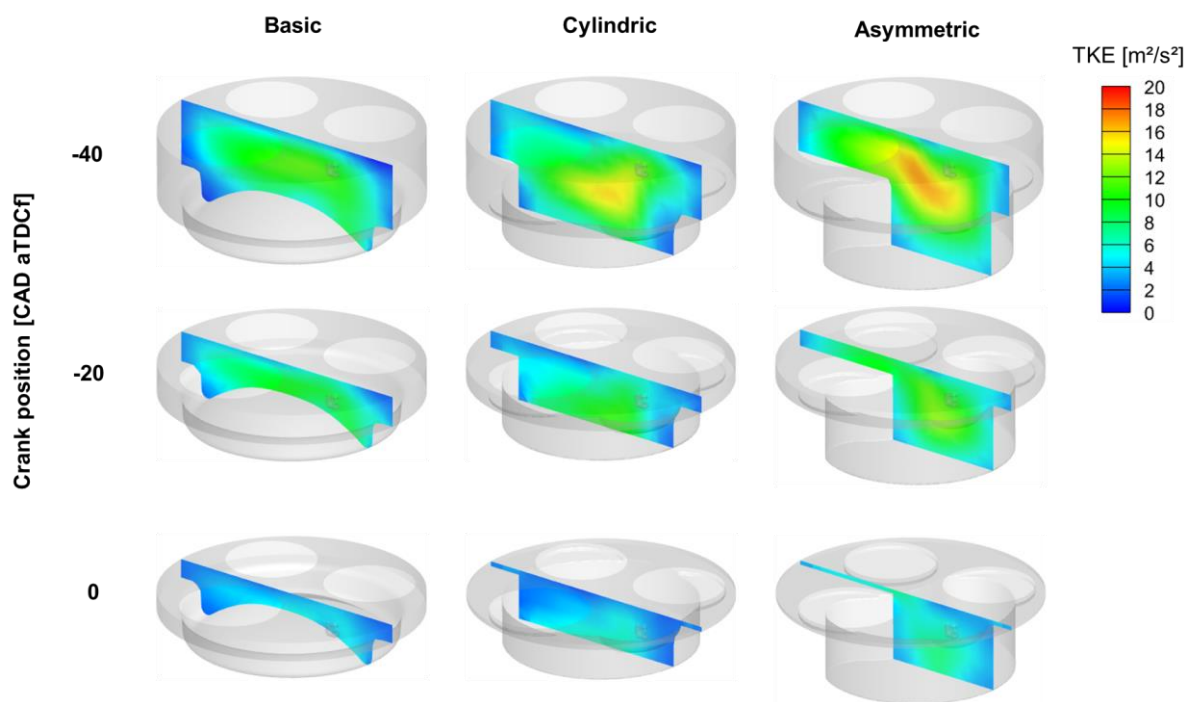

Figure 29: TKE during compression within the combustion chamber with basic, cylindric, and asymmetrically-shaped piston crown (air cycle at wide-open-throttle)

6.3 Experimental Investigation of the Combustion Process

To investigate the effects of the piston crown geometries on the combustion process, the defined piston crowns are milled on the specially designed piston blanks and implemented in the research engine. The engine efficiency and emissions are

analyzed during lean operation and operation with EGR (λ=1). The evaluations occur in the nominal operating point defined by the fixed intake pressure (875 mbar$_a$) and a constant engine speed of 1500 rpm (essentially giving a constant charge flow), reproducing the engine's operating conditions in the biomass power plant. Under these conditions, the pumping work remains unchanged, making it distinct from conventional engines, where the desired load is adjusted by mixture flow throttling. The air, and fuel flows are varied on the test bench to maintain intake pressure constant for various mixture dilution rates, resulting in different engine power outputs. Every piston crown geometry sets the geometric compression ratio ε=11. The ignition timing is set to give the maximum IMEP for given engine operating parameters (IT=IT$_{IMEP=max}$).

6.3.1   Effects of Combustion Chamber Geometry on Combustion Process

The combustion process in the engine adapted with different combustion chambers is analyzed at λ=1,1 in the following. The engine operating parameters of every investigated operating point remain unchanged.

Figure 30 shows the apparent heat release rate (AHRR) determined on the research engine with the basic, cylindrical, and asymmetrical piston crowns. The intensive charge motion within asymmetrically-shaped piston crown results in a significantly faster heat release rate compared to basic and cylindrical designs. The heat release rate in the cylindrical piston crown is slightly higher than in the basic variant due to slightly improved in-cylinder flow motion (see Figure 28). The optimal ignition timing (IT$_{IMEP=max}$) occurs significantly closer to TDC due to improved flame propagation and a shorter length of flame travel path at asymmetrical piston crown compared to cylindrical and basic geometry. The robust asymmetrical piston crown is positioned on the side of the spark plug, bringing most of the cylinder charge closer to the spark plug as the piston approaches the cylinder head, making the flame travel path shorter than at the other piston crown variants.
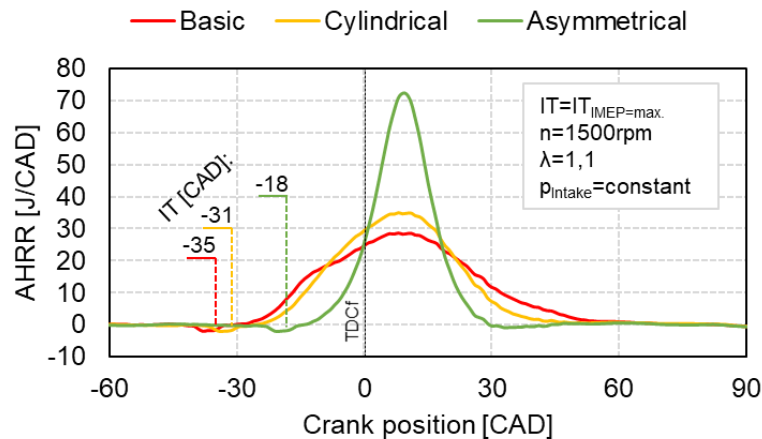
Figure 30: AHRR determined on the engine test bench during operation with different piston crowns – results of measurements at nominal engine operating point (at constant intake pressure =875 mbar$_{absolut}$)

Figure 31 shows the combustion duration, ignition delay, COV$_{IMEP,}$ and raw exhaust gas emissions during engine operation with different piston crowns. The cylindrical and asymmetrical piston crowns accelerate the combustion process, reducing combustion duration by 10 and 25 CAD compared to the basic variant, respectively. The reduced COV$_{IMEP}$ indicates improved combustion stability with cylindrical and asymmetrical piston crowns during engine operation.
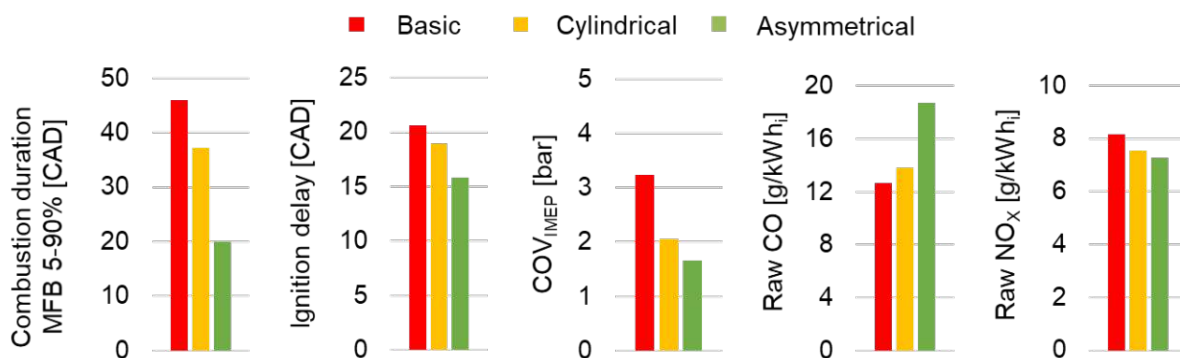
Figure 31: Combustion duration, ignition delay (defined as CAD between IT and MFB5%), cycle-by-cycle variations (COV$_{IMEP}$), and raw pollutant emissions – results of measurements at nominal wood gas engine operating point (n=1500rpm, IT=IT$_{MFB50\%=opt.}$, λ=1,1 and p$_{intake}$=0,875bar$_a$)

CO emissions from engines fueled with wood gas originate mainly from unburned fuel containing CO. The lowest CO emissions are observed at the basic piston crown with no squish area and a smaller crevice volume. The higher CO emissions occur during operation with cylindrical and asymmetrically-shaped piston crowns mainly due to the flame quenching in the dead volume of the squish area and crevice volume – a higher proportion of the fresh charge does not participate in combustion resulting in higher

unburned CO concentrations in the exhaust gas and also adversely affecting the engine efficiency.

The raw NO$_X$ emissions at cylindrical and asymmetrical piston crowns are lower than at the basic variant in the investigated operating point by 3% and 10%, respectively. <u>Figure 32</u> shows the cumulative heat release (a) and burned gas temperatures [7] determined by the thermodynamical analysis (b) for investigated piston crowns. Since the combustion begins earlier (see Figure 30) and a significantly higher amount of fuel heat is released before TDC at basic and cylindrical variant, higher burned mixture temperatures are achieved compared to the asymmetrical piston crown. Thus, lower combustion temperatures reduce the NO$_X$ formation at asymmetrical piston crown.
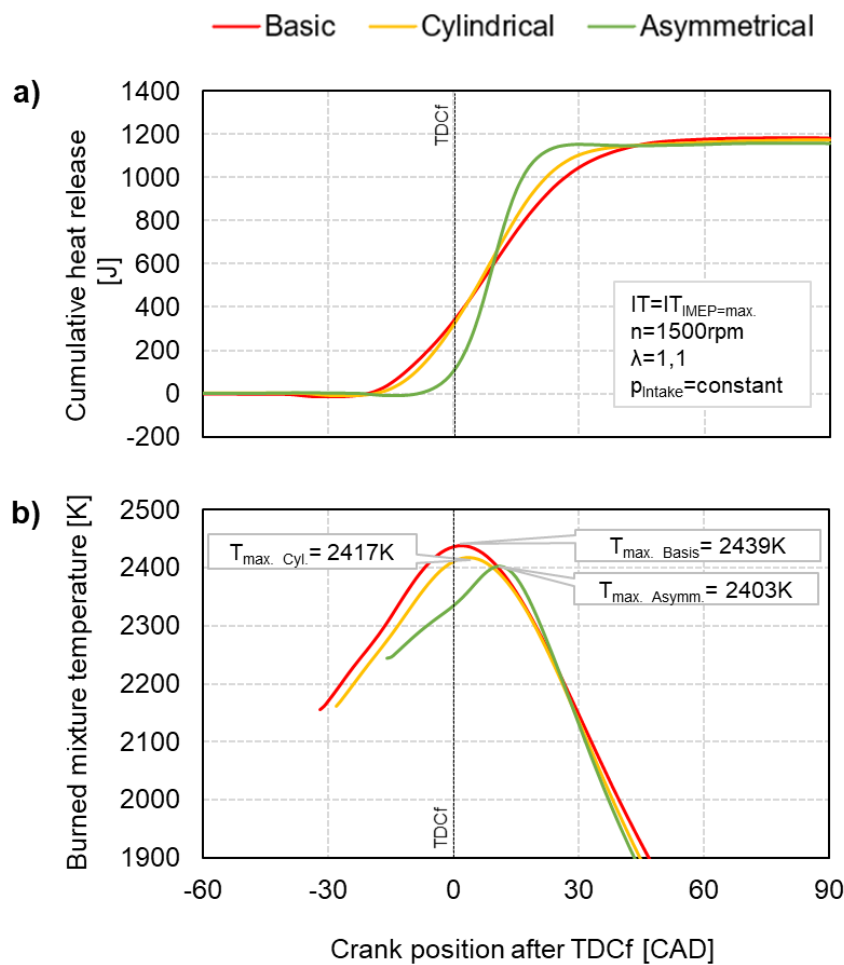
Figure 32: Results determined by the thermodynamical analysis: cumulative heat release (a) and burned mixture temperatures (b) at the investigated piston crowns for engine operation in nominal operating point (n=1500rpm, IT=IT$_{MFB50\%=opt.}$, λ=1,1 and p$_{intake}$=0,875bar$_a$)

---

[7] Burned mixture temperature is calculated according the two-zone combustion methodology and the heat transfer coefficients are determined according to Woschni's correlation [95]

Figure 33 shows the indicated efficiencies (η_i) and related losses for the investigated piston crown geometries. The calculated efficiency losses are deducted from the theoretical efficiency of the ideal cycle (at constant volume, see Chapter 5.4.1) and visualized in the bar chart. The indicated efficiencies of the engine operating with cylindrical and asymmetrical piston crowns are higher than with the basic variant. The losses occurring due to the fluid properties remain in the same range for the investigated variants. The efficiency loss due to unburned fuel is the lowest at the basic variant and increases at cylindrical and asymmetrical piston crowns. It results from the incomplete combustion of fuel, which is reflected in higher unburned fuel emissions. However, the lower efficiency loss due to combustion duration compensates for this disadvantage at the asymmetrical piston crown. The wall heat transfer is in a similar range in all three variants, although the surface-to-volume ratio is lower at cylindrical and asymmetrical piston crowns compared to the basic variant. This trend can be explained by the intensive charge motion at cylindrical and asymmetrical variants, which increases the wall heat transfer and reduces the benefit of a lower surface-to-volume ratio. The gas exchange losses are in the same range. Hence, the efficiency improvement at asymmetrically shaped piston crown results is mainly due to faster combustion and reduced related losses compared to the other variants. Although the efficiency improvement in the investigated nominal operating point at $\lambda=1,1$ is modest, the intensive charge motion ensures a fast and stable combustion process essential for boosting the efficiency in EGR- or lean engine operation.
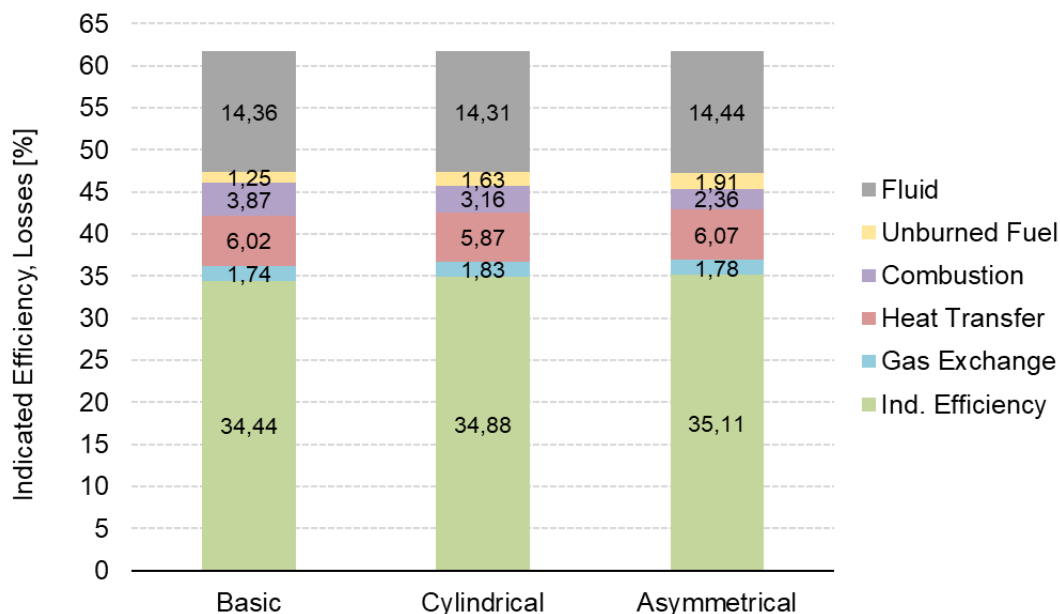

Figure 33: Results of the thermodynamical analysis: indicated efficiency and efficiency losses for engine operation in nominal operating point (n=1500rpm, IT=IT$_{IMEP=max.}$, $\lambda=1,1$ and p$_{intake}$=0,875bar$_a$) with the basic (OP 1), cylindrical (OP 2), and asymmetrical piston crown (OP 3)

6.3.2   Lean Combustion Process

The experimental investigation concerning lean operation is presented in the following. Figure 34 shows the optimal ignition timing, ignition delay, combustion duration (MFB5%-90%), and COV_{IMEP} during lean engine operation with basic, cylindrical, and asymmetrically-shaped piston crowns. As the λ increases, the optimal ignition timing is more advanced, and the ignition delay, combustion duration, and COV_{IMEP} increase at each piston crown variant due to changed fresh charge properties. With increasing λ, the composition-depended laminar flame velocity decreases, and the reaction time increases due to lower temperatures resulting in a slower flame development, deteriorations in combustion stability, and a longer combustion duration. However, the intensive charge motion generated by the asymmetrical piston crown accelerates flame propagation. Thus, the latest ignition timing and the shortest ignition delay occur at the asymmetrically-shaped piston crown. The basic geometry demands the most advanced ignition timing and exhibits the most prolonged ignition delay. Optimizing the combustion chamber significantly reduces the combustion duration and stabilizes the combustion process in the lean operation. For example, during operation at λ=1,8 with the asymmetrically-shaped piston crown, the combustion duration is 40 CAD shorter, and COV_{IMEP} (a measure of combustion stability) reaches a significantly lower level than with the basic geometry. As a result, a significant increase of η_i is achieved compared to the basic variant during the lean operation.
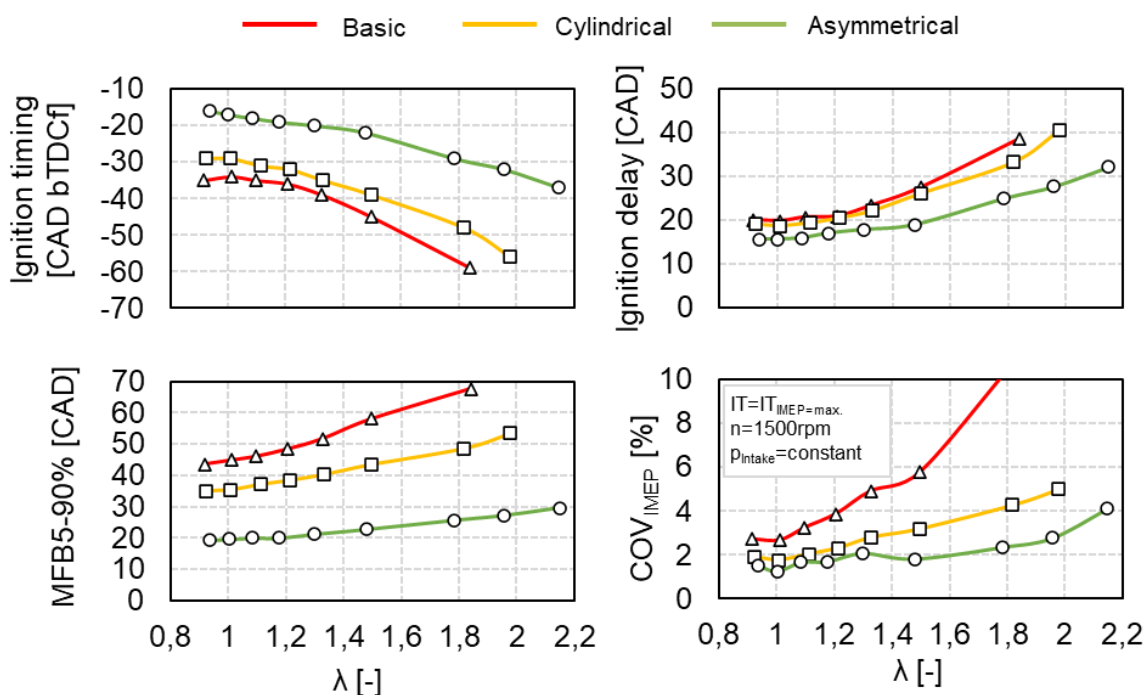

Figure 34: Optimal ignition timing (IT=IT$_{IMEP=max}$), ignition delay, combustion duration, and COV$_{IMEP}$ during lean engine operation with different piston crowns

Figure 35 shows the indicated efficiency and the raw exhaust emissions measured on the single-cylinder research engine during lean operation with the different piston crowns. The indicated efficiency increases as the λ increases and reaches its maximum at different λ for each piston variant. As the fresh charge is more diluted, the η_i decreases due to the negative effect of longer combustion duration and deterioration of combustion stability. However, the intensive charge motion generated by the asymmetrically-shaped piston crown enables rapid and stable combustion of the mixture with excess air and extends the lean limit to λ>1,8. Among the investigated variants, the asymmetrical piston crown achieved the highest η_i at λ=1,5, resulting in an improvement of 2,5 percentage points compared to the basic and 0,7 percentage points compared to the cylindrical piston crown at the same λ.
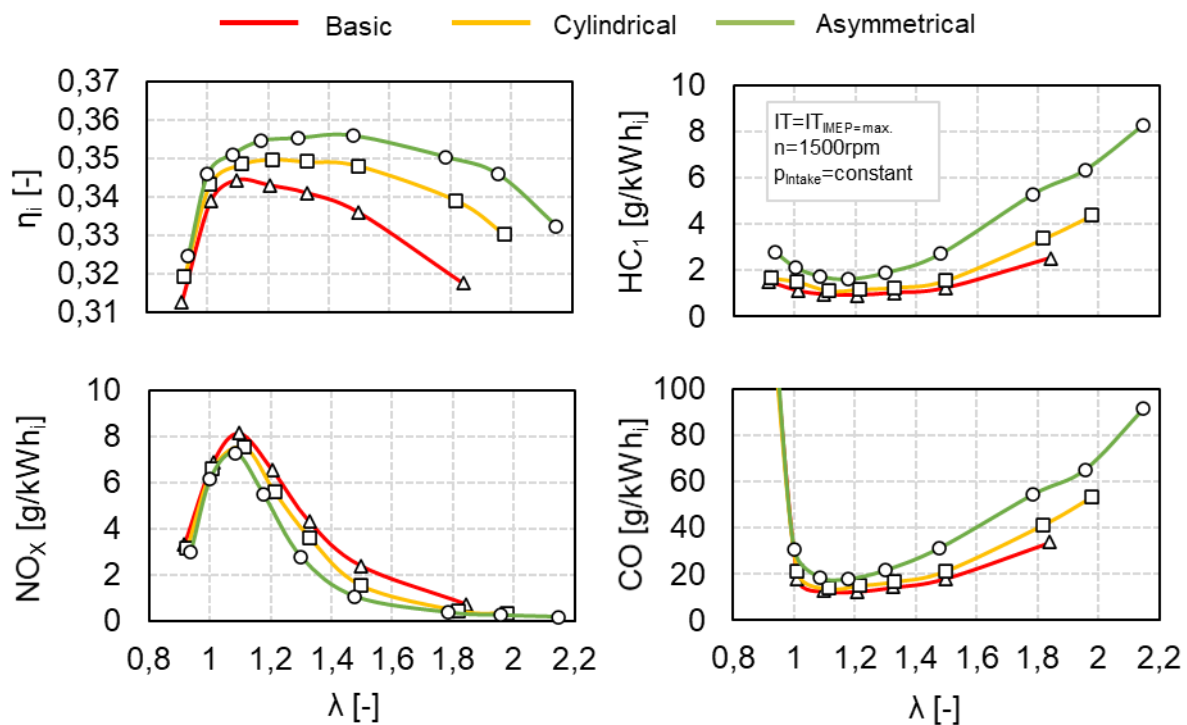

Figure 35: Indicated efficiency and raw exhaust gas emission in lean engine operation with different piston crows

Further, the NO_X emissions reach a maximum at λ~1,1 at each variant due to the highest temperature and sufficient oxygen and nitrogen concentrations in the burned mixture. As the λ increases, the N_2 and O_2 concentrations increase, but the burned gas temperature decrease reducing the NO_X formation. The NO_X emissions are lower during engine operation with asymmetrically-shaped piston crown than with the cylindrical and basic variants in the wide lean operating range due to the abovementioned reasons (see Chapter 6.3.1), and they approach close to zero at λ>1,8. A similar NO_X tendency is observed by a comparison of high-turbulence piston

crowns and flat pistons reported in [49] for lean engine operation on natural gas (λ>1,2) and in [22] for wood gas engine operation (λ>1,5).

The highest CO and hydrocarbon emissions (HC_1) levels are attained with the asymmetrically-shaped piston crown due to the flame quenching within large crevice volume and squish area. Additionally, the CO and HC_1 emissions increase with increasing λ mainly due to the reduced reaction rates at lower temperatures, the increasing importance of flame quenching during the flame contact with the wall, and reduced oxidation at lower temperatures. Since the wood gas contains a petite portion of hydrocarbon components, the HC_1 emissions in the exhaust gas also reach a low level. HC_1 shows a similar trend as CO emissions. However, even in lean engine operation, CO and HC_1 emissions can be effectively reduced through exhaust gas aftertreatment.

A disadvantage of lean operation is a significant decrease in engine power output of 17% at λ=1,5 compared to λ=1,1 with the asymmetrical piston crown (not shown in Figure 35). However, the power derating caused by lean operation can be omitted by boosting the intake pressure.

Comparing the highest efficiency achieved with the asymmetrical piston crown in the operating point at λ=1,5 and the nominal operating point of the basic engine at λ=1,1, an efficiency improvement potential of 1,12 percent points and NO_X reduction of 85% is achieved.

6.3.3   EGR Combustion Process

The effects of the combustion chamber geometry on the combustion process during engine operation with EGR at λ=1 are assessed on the research engine and presented in the following. Figure 36 shows the ignition timing (IT=$IT_{IMEP=max}$), ignition delay, combustion duration (MFB5%-90%), and COV_{IMEP} in engine operation with basic and asymmetrically-shaped piston crowns. With an increasing rate of EGR, the optimal ignition timing is advanced for both variants. Compared to the basic variant, a later optimal ignition timing, and correspondingly shorter ignition delay occur at the asymmetrical piston crown. The combustion duration is significantly reduced and stabilized with the asymmetrical piston crown and increases slightly as the EGR rate increases. COV_{IMEP} reaches a significantly lower level than with the basic geometry. The asymmetrical piston crown extends the limit of stable operation to over 18% EGR rate, whereby the combustion occurs stable and COV_{IMEP} remains around 2%.
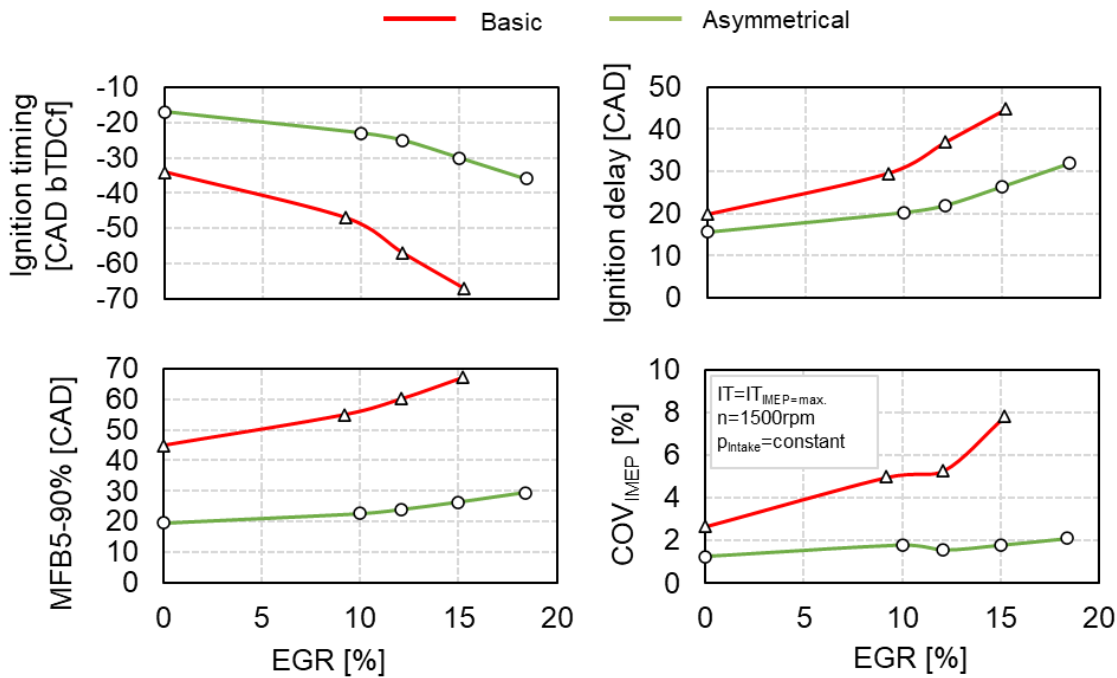
Figure 36: Optimal ignition timing (IT=IT$_{IMEP=max}$), ignition delay, combustion duration, and COV$_{IMEP}$ in engine EGR operation with different piston crowns

As a result of fast and stable combustion, a significantly higher η_i is achieved during the operation with asymmetrical piston crown compared to basic variants – see Figure 37. As the EGR rate increases, the η_i of the engine with asymmetrically-shaped piston crown slightly increases, reaches its maximum at 10% EGR, and further decreases with higher EGR rates. The η_i of the basic piston crown immediately decreases as the rate of EGR increases due to significantly increased combustion duration and deterioration in combustion stability (increasing COV$_{IMEP}$).

Figure 37 also shows the measured raw exhaust emissions during EGR operation with the different piston variants. It can be seen that the NO$_X$ emissions significantly decrease with increasing EGR rates. The diluting of fresh charge by 10% EGR reduces NO$_X$ emissions by more than 66% at both piston crowns. The NO$_X$ formation rates decrease due to decreasing peak temperatures of burned gas with increasing EGR rates. The NO$_X$ emissions are lower when operating with asymmetrically-shaped piston crowns compared to the basic variant due fast combustion closer to the optimal combustion center and thus lower combustion temperatures (see Chapter 6.3.1). Similar NO$_X$ behavior during the engine operation with high-turbulence piston crowns (with squish area) and flat pistons is reported in [49] for EGR engine operation on natural gas, whereby the dilution with up to 30% is achieved.

Further, the CO and HC$_1$ emissions show similar trends and increase significantly as the EGR rate increases above 10% for both variants of piston crowns. This effect occurs mainly due to the increasing importance of flame quenching at lower gas

temperatures, reduced oxidation, and increased cycle-by-cycle variations. The highest CO and HC_1 emission levels are attained with the asymmetrically-shaped piston crown due to the larger crevice volume and flame quenching within the larger squish area, similar to lean engine operation. However, the pollutant emissions can be effectively reduced by a three-way catalytic converter due to the stoichiometric operation.

The engine operation with the asymmetrically-shaped piston crown and 10% EGR rate offers a minor efficiency improvement potential of 0,315 percentage points compared to the nominal operating point with the basic variant at λ=1,1 (see Figure 35). However, a significant reduction of NO_X emissions by 88% is achieved.
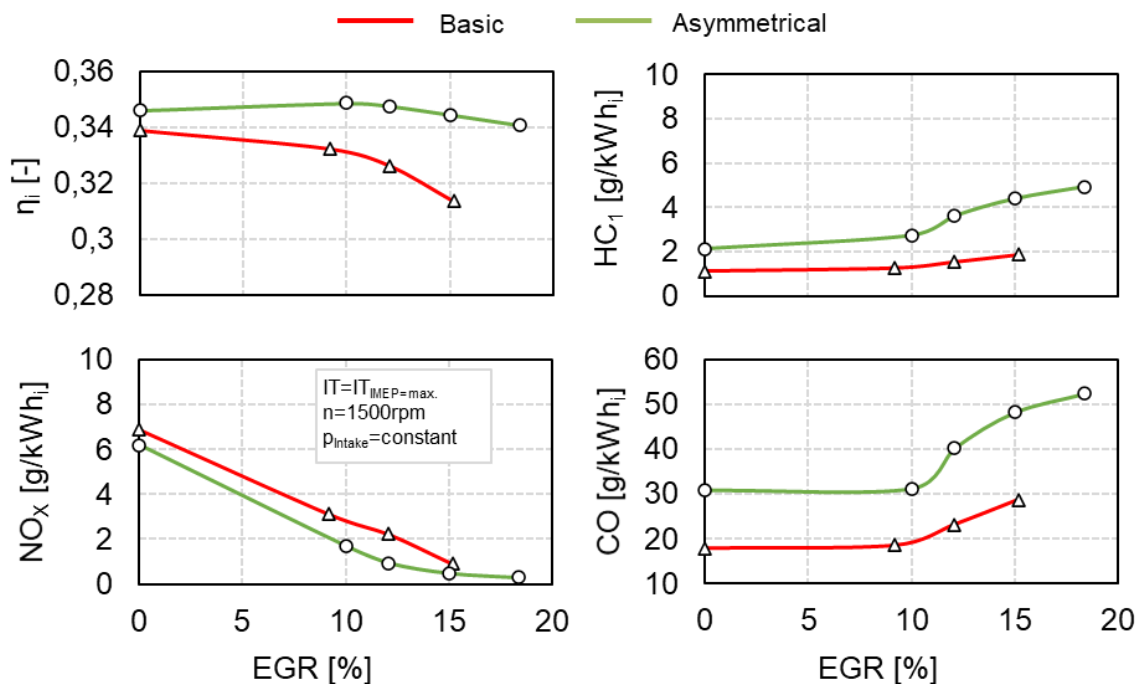

Figure 37: Indicated efficiency and raw NO_X, HC_1, and CO exhaust gas emission in EGR engine operation with different piston crowns

6.3.4   Comparison of Lean and EGR Combustion Concepts

The operating points with gradually increased mixture dilution rates (with EGR at λ=1 and excess air) of the engine with asymmetrically shaped piston crown are analyzed in more detail to highlight the differences between EGR and lean wood gas engine operation. To compare the dilution effects of EGR and excessive air, a total charge mass-based relative air-fuel ratio λ_m is applied according to [100] and defines the dilution rate (see Equation 12):

$$Dilution\ rate = (\lambda_m - 1) \cdot 100\% = \left(\frac{\left(^C/_F\right)_{Actual}}{\left(^A/_F\right)_{Stoichiometric}} - 1\right) \cdot 100\ [\%] \qquad (12)$$

C	total intake mass flow	(kg/h)
A	air mass flow	(kg/h)
F	fuel mass flow	(kg/h)
EGR	EGR mass flows	(kg/h)
λ_m	reactant and fuel ratio irrespective of the diluent type (-)	

The total intake mass flow comprises air and EGR mass flows: $C = (A + EGR)$, (kg/h). λ_m gives the reactant and fuel ratio irrespective of the diluent type. When only air dilutes the fresh charge, then is $\lambda = \lambda_m$ valid. The effects of increasing the mixture dilutions with excess air and EGR (at λ=1,0) on efficiency, combustion stability, and exhaust gas emissions of a naturally aspirated wood gas engine with an asymmetrical piston crown are depicted in Figure 38.
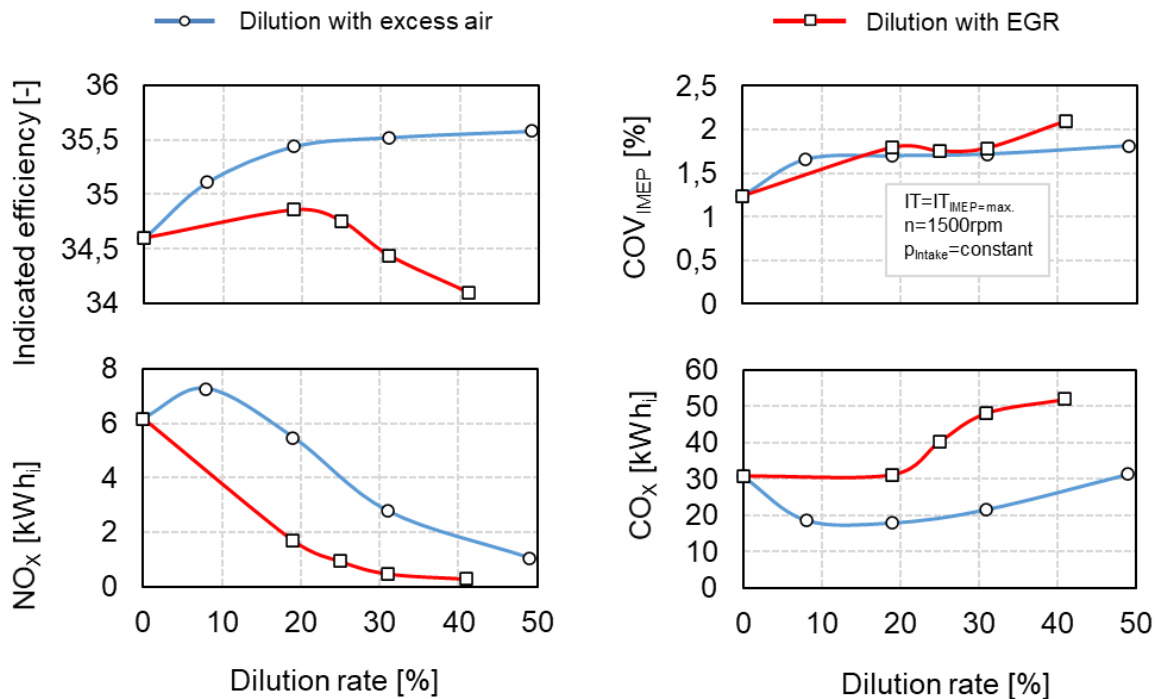

Figure 38: Effects of fresh mixture dilution with excess air and EGR at λ=1 on indicated efficiency, combustion stability, and exhaust gas emissions of the naturally aspirated wood gas engine at constant p_{intake} and 1500rpm

Lean engine operation gives significantly higher efficiency benefits, lower CO, and higher NO_X emissions at the same combustion stability level (COV_{IMEP}) compared to EGR operation. Increasing the EGR rate decreases the NO_X emissions significantly faster than dilution with excess air. However, CO emissions (and HC_1 not shown in the diagram due to relatively low content) increase more rapidly as the mixture is diluted with EGR. A comparison of operating points with the same dilution rates of EGR and

excessive air is presented in the following. <u>Table 7</u> gives the operating parameters and measured flows.

Table 7: Operating parameters and measured flow rates during EGR and lean engine operation with asymmetrical piston crown at 1500rpm

Parameter	Operating point	p_{Intake}	Wood gas flow	Air flow (wet)	EGR flow	$(A/F)_{stoich.}$	λ	EGR Rate	Dilution rate
Dilution with air	OP 4	879 mbar$_a$	10,31 kg/h	19,72 kg/h	-	1,61 kg$_A$/kg$_F$	1,19	0 %	19 %
Dilution with EGR	OP 6	875 mbar$_a$	10,23 kg/h	16,76 kg/h	2,98 kg/h	1,62 kg$_A$/kg$_F$	1,01	10 %	19 %

<u>Figure 39</u> compares in-cylinder composition, heat capacity ratios, burned mixture temperature, and heat flux during the lean and EGR operating points (19% dilution rate) determined by the thermodynamical analysis. During the operation with EGR, CO_2 and H_2O fractions of the mixture are higher than in lean operation, resulting in lower combustion temperatures due to a higher charge heat capacity. The higher amount of tri-atomic molecules minorly affects the temperature-dependent heat capacity ratio and, thus, the efficiency. Due to higher burned mixture temperatures during lean operation, a higher heat transfer to the walls occurs.
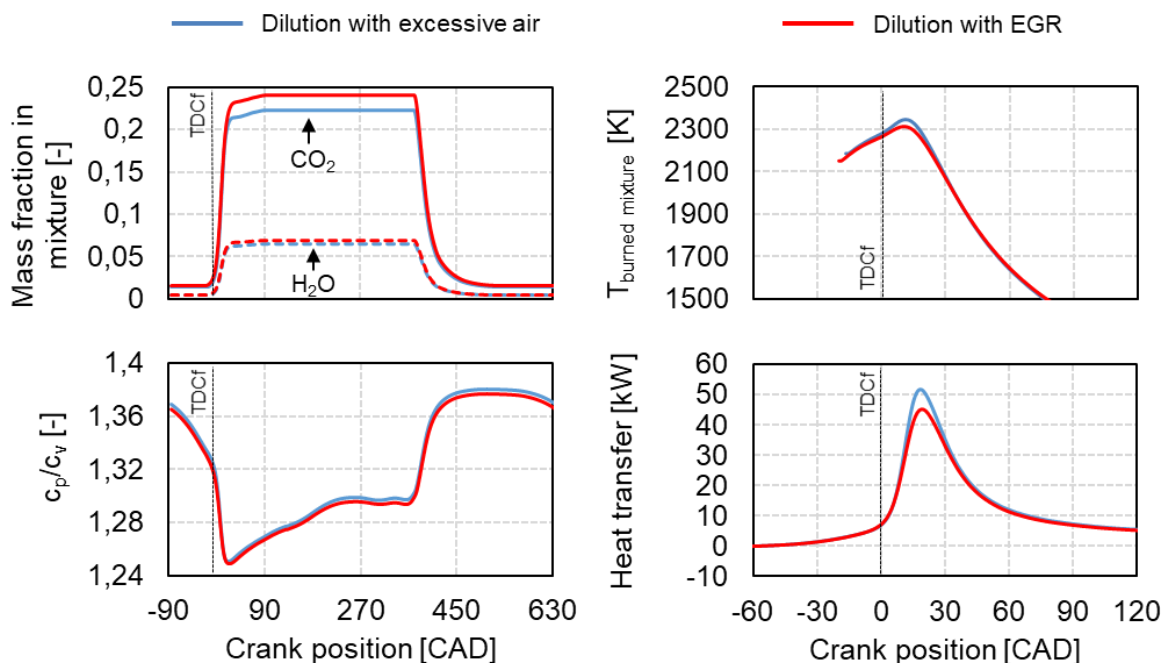

Figure 39: Results of thermodynamical efficiency analysis – comparison of dilution effects with excess air and EGR: CO_2 and H_2O mass fractions, burned mixture temperature, heat capacity ratio (c_p/c_v) and heat flux from gas to the wall at 19% dilution rate, constant $p_{intake,}$ and 1500rpm

The results of the efficiency loss analysis are shown in <u>Figure 40</u>. During the engine operation on wood gas, the mixture dilution with excess air results in a higher indicated efficiency compared to the mixture dilution with EGR at the same dilution rate due to the higher importance of efficiency losses visualized in the bar chart. Higher unburned CO and HC_1 emissions during operation with EGR adversely affect the indicated efficiency. The increasing importance of flame quenching at the combustion chamber walls and reduced reaction rates (due to lower in-cylinder mixture temperature) result in higher combustion efficiency loss (unburned fuel – see Figure 40). The combustion duration is short in both cases, resulting in low efficiency losses related to the real combustion process. Slightly slower combustion duration and, thus, higher losses due to real combustion during operation with EGR are related to a lower temperature-dependent laminar flame speed. However, lower mixture temperature during EGR operation results in a lower wall heat transfer (see Figure 39) and slightly lower efficiency loss compared to lean operation (Figure 40). A slightly lower efficiency loss related to the thermodynamic fluid properties and charge composition is achieved during lean operation. The gas exchange losses are similar in both cases and negatively affect the indicated efficiency.

Overall, the lean mixture exhibits favorable thermodynamic properties during compression and expansion strokes, improving efficiency more than EGR operation. Although a noticeable efficiency improvement during EGR operation on natural gas is reported in [48], the adverse effects of higher CO_2 and H_2O fractions in fresh charge outweigh the positive effects of EGR during operation on wood gas. Similar adverse effects of diluting the fresh mixture with high CO_2 fraction on the engine efficiency (propane operation) are reported in [101].
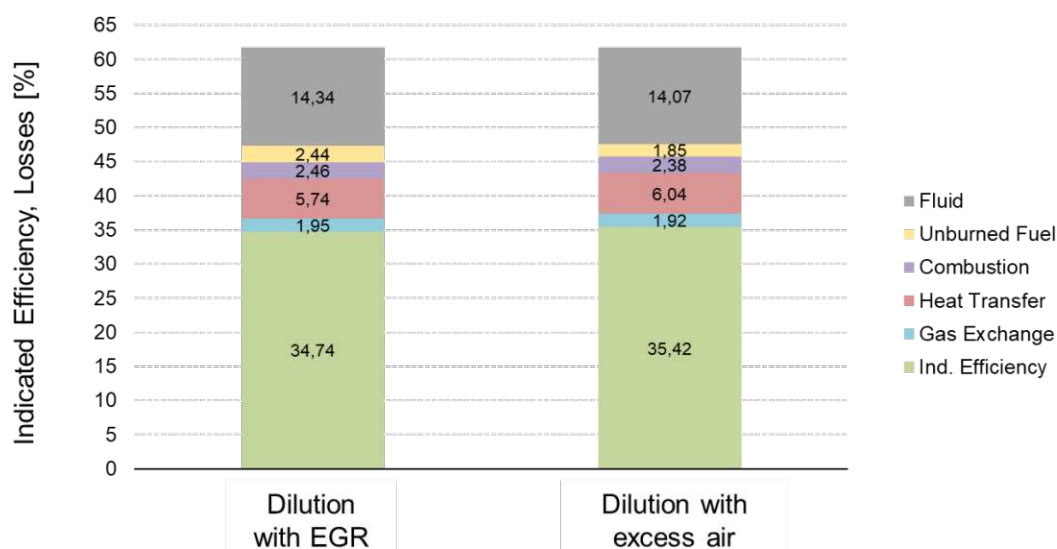

Figure 40: Results of thermodynamical efficiency analysis – comparison of dilution effects with excess air and EGR: indicated efficiency and efficiency losses at 19% dilution rate, constant p_{intake}, and 1500rpm with the asymmetrical piston crown

6.4 Chapter Summary

The intensive in-cylinder charge motion generated by the asymmetrically-shaped piston crown enables rapid and stable combustion of the diluted mixture, essential for efficient wood gas engine operation. The lean limit is extended to $\lambda>1,8$, and the EGR limit to 18% by applying the asymmetrical piston crown. The highest efficiency is achieved with the asymmetrical piston crown in the operating point at $\lambda=1,5$ resulting in an efficiency improvement of 1,12 percent points and NO_X reduction of 85% compared to the basic piston crown at nominal OP ($\lambda=1,1$). On the other hand, the EGR engine operation results in lower NO_X emissions compared to lean operation.

7 Compression Ratio Increase and Spark-Assisted Compression Ignition

A possible approach to increase the SI engine efficiency is raising the compression ratio ε. The increase of compression ratio is limited by the engine knocking and uncontrolled autoignition, which also depend on the fuel properties and engine operating conditions. However, controlled autoignition combustion concepts such as SACI represent a promising approach for boosting the efficiency of SI engines. The investigations presented in this chapter aim to determine the potential for efficiency improvement and emission reduction through the increase of compression ratio for the SI combustion concept and by applying the SACI combustion on the wood gas engine.

<u>Figure 41</u> schematically depicts the altering of piston crown depth (left) and the surface-to-volume ratio at TDC (right) as the compression ratio changes. The compression ratio of the asymmetrically-shaped piston crown is adjusted by increasing the piston crown´s depth. Thus, the shape and position of the piston crown (also the quench area), and the distance between the top edge of the piston and the cylinder head at the TDC remain unchanged. The crevices volume also prevails constantly. The surface-to-volume ratio at TDC intensively increases with increasing the compression ratio due to a significant decrease in volume and a slight decrease in surface area.

The lean engine operation at a constant speed, intake temperature, pressure (naturally aspirated operating mode), and wood gas composition is investigated. The ignition timing (spark timing) is set for the highest IMEP in every operating point (IT=IT$_{IMEP=max}$).
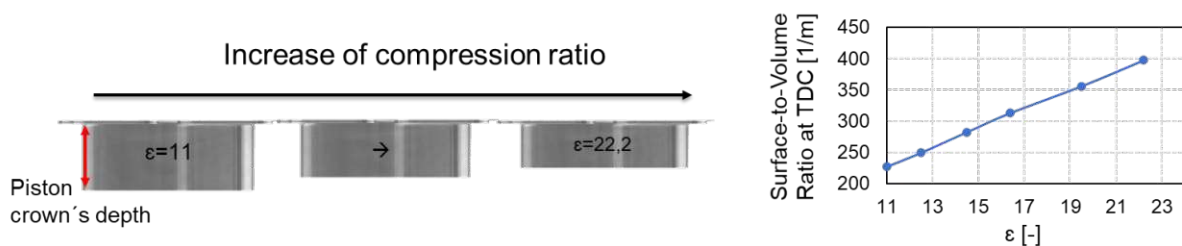

Figure 41: Increase of ε by adjusting the depth of the asymmetrically-shaped piston crown (left) and the surface-to-volume ratio at TDC (right)

7.1 Spark-Assisted Compression Ignition on Wood Gas Engine

For investigating its effects on the combustion process, the geometric compression ratio is gradually increased from ε=11 to ε=22,2. <u>Figure 42</u> shows the cylinder pressure curves of the single cycle at different compression ratios (at λ=1,5). The peak cylinder pressure increases with the gradual increment of ε. As ε increases from 19,5 to 22,2, a wrinkle with a high pressure gradient characteristic for autoignition appears on the

pressure curve (black line). The intensive pressure gain starts above the cylinder pressure of 65 bar, implying a critical autoignition threshold at the operating point under given in-cylinder conditions (temperature, pressure, and charge composition).
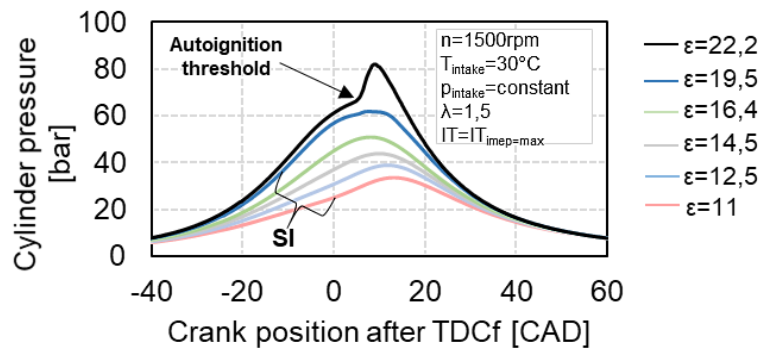

Figure 42: The cylinder pressure of the single cycle at different compression ratios (engine operation at λ=1,5, and constant intake pressure)

Figure 43 shows the determined AHRR and second derivative of AHRR (d²AHRR/dCAD²) for a single cycle at ε=19,5 and ε=22,2 – the difference between the heat release rate is significant.
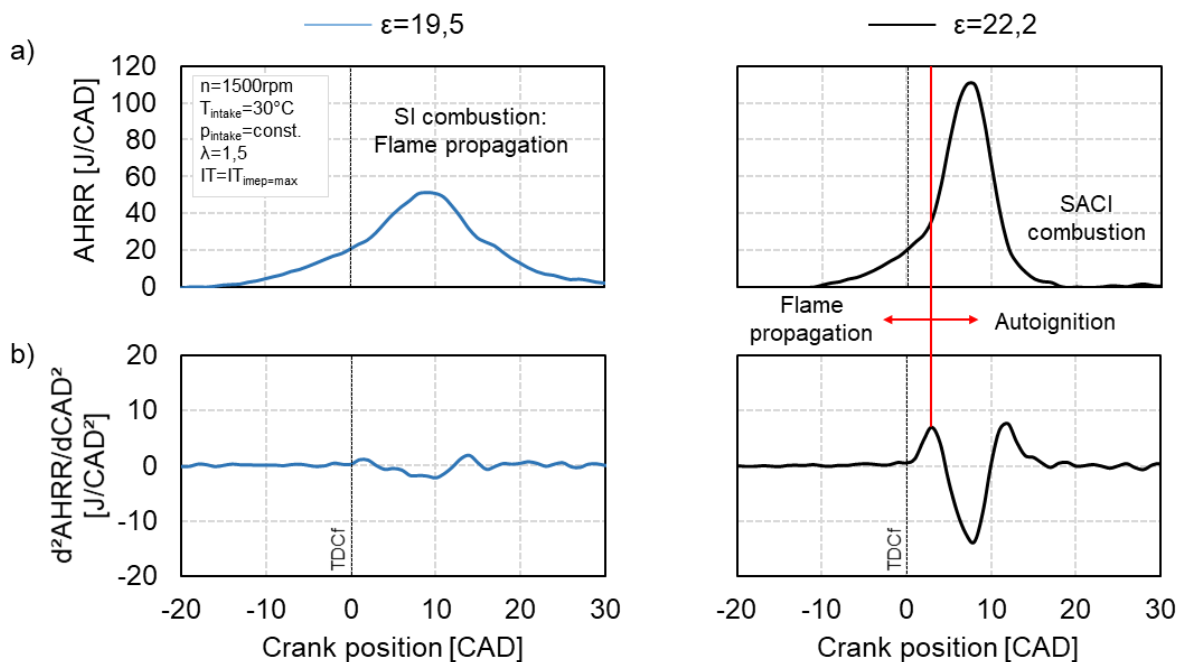

Figure 43: Single cycle results: AHRR a), and second derivative of AHRR, which indicates the shift from flame propagation to the autoignition phase of SACI combustion b) at λ=1,5 and 1500rpm

At ε=22,2, an initial region of slow heat release rate, where flame propagation occurs (SI), is followed by a rapid heat release rate characteristic for bulk autoignition. This combined combustion consisting of flame propagation and autoignition represents

SACI. The autoignition can only be achieved with spark assistance since the maximal motored pressure of 55 bar (not given in the figure) is below the autoignition threshold at 65 bar under given conditions at ε=22,2. According to [88], the transition from the SI combustion mode to the faster autoignition is also determined using the second derivative of the AHRR. The brink in Figure 43 (bottom right) implies the highest altering in the combustion speed and, therefore, the shift from flame propagation (characteristic for SI) to autoignition (characteristic for HCCI). This result shows that SACI is achieved in the present wood gas engine by sufficiently increasing the compression ratio. No irregular combustion phenomena (knocking, glow ignition) occur under investigated operating conditions.

Engine operating parameters such as ignition timing, air-fuel ratio, or intake temperature influence the combustion and affect the transition from SI to SACI or vice versa. Figure 44 shows the cylinder pressure and AHRR at different λ for a single cycle. As the λ increases, a lower peak cylinder pressure is achieved, and the heat release rate is reduced. At λ=1,8, the transition from autoignition to flame propagation occurs, whereby the SACI is not achieved in every cycle under investigated operating conditions. The blue line in Figure 44 stays for a single cycle at λ=1,8 without SACI, whereby flame propagation occurs. The optimal ignition timing (i.e., spark timing, $IT=IT_{IMEP=max}$) approaches the TDC as the λ sinks, and the autoignition threshold occurs on lower pressure. This trend shows the importance of local in-cylinder temperature and composition for autoignition initiation.
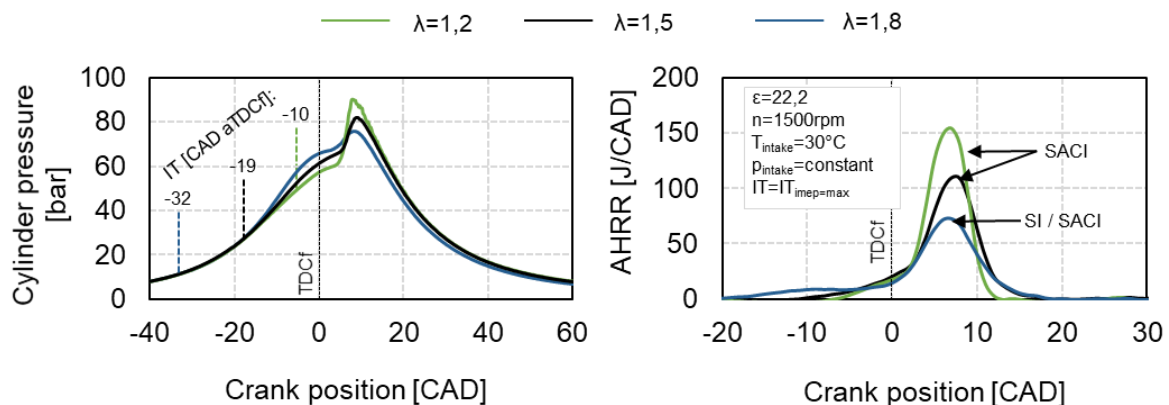

Figure 44: Effect of air-fuel ratio on combustion mode: single cycle in-cylinder pressure (left) and AHRR (right) at ε=22,2 and T_{intake}=30°C

Adjusting the intake temperature is another possible approach for achieving SACI on wood gas engines. SACI is realized by increasing the intake temperature to 150°C at ε=11 and λ=1,1. Figure 45 shows the effect of ignition timing (i.e., spark timing) on combustion mode. It can be seen that a rapid heat release occurs at significantly lower peak pressure than with ε=22,2 and T_{intake}=30°C implying the high importance of the intake temperature on the autoignition process. As the ignition timing approaches the

TDC, the peak cylinder pressure decreases, and the heat release rate is reduced. At a late ignition timing (-9 CAD after TDCf), the autoignition conditions are not achieved, resulting in a SI flame propagation mode. At advanced IT (-19 CAD aTDCf), engine knocking can occur. Thus, the optimal IT (spark timing) is essential to ensure the best conditions and timing for bulk autoignition. However, this approach for achieving SACI by increasing the intake temperature is further not discussed in more detail since the increment of intake temperature adversely affects the temperature-dependent thermodynamic fluid properties and related losses resulting in a low indicated efficiency, despite the rapid combustion.
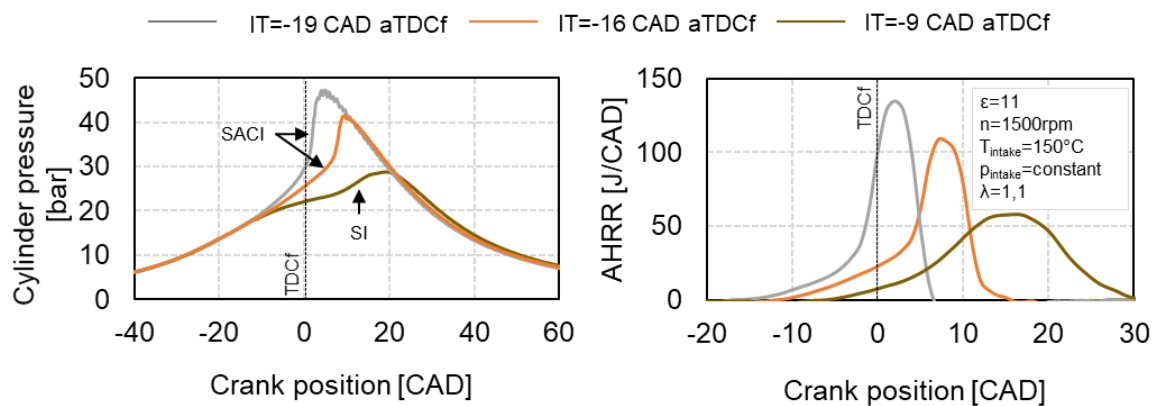

Figure 45: Effect of ignition timing (IT, i.e., spark timing) on combustion mode: in-cylinder pressure (left) and AHRR (right) at $\varepsilon=11$ and intake temperature of 150°C (optimal IT=IT$_{IMEP=max}$ is at -16CAD aTDCf)

These results demonstrate two possible approaches for achieving SACI on the wood gas engine: increasing the SI engine's compression ratio and intake temperature. In the following, the combustion process is analyzed in more detail to evaluate the potential for efficiency improvement and emissions reduction by increasing the compression ratio.

7.2 Effects of Compression Ratio on Combustion Process

This chapter presents the results of the experimental investigations and efficiency analysis assessing the effects of compression ratio on wood gas engine efficiency. Table 8 lists the operating parameters of the investigated operating points.

Table 8: Engine operating parameters at investigated compression ratios with asymmetrical piston crown at 1500rpm

Parameter	ε=11 (OP 5)	ε=12,5 (OP 7)	ε=14,5 (OP 8)	ε=16,4 (OP 9)	ε=19,5 (OP 10)	ε=22,2 (OP 11)
p_{Intake} [mbar$_a$]	876	880	881	883	880	887
λ [-]	1,48	1,48	1,49	1,47	1,52	1,5
LHV$_{Mixture}$ [kJ/kg]	1,67	1,67	1,66	1,67	1,64	1,65
Combustion mode	SI	SI	SI	SI	SI	SACI

Figure 46 shows that the efficiency increases with rising ε up to ε=14,5 at a decreasing rate by more than 1,1 percent points. A further compression ratio increment to ε=19,5 offers no benefits, while an efficiency breakthrough by more than 1 percent point is achieved at ε=22,2 due to the transition from SI to SACI combustion resulting in a total efficiency improvement of more than two percentage points. The relationship between IMEP and compression ratio follows the trends of the indicated efficiency and ε – since a higher amount of heat is converted to the work, the IMEP increases with increasing compression ratio.
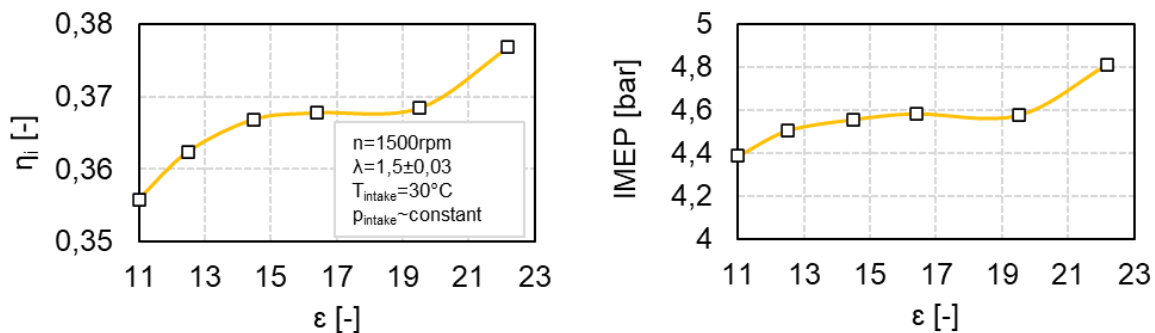

Figure 46: Indicated efficiency η$_i$ and IMEP as a function of compression ratio

Figure 47 gives an efficiency analysis and quantifies the individual losses of the investigated operating points. The theoretical achievable efficiency of the ideal cycle defined in equation 11 (which is calculated under assumption of constant γ=1,4, and represents the sum of indicated efficiency and losses) significantly increases with increasing ε. However, the indicated efficiency increases less intensively due to related efficiency losses.
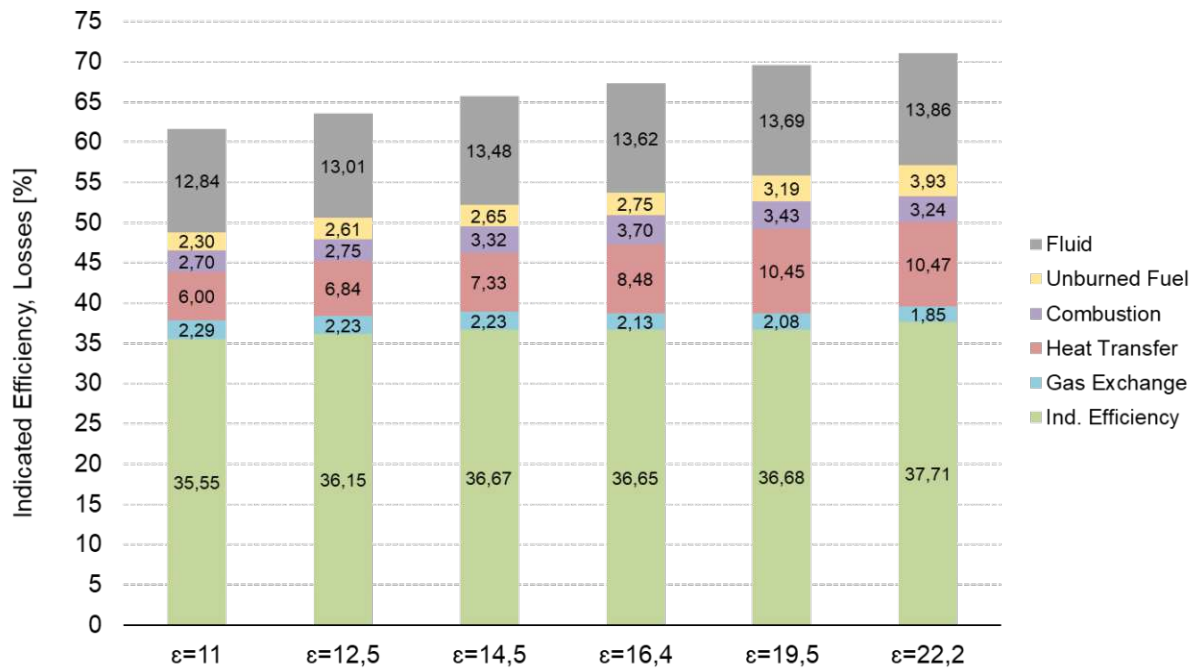
Figure 47: Results of thermodynamical efficiency analysis – effects of compression ratio on indicated engine efficiency and efficiency losses under constant operating conditions (T_{intake}=30°C, p_{intake}=875mbar$_a$, λ=1,5, 1500rpm with asymmetrical piston crown)

The highest thermodynamic efficiency loss occurs due to fluid properties. Figure 48 presents the in-cylinder temperature of burned and unburned zones and the heat capacity ratios of the mixture for ε=11 and ε=22,2 determined by the thermodynamic analysis. As the compression ratio increases, higher in-cylinder temperatures occur during the compression and a part of the expansion stroke (during combustion). Higher temperatures result in a lower temperature- and composition-dependent heat capacity ratio γ. The heat capacity ratio is also affected by the gas composition and is lower compared to the air. Consequently, the related efficiency loss slightly increases with the increased ε, as depicted in the bar chart (grey, "Fluid"). Additionally, the residual gas fraction of the trapped in-cylinder mass decreases with increasing ε from 6,7% at ε=11 to 4,2% at ε=22,2 due to slightly reduced volumetric efficiency. A gradually decreasing residual gas fraction in the fresh charge also contributes to a less intensive increase of efficiency losses caused by the fluid properties with increasing ε.
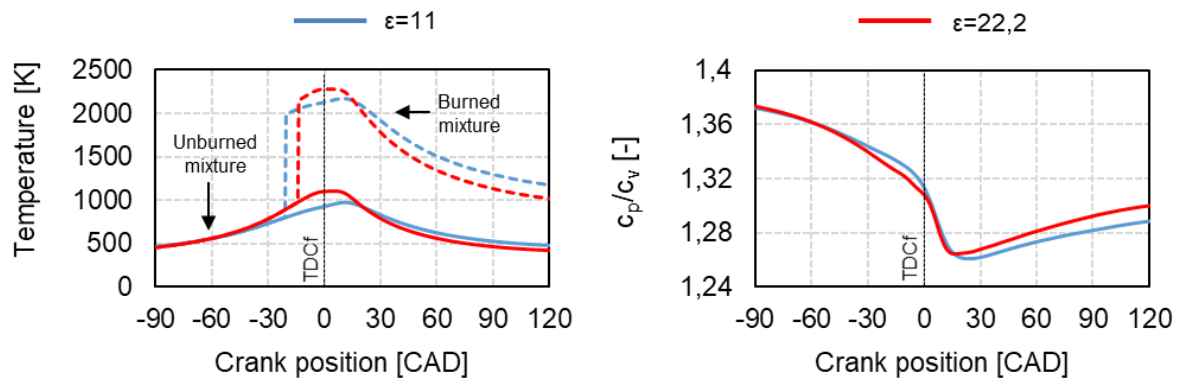
Figure 48: Results of thermodynamical efficiency analysis – charge temperature (burned and unburned zone) and heat capacity ratios (c_p/c_v) over the crank position at ε=11 and ε=22, constant p_{intake}, and 1500rpm

The in-cylinder peak temperatures also affect the NO_X formation significantly. Figure 49 shows the measured raw NO_X and CO emissions as a function of ε. The increasing trend of raw NO_X emissions occurs due to increasing peak combustion temperatures at higher ε, encouraging thermal NO_X formation (see Figure 48). As ε gradually increases from 11 to 22,2, the NO_X emissions increase more than five times at ε=22,2 under the investigated operating conditions. The CO emissions mainly originate from incomplete combustion and increase slightly with the compression ratio. Due to increasing cylinder pressure, a higher mass fraction of fresh charge is captured within the crevices volume and remains unburned as the ε increases. The THC emissions are significantly lower than CO emissions and show a similar trend (not depicted in the figure). Thus, the CO and THC emissions increase with increasing ε due to the higher importance of crevice volume and flame quenching within the squish area, causing efficiency loss due to incomplete combustion. It increases with an increased compression ratio, as depicted in the bar chart (Figure 47).
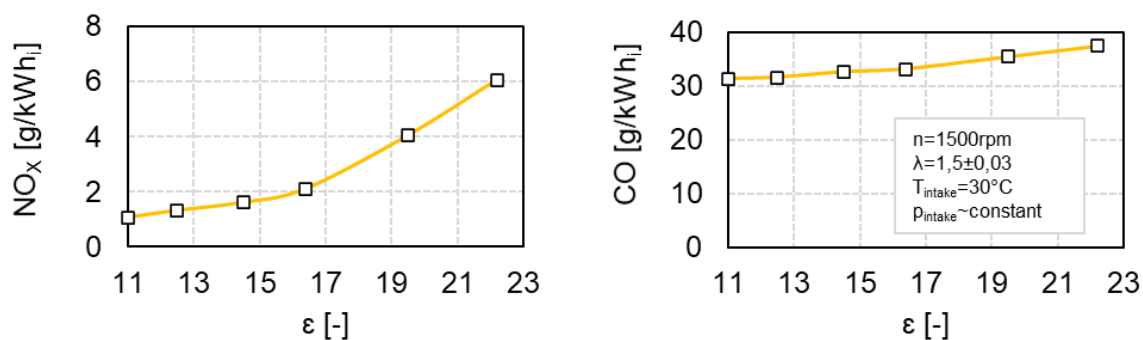

Figure 49: Raw NO_X and CO emissions as a function of compression ratio measured on the test bench

The ignition delay, combustion duration (MFB5-90%), COV_{IMEP} (as a measure of combustion stability), and exhaust temperature as a function of compression ratio are depicted in Figure 50. The ignition delay decreases since the optimal ignition timing

slightly approaches the TDC with an increased compression ratio. This effect can be explained by the increased laminar flame velocity at higher temperatures, which enhances early flame development. The cycle-to-cycle variations increase slightly with increasing compression ratio, indicating a slight deterioration in combustion stability. The exhaust gas temperature decreases as the heat converted to the work increases with increasing ε.
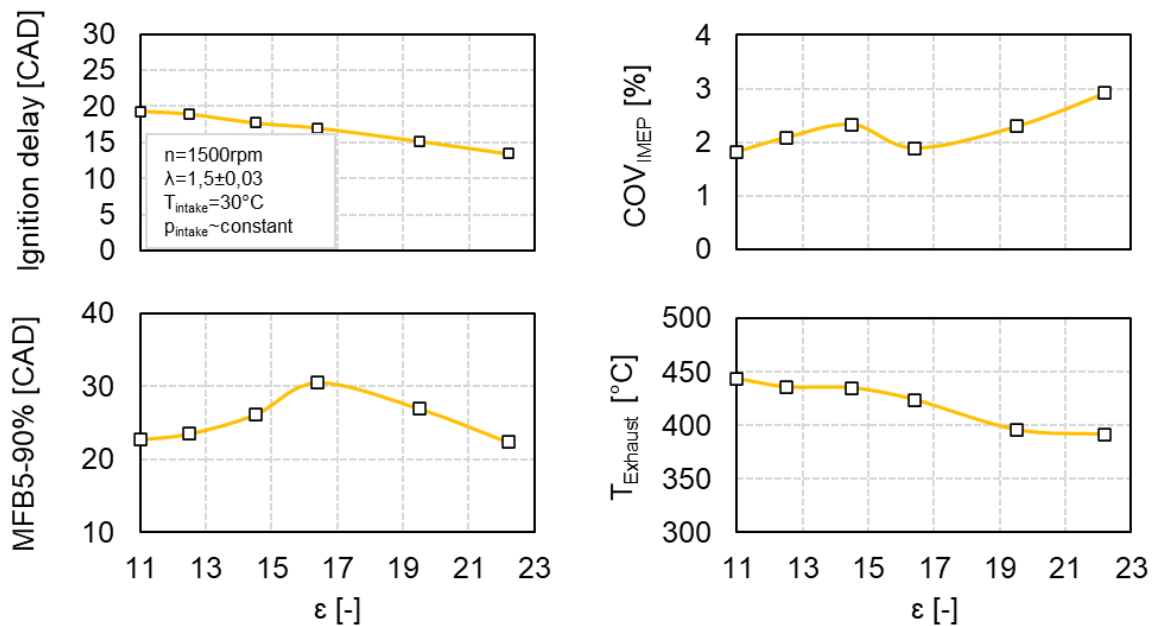

Figure 50: Ignition delay, combustion duration (MFB5-90%), COV$_{IMEP}$, and exhaust gas temperature as a function of compression ratio

The combustion duration increases with increasing ε, reaches a maximum at ε=16,4, and starts decreasing at ε=19,5 with the same intensity. The effects of piston chamber geometry alterations and related in-cylinder charge distribution on flame propagation can explain the increasing trend of combustion duration. Since only the volume of the piston crown is reduced (due to the reduced depth of the piston crown), and the squish area and crevice volume remain unchanged as the ε increases, the mass fraction of the charge captured within the volume of the crevices and squish area increases. Thus, the propagating flame rapidly captures a lower mass fraction within the piston crown as the ε increases. Within the narrow squish area, the flame propagates aggravated due to adverse effects, such as the higher importance of flame quenching, resulting in a longer combustion duration. Correspondingly, the fraction of the mixture burned in the top dead center region decreases with the increasing ε. This increasing tendency toward nonconstant volume combustion with increasing ε adversely affects the indicated efficiency improvement. Also, the importance of the chemical dissociation of combustion products increases with charge temperature increment caused by

increased ε. The dissociation and the subsequent recombination of the molecules adversely affect the combustion duration.

However, as the ε increases from 19,5 to 22,2, the occurring bulk autoignition initiated by flame propagation ensures a rapid heat release shifting the combustion closer toward the constant volume, as in the ideal cycle. Consequently, the efficiency loss due to combustion duration sinks as the SI combustion shifts to SACI, reducing the importance of the aggravated flame propagation (see Figure 47).

The heat transfer to the wall at ε=11 and ε=22,2 is presented in Figure 51. It increases significantly with increasing ε during the compression and expansion strokes while combustion occurs due to higher charge temperatures (see Figure 48), resulting in an increased efficiency loss. The combustion chamber surface and surface-to-volume ratio also significantly affect the wall heat loss. With increasing ε, the surface-to-volume ratio of the combustion chamber increases significantly, increasing the heat transfer (see Figure 41). However, as the transition from SI to SACI occurs, the reduced combustion duration hinders the increment of heat losses, although the ε increases. Also, the reduced intensity of the in-cylinder charge motion with increasing ε contributes to less increasing heat transfer losses, according to [58].
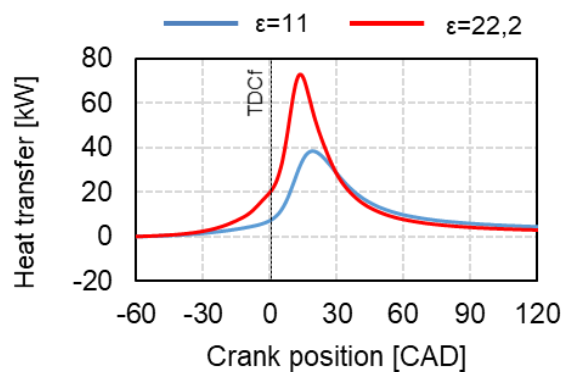

Figure 51: Results of thermodynamical efficiency analysis – heat transfer from gas to the wall at ε=11 and ε=22,2; constant $p_{intake,}$ and 1500rpm

The gas exchange efficiency losses slightly decrease with increasing ε, positively affecting the indicated efficiency improvement (see Figure 47). This effect can be explained by the slightly lower cylinder pressure during the expansion stroke at a higher ε – see Figure 52. Thus, the negative pumping work (from the piston to gas) during the exhaust stroke decreases as the ε increases, resulting in lower gas exchange efficiency loss. Since the valve timing remains unchanged, the cylinder pressure increases more intensively as the piston approaches TDC (gas exchange) at a higher ε, reducing the benefit in efficiency.
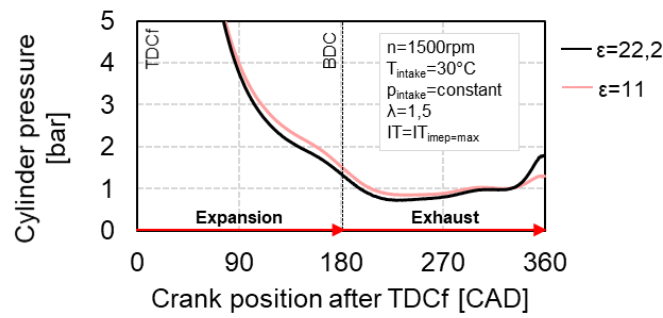
Figure 52: Cylinder pressure during expansion and exhaust stroke at ε=11 and ε=22,2

The effects of the ε on the combustion process are assessed over the wide lean operating range in the following. The combustion duration (MFB5-90%), COV_{IMEP}, indicated efficiency and raw NO_X emissions in lean engine operation at different ε are depicted in Figure 53. The combustion duration and COV_{IMEP} increase with increasing λ at each ε due to related effects on combustion, such as a slower kinetic reaction behavior and flame quenching (see Chapter 3.2.1). The increasing importance of flame quenching also gains COV_{IMEP}, as ε increases. The combustion duration increases as ε increases at SI combustion mode (up to ε=19,5) and decreases at ε=22,2 due to SACI in the investigated lean operation, as described above. As λ increases, the indicated efficiency reaches a maximum and decreases with further increasing λ at each ε. The rate of η-decrease is more intensive at higher ε. The increasing ε results in significant efficiency improvement during the lean operation at λ<1,8. For λ>1,8, the adverse effects, such as deterioration in combustion stability, overcome the benefits of higher ε, resulting in low efficiency. However, the highest efficiency is achieved at ε=22,2 due to the SACI combustion mode for λ<1,8. The achieved autoignition at ε=22,2 overcomes the limitations of conventional flame propagation and increases efficiency compared to ε=19,5 during the wide lean operating range. NO_X emissions increase with increasing ε due to the increased peak combustion temperatures. They achieve a maximum around λ=1,1 and approach zero as the λ increases at each ε. In the presented operating points, no irregular combustion phenomena occur.
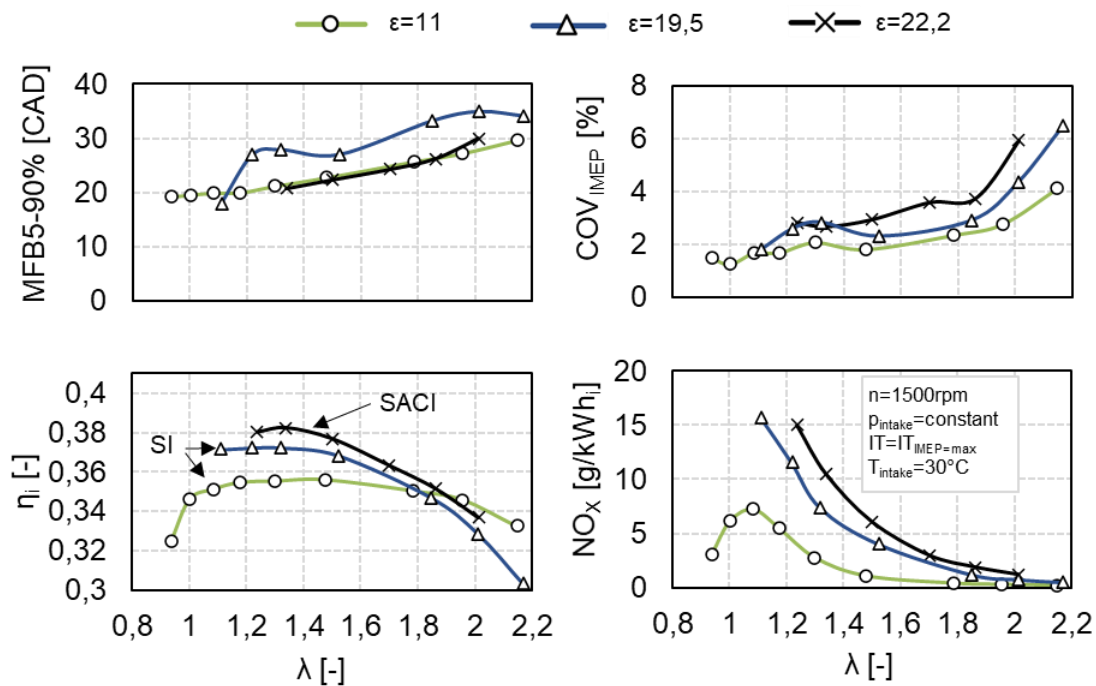
Figure 53: Combustion duration (MFB5-90%), COV_{IMEP}, indicated efficiency η_i, and raw NO_X emissions in SI and SACI combustion modes at different ε

The efficiency analysis showed that intensive heat transfer and incomplete combustion are the main factors limiting the efficiency improvement at high ε. They can be diminished through a targeted improvement of the combustion chamber shape by adjusting the surface-to-volume ratio and squish area. Regarding the SACI combustion mode, the effects of the ignition timing, intake temperature, fresh charge composition, and combustion chamber geometry (e.g., shape for targeted turbulence intensity or unscavenged pre-chamber) represent the relevant parameters for engine optimization. A dedicated engine layout for SACI meeting an optimum of the above-listed parameters is a prerequisite for achieving further efficiency improvement at related operating conditions in biomass power plants.

7.3 Chapter Summary

To sum up, the presented results demonstrate a potential for improving the efficiency of the wood gas engine during lean operation by increasing ε. The increment of ε from 11 up to 16,4 improves the indicated efficiency of the SI wood gas engine by 1,13 percentage points. The transition from SI to SACI is demonstrated by increasing the ε from 19,5 to 22,2. The SACI overcomes the efficiency losses related to the limitations of SI combustion, which are reflected mainly in a relatively slow flame propagation compared to bulk autoignition and heat transfer losses due to a longer combustion duration. Thus, an efficiency breakthrough of the wood gas engine at investigated operating conditions of additional 1,03 percentage points is achieved by applying the SACI.

8 Intake Pressure Boosting and Combustion Control

This chapter investigates the potential of technologies for intake pressure boosting and combustion control for efficiency improvement and emission reduction of the wood gas engine. The results are determined experimentally on the test engine by reproducing the operating conditions and behavior of the related technology. The potential for efficiency improvement and emission reduction is independently identified for each optimization measure.

8.1   Intake Pressure Boosting

Since the aspiration of the wood gas through the biomass power plant's gasification and gas purification systems is driven by the engine, it operates at an intake pressure below atmospheric (~875 $bar_{absolute}$). The engine operation at different intake pressure levels (simulation of boost operation) is examined on the single-cylinder research engine with an electrically driven supercharger to evaluate the effects of the engine intake pressure on efficiency and exhaust gas emissions. In addition, the engine operation at constant load (IMEP – λ sweep) is investigated to evaluate the engine performance over the wide lean engine operating range. As the intake pressure is increased slightly above the atmospheric pressure level, the exhaust pressure is set to the same level to reproduce the operating conditions of a turbocharging system. The ignition timing (IT) is adjusted to meet the optimal center of combustion for a given engine operating parameters (IT=$IT_{IMEP=max.}$). The work done by the compressor is not considered in these analyses.

8.1.1   Effects of Intake Pressure Boosting on Wood Gas Engine

The engine is operated at different pressure levels, λ=1,5, and constant speed (1500 rpm). The relative air-fuel ratio λ is regulated by adjusting the wood gas flow at the defined intake pressure. The measurements occurred at different compression ratios.

<u>Figure 54</u> depicts IMEP, indicated efficiency, ignition delay, and combustion duration at different pressure levels and compression ratios. The IMEP (i.e., engine load) increases linearly with the intake pressure, i.e., proportionally to the supplied fuel energy. At the constant intake pressure (i.e., the same amount of supplied fresh mixture), a higher IMEP is achieved at higher ε due to higher indicated efficiency. The ignition delay and combustion duration remain constant as the intake pressure increases.

The indicated efficiency increases sharply as the intake pressure increases from 0,87 to 1,1 bar_{abs} for both compression ratios. Intake pressure boosting minimizes the gas exchange work (negative pumping work) and the related gas exchange losses as the

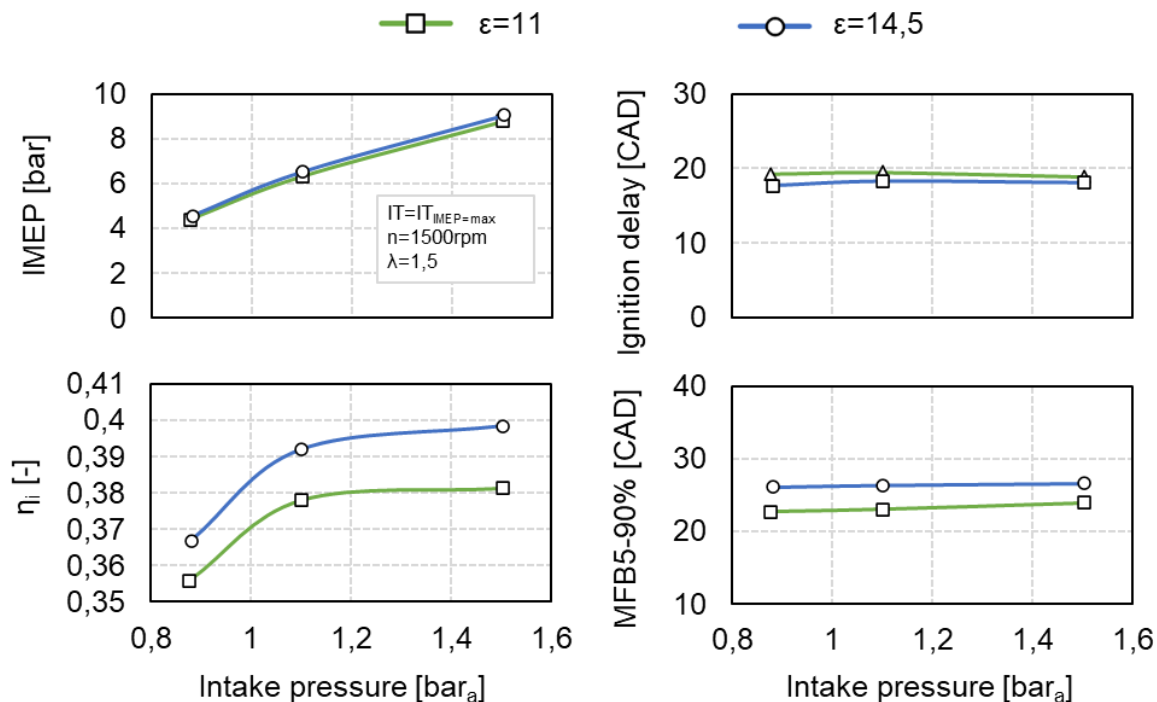intake pressure increases until the level of the exhaust pressure (slightly above the atmospheric pressure).

Figure 54: IMEP (i.e., load), ignition delay, combustion duration (MFB5%-90%), and indicated efficiency during lean engine operation at different pressure levels and ε

As the intake pressure is increased from 1,1 up to 1,5 bar$_{abs}$, the efficiency further increases due to decreasing wall heat losses at higher engine loads (however, absolute heat transfer increases). The losses due to wall heat transfer tend to decrease with increasing load (higher heat release) as the wall area of the combustion chamber remains unchanged at a particular engine. Although the absolute wall heat transfer tends to increase with increasing load (i.e., higher heat release), the pressure-dependent heat transfer coefficient increases less intensively, resulting in a lower wall heat loss (regarding the total amount of released heat) [47], [102]. The importance of these effects increases at a higher compression ratio, resulting in a higher efficiency improvement with increasing intake pressure (i.e., load). Similar trends are reported in [37] and [58], confirming that the efficiency improvement by increasing ε also depends on the operating conditions – a higher efficiency improvement is demonstrated at the wide-open-throttle operation compared to the part load.

<u>Figure 55</u> shows the raw CO and NO$_X$ emissions over the intake pressure. The unburned CO emissions slightly decrease as the engine operates at a higher intake pressure (i.e., load). More intensive oxidation of unburned CO due to the slightly higher exhaust gas temperatures (and temperatures during the expansion stroke, not shown here) can explain this trend. The NO$_X$ emissions increase with increasing engine load

(i.e., intake pressure) due to higher peak combustion temperatures which drive the NO_X formation. The NO_X increases intensively at higher ε.
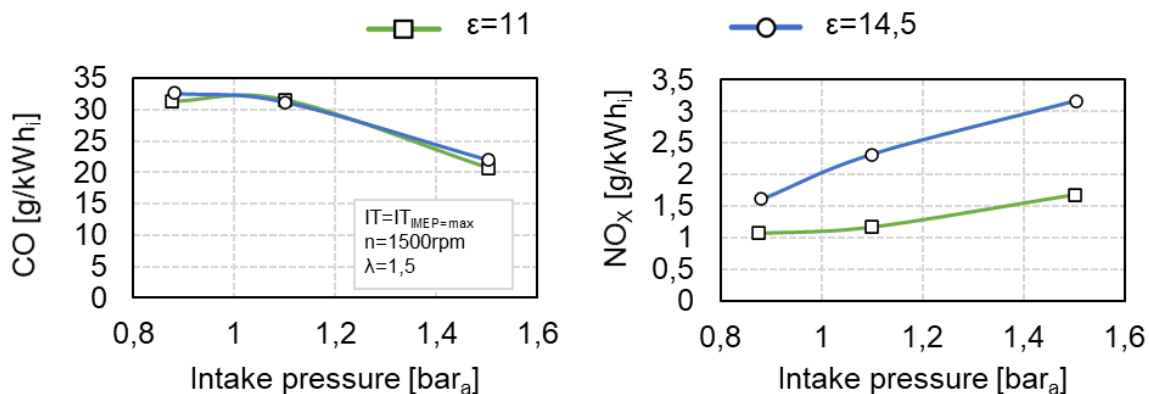

Figure 55: Raw exhaust gas emissions during engine operation at different pressure levels and ε – CO (left) and NO_X (right)

The presented results demonstrate the advantages of intake pressure boosting on wood gas engine efficiency, arising mainly from reduced gas exchange work and lower heat loss related to higher engine load. The supercharger and turbine efficiencies are not considered in the presented analyses. However, the wood gas supply and engine operating conditions (which affect the exhaust gas enthalpy for turbocharging) can limit the intake pressure increase for a wood gas engine integrated into a small biomass power plant. Hence, the lean engine operation at two representative loads and the operating conditions are investigated in the following.

8.1.2 Lean Engine Operation at Constant Load (IMEP) – λ Sweep

The engine is operated at constant load (IMEP) and speed (1500 rpm) at ε=11. The relative air-fuel ratio λ is regulated by adjusting the wood gas flow and the intake pressure.

Figure 56 shows the intake and exhaust pressures, the ignition delay, the combustion duration (MFB5%-90%), and indicated efficiency during the lean engine operation at two different loads (IMEP). The lower load (black line) represents the nominal load achieved during near-stoichiometric and naturally aspirated engine operation in the biomass power plant. The absolute intake pressure is gradually increased to achieve the defined load as the mixture becomes lean. A higher intake pressure is necessary for a higher load. The ignition delay and combustion duration increase linearly as the mixture becomes leaner. However, despite the different pressure levels, they are in the same range at both engine loads.

The indicated efficiency increases as the λ increases at both loads due to the advantages of lean engine operation. At nominal low-load operation (black line), the intake pressure is below exhaust gas pressure (dashed line) for λ<1,8, causing efficiency losses due to gas exchange (negative pumping work). An efficiency improvement higher than one percentage point is achieved for λ<1,8 at a higher load (orange line) due to increased intake pressure. Also, a lower heat loss related to a higher engine load positively affects the efficiency; however, its extent is not analyzed in more detail. For λ>1,8, the intake and exhaust pressures are balanced at both loads, resulting in the same efficiency, although the engine operates at different pressure levels. However, the increased combustion duration and the deterioration in combustion stability adversely affect the engine efficiency and overcome the positive effects of intake pressure boosting, resulting in efficiency decrease as the λ increases above 1,5.
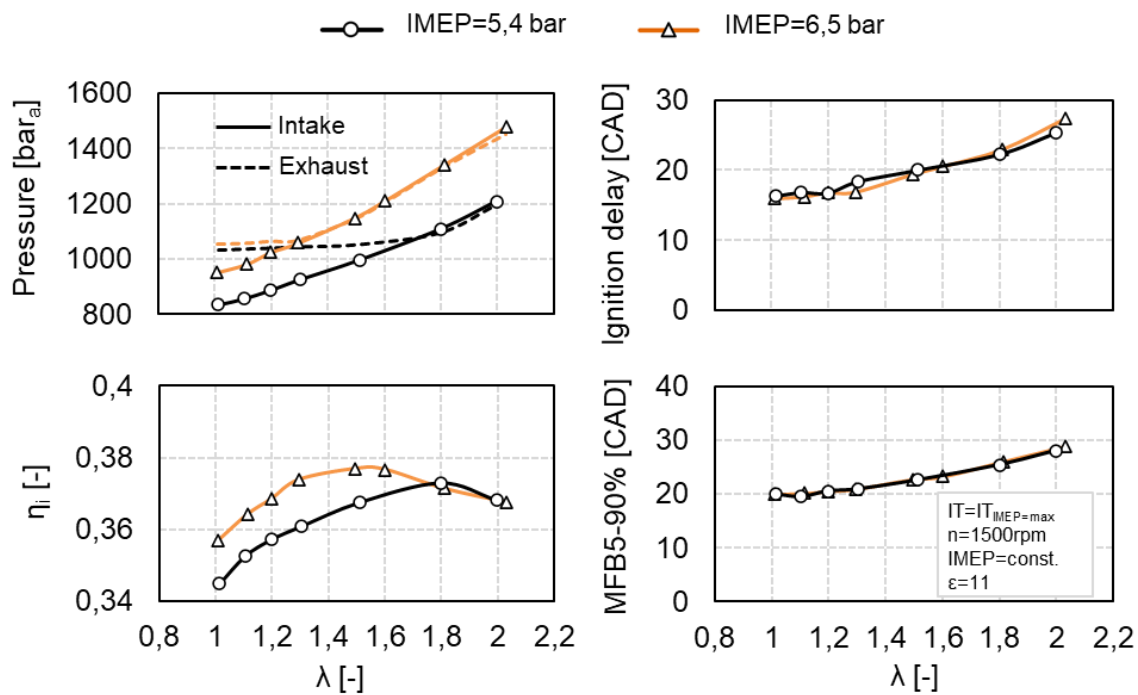
Figure 56: Absolute intake and exhaust pressures, ignition delay, combustion duration, and indicated efficiency during lean engine operation at a constant load

Figure 57 shows the raw exhaust gas emissions measured on the single-cylinder research engine. Similar CO emissions can be seen for both loads on the left diagram. They decrease during the operating range from λ=1 to λ=1,1 and increase linearly as the λ increases above λ=1,1. At the nominal lower load (black line), CO emissions are higher compared to the high load at λ>1,8. This effect can be explained by slightly lower exhaust gas temperatures at lower load, resulting in reduced CO oxidation. Unburned HC_1 exhaust gas emissions are significantly lower than CO; however, HC_1 emissions exhibit similar trends (not shown in the figure). The CO and HC_1 emissions

can be effectively reduced by exhaust aftertreatment, even in operation leaner than stoichiometric.

NO_X emissions are depicted in Figure 57 – right. As the fresh charge becomes leaner than stoichiometric, they increase, reaching the maximum at λ~1,1 and further intensively sink approaching "Near Zero NO_X" at λ>1,8 for both loads. Slightly higher NO_X emissions are achieved at IMEP 6,5 bar compared to IMEP 5,4 bar at λ=1 – 1,2 due to a higher combustion peak temperature which drives the NO_X formation.

The highest efficiency is achieved at λ=1,5 at the higher load – see Figure 56. Compared to the operating point of the basic engine at λ=1,1 at the lower load (IMEP=5,4bar), the efficiency increases by more than 2%. NO_X emissions are reduced by more than 75% (Figure 57).
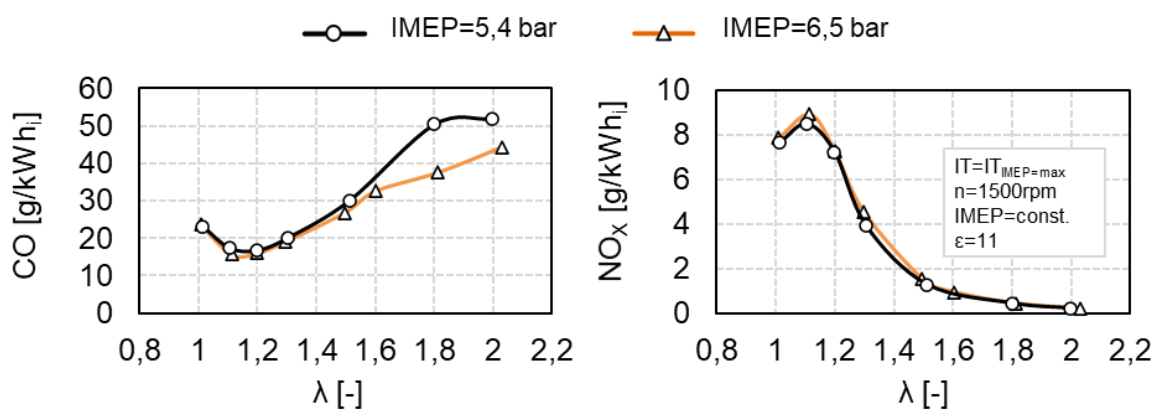
Figure 57: Raw exhaust gas emissions during lean engine operation at constant load – CO (left) and NO_X (right)

The presented results demonstrate a potential for wood gas engine efficiency improvement by boosting the intake pressure. That way, the related engine efficiency losses (e.g., pumping work in naturally aspirated engine operation) caused by biomass power plant low-pressure operating mode can be avoided. Additional benefits arise from lower heat loss related to higher engine load. After the positive potential has been shown, in the further course of the research, possible intake pressure boosting strategies such as supercharging, turbocharging, and advanced solutions such as electric turbo compound are to be evaluated concerning effects on the gasification process and gas purification. Depending on the operating conditions of the gasification process and available exhaust gas enthalpy for the turbine drive, the gasifier intake pressure boosting represents a possible approach for improving the biomass power plant.

8.2 Potential for Efficiency Improvement through Combustion Control

A possible manipulated variable for a combustion control system (such as cylinder-pressure-based combustion control) represents the ignition timing. Its effect on the engine efficiency is evaluated by the ignition timing variations. Thereby the engine utilizes average wood gas with an H_2 fraction of 14%vol. (see Table 4). The effect of wood gas composition on the engine efficiency and altering the ignition timing is also evaluated. For this purpose, the H_2 fraction in wood gas is increased up to 45%, reproducing the possible extremes of composition fluctuations depending on gasification conditions or wood quality. That way, the viability of a cylinder-pressure-based combustion control system for an application on a wood gas engine is assessed on the test bench (naturally aspirated engine operating mode). The measurements occur at the constant engine speed (1500 rpm), intake pressure, and the relative air-fuel ratio λ. λ is set by adjusting the wood gas flow and the throttle valve for air. The total mass flow remains unchanged and, therefore, the intake pressure, but the engine load increases by increasing the H_2 content, i.e., heating value. This kind of mixture control is characteristic for naturally aspirated wood gas engines and reproduces the real conditions in biomass power plants.

Figure 58 depicts how altering the ignition timing affects the efficiency, the center of combustion MFB50%, and NO_X emissions. The optimal engine operating point with the particular ignition timing (IT=$IT_{IMEP=max}$) gives the highest IMEP at a constant speed, mixture composition, and flow rate (i.e., highest efficiency). Retarding the ignition timing for 5 CAD or more reduces the engine efficiency by more than 1 % and NO_X by 30%. Additionally, the threat of engine knocking is avoided.
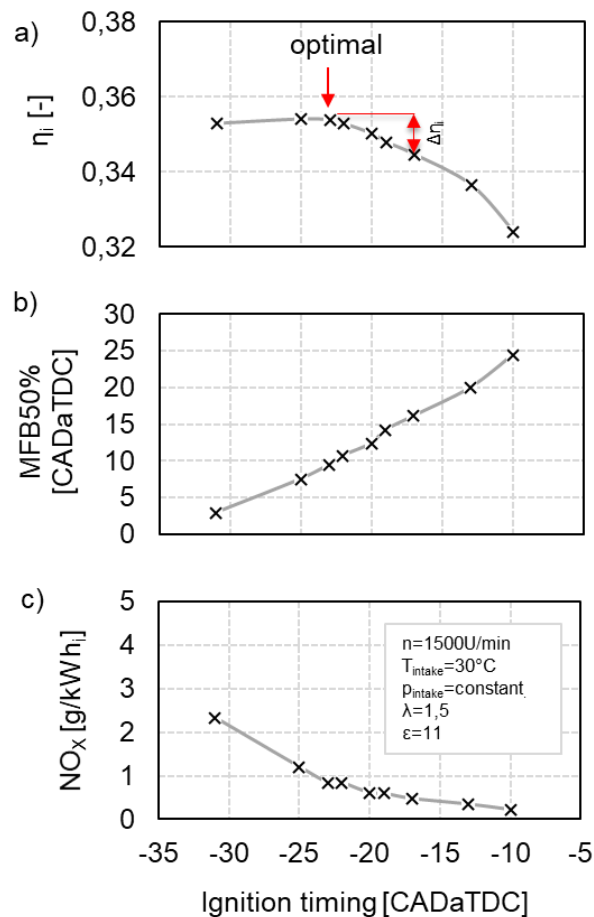
Figure 58: Effect of ignition timing on indicated efficiency, MFB50%, and NO$_X$ emissions – wood gas composition: H$_2$=14%vol.

Figure 59 shows engine efficiency, ignition timing, and raw NO$_X$ emissions for operation on different wood gas compositions. The ignition timing (IT) is set to meet the optimal center of combustion (IT=IT$_{IMEP=max}$) for given engine operating parameters. The engine efficiency increases with increasing H$_2$ fraction in wood gas due to a higher laminar flame velocity which ensures stable and faster combustion and favorable thermodynamic properties of the mixture. As the H$_2$ fraction rises, the efficiency increment occurs moderately due to the higher effect of related efficiency losses (e.g., wall heat transfer). For optimal engine operation (operating point with the highest efficiency), the ignition timing shifts closer to TDC for 5 CAD as the H$_2$ fraction increases by 10%. The NO$_X$ emissions rise significantly at higher H$_2$ content due to higher combustion temperatures. No engine knocking or backfire due to high H$_2$ fraction occurred at the investigated engine operating points.

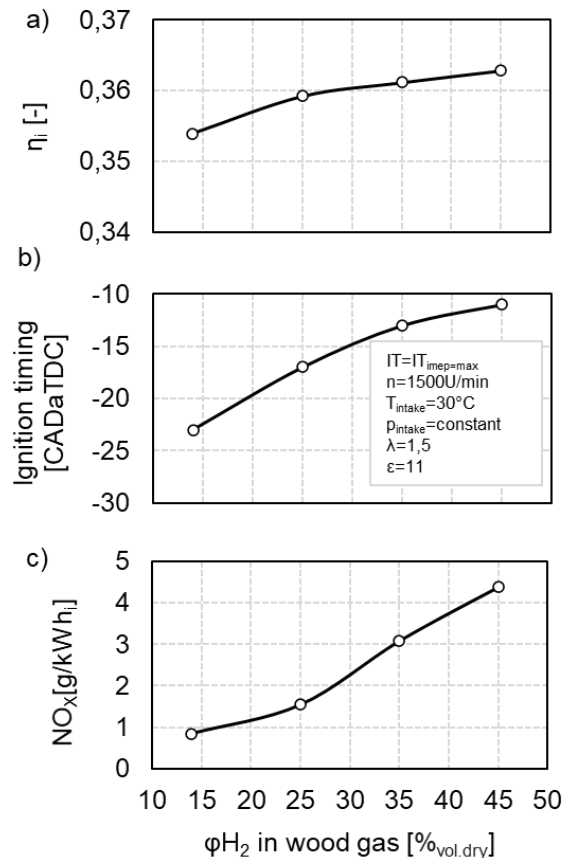**Figure 59:** Effect of H_2 fraction in wood gas composition on indicated efficiency, ignition timing for operating point with the highest efficiency, and NO_X emissions. Changing the H_2 fraction in wood gas reproduces possible extremes of composition fluctuations occurring in biomass power plants.

The presented results demonstrate the effects of ignition timing as a manipulated variable in terms of combustion control on engine efficiency and NO_X emissions. The necessary shifts of ignition timing for adjusting the efficient engine operation or avoiding high NO_X emissions depend on the wood gas fluctuations and span more than 10 CAD. By applying a control system for adjusting the spark timing to optimum, the efficiency loss of more than 1 % can be avoided during the composition fluctuations. Further, the implemented tolerances for the conventional open-loop control can be minimized, thereby ensuring efficient engine operation in optimal operating point at the knock limit. The engine operation can also be adjusted to reach the NO_X emissions below the limitations. In the long-term operation, the combustion control system can improve the rentability and durability of the biomass power plant. In further steps, the viability of the combustion control system is to be investigated in the biomass power plant during long-term operation, and the costs of the system are to be evaluated.

9 Improvement Measures Combination: Optimal Wood Gas Engine Setup

The results presented in previous chapters demonstrate the potential for efficiency improvement of investigated optimization measures independently. An optimal wood gas engine setup is defined by holistically implementing the auspicious optimization measures on the single-cylinder test engine. This setup comprises conventional optimization measures such as optimized combustion chamber geometry, a high compression ratio, and intake pressure boosting. For adjusting the optimal parameters, the interaction of the measures is considered, and the engine operation is analyzed.

Figure 60 shows the indicated efficiency and raw NO_X emissions over λ. Application of the optimized asymmetrically-shaped piston crown geometry enables stable, rapid combustion and efficient lean engine operation. Thus, a higher indicated efficiency and significantly lower NO_X emissions are achieved with the asymmetrical piston crown (yellow line) compared to the basic piston geometry (red line). The increase of ε from 11 to 14,5 enables a further increase in the efficiency of SI combustion mode over the lean operating range and without the occurrence of irregular combustion phenomena (blue line). To evaluate the effects of the intake pressure boosting, the intake and exhaust pressures are balanced at 1,5bar$_a$ (absolute) to reproduce the possible operating conditions of a turbocharging system. The higher intake pressure reduces high gas exchange losses and significantly increases the efficiency of the SI wood gas engine (green line). The efficiency improvement results from avoiding the negative engine pumping work occurring on the real biomass power plant by aspiration of wood gas through the gasifier and reduced wall heat losses. Additionally, boosting the intake pressure allows overcoming the power derating caused by the lean engine operation. The highest efficiency and the lowest raw NO_X emissions are achieved in lean operation (marked as a star). Compared to the nominal operating point of the basic engine (marked as a circle), an efficiency improvement potential of 5,55 percentage points is achieved. Thereby, the NO_X emissions are reduced by 52% – far below the emission limitation according to Austrian legislation. With increasing λ, NO_X emissions decrease and approach "Near-Zero NO_X" in ultra-lean operation (λ>1,8). However, the efficiency slightly decreases as the λ increases above 1,5.

Further, the SACI combustion is accomplished by increasing ε of the naturally aspirated wood gas engine up to 22,2. It results in an efficiency improvement potential of 3,27 percentage points at the optimal operating point (marked as a triangle). Thereby the NO_X emissions meet the limitation according to Austrian legislation. Hence, the engine operation in optimal operating points for SI and SACI combustion modes allows the complex exhaust gas aftertreatment, such as Selective Catalytic Reduction (SCR)

system and related costs, to be omitted due to raw NO_X emissions below the limitation. Nonetheless, the CO emissions are above limitations in every operating point. The CO and HC_1 (not shown in the figure) can be effectively reduced by an oxidation catalyst.
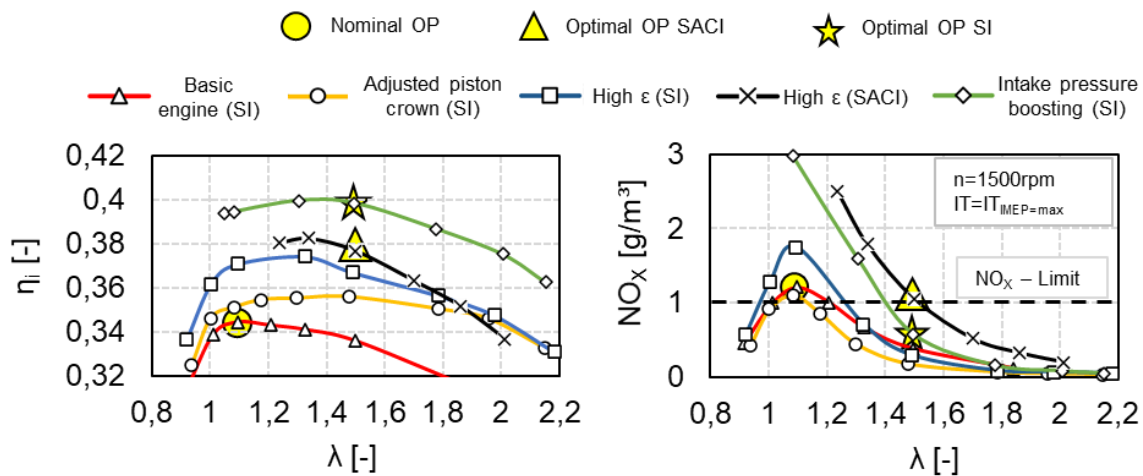
Figure 60: Holistic implementation of optimization measures on a small high-speed wood gas engine – indicated efficiency η_i (left) and raw NO_X emissions (right). NO_X-limitation according to [26].

Finally, the efficiency improvement achieved by gradually implementing the individual measures and adjusting engine parameters is given quantitatively on the roadmap for the evolution of the wood gas engine in <u>Figure 61</u>.
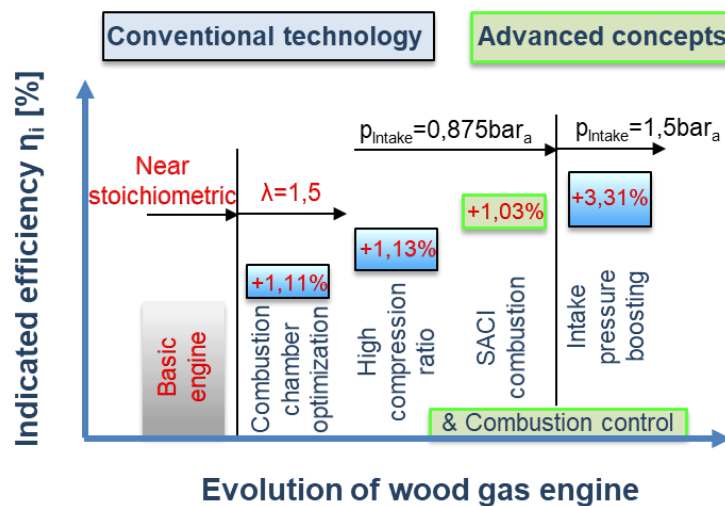
Figure 61: Roadmap of wood gas engine development

Combining conventional technologies such as lean fast-burn SI combustion, high compression ratio, and intake pressure boosting with advanced concepts such as SACI combustion demands an adaptive combustion control that can assure efficient engine operation with low NO_X emissions despite the wood gas composition fluctuations.

10 Summary

The doctoral thesis aims to investigate and improve the combustion process for efficient and low-emissions operation of small high-speed wood gas engines. The potential for engine efficiency improvement and emissions reduction is determined by applying selective optimization measures on the small high-speed wood gas engine.

The methodological approach and engine optimization measures are defined based on the literature review and the assessments of the operating biomass power plant in the field. A wood gas composition mixer and single-cylinder research engine, which enable accurate experimental investigations of the combustion process, are developed on the test bench and verified. The selective optimization measures such as combustion chamber adjustment, lean and EGR combustion concepts, high compression ratio, spark-assisted compression ignition combustion concept, engine intake pressure boosting, and combustion control are investigated independently. Thus, applying a specific combination and interaction of the well-known engine optimization measures on a small high-speed wood gas engine represents the main contribution of this thesis. The main achievements are summarized below:

- The particular piston crown design and high compression ratio ensure an intensive in-cylinder charge motion and a rapid and stable combustion process of diluted fresh charge. The lean mixture exhibits favorable properties for the combustion process, resulting in higher engine efficiency than the EGR operation, and represents a viable combustion strategy for a wood gas engine.

- The lean engine operation demonstrates a high potential for reducing raw NO_X emissions compared to the basic engine. However, high unburned fuel emissions (CO and HC_1) demand an exhaust aftertreatment system (e.g., an oxidation catalyst).

- The Spark-Assisted Compression Ignition (SACI) is accomplished by increasing the compression ratio up to 22,2 in the lean operation of a naturally aspirated engine. An efficiency breakthrough occurs due to rapid and stable controlled autoignition of the fresh charge, which overcomes the limitations of the SI concept related to combustion duration losses.

- The engine intake pressure boosting overcomes the gas exchange loss caused by the low-pressure operation of the biomass power plant and improves the engine performance.

- The optimal ignition timing, which represents a possible manipulated variable for an adaptive combustion control system, depends on the wood gas composition and spans more than 10 CAD. Thereby, the efficiency reduction of more than 1% can be avoided by appropriately adjusting the IT according to gas composition fluctuations.

An overall indicated efficiency improvement of 5,55 percentage points is achieved by holistically applying the conventional optimization measures comprising ultra-lean and fast-burn SI concept, high compression ratio, and intake pressure boosting on the wood gas research engine. The NO_X emissions of optimal engine setup are reduced by 52% compared to the basic engine in the nominal operating point. The achieved NO_X emissions are below the limitations and approach "Near Zero NO_X" with increasing λ allowing the complex exhaust gas aftertreatment to be omitted. However, the CO emissions during lean engine operation are above limitations and can be effectively reduced by an oxidation catalyst.

References

[1] Crutzen, P.: Geology of mankind. Nature, 2002, 415, p. 23, DOI: https://doi.org/10.1038/415023a.

[2] Barker, J. R.; Ross, M. H.: An introduction to global warming. American Journal of Physics, 1999, 67, p. 1216–1226. DOI: https://doi.org/10.1119/1.19108.

[3] Lüthi, D.; Le Floch, M.; Bereiter, B.; Blunier, T.; Barnola, J. M.; Siegenthaler, U.; Raynuad, D.; Jouzel, J.; Fischer, H.; Kawamura, K.; Stocker, T. F.: High-resolution carbon dioxide concentration record 650,000-800,000 years before present. Nature, 2008, 453, p. 379–382. DOI: https://doi.org/10.1038/nature06949.

[4] MacFarling Meure, C.; Etheridge, D.; Trudinger, C.; Steele, P.; Langenfelds, R.; van Ommen, T.; Smith, A.; Elkins, J.: Law Dome CO_2, CH_4 and N_2O ice core records extended to 2000 years BP. Geophysical Research Letters, 2006, 33, p. 1-4. DOI: https://doi.org/10.1029/2006GL026152.

[5] Keeling, R. F.; Keeling, C. D.: Atmospheric Monthly In Situ CO2 Data - Mauna Loa Observatory, Hawaii (Archive 2022-11-02). In Scripps CO2 Program Data. UC San Diego Library Digital Collections. 2017. DOI: https://doi.org/10.6075/J08W3BHW.

[6] Schwartz, S.E.: Resource Letter GECC-2: The Greenhouse Effect and Climate Change: The Intensified Greenhouse Effect. American Journal of Physics, 2018, 86, p. 645-656. DOI: https://doi.org/10.1119/1.5045577.

[7] Al-Ghussain, L.: Global warming: review on driving forces and mitigation. Environmental Progress and Sustainable Energy, 2019, 38, p.13–21. DOI: https://doi.org/10.1002/ep.13041.

[8] Schwartz, S.E.: Resource Letter GECC-1: The Greenhouse Effect and Climate Change: Earth's Natural Greenhouse Effect. American Journal of Physics, 86, 2018, p. 565–576. DOI: https://doi.org/10.1119/1.5045574.

[9] Intergovernmental Panel on Climate Change (IPCC): Climate change 2013 – The Physical Science Basis. Contribution of Working Group I to the Fifth Assessment Report of the Intergovernmental Panel on Climate Change. New York: Cambridge University Press, ISBN: 781107057999, 2014.

[10] EDGAR/JRC: Distribution of Global Carbon Dioxide Emissions in 2021, by sector. 2022, [Online]. Available: https://www.statista.com/statistics/1129656/global-share-of-co2-emissions-from-fossil-fuel-and-cement/, Accessed on 7th May, 2023.

[11] Scarlat, N.; Prussi, M.; Padella, M.: Quantification of the carbon intensity of electricity produced and used in Europe. Applied Energy, 2022, 305, p. 1–15, DOI: https://doi.org/10.1016/j.apenergy.2021.117901.

[12] Hondo, H.: Life cycle GHG emission analysis of power generation systems: Japanese case. Energy, 2005, 30, pp. 2042–2056, DOI: https://doi.org/10.1016/j.energy.2004.07.020.

[13] Thomson, R.; Kwong, P.; Ahmad, E.; Nigam, K.D.P.: Clean syngas from small commercial biomass gasifiers; a review of gasifier development, recent advances and performance evaluation. International Journal of Hydrogen Energy, 2020, 45, p. 21087–21111, DOI: https://doi.org/10.1016/j.ijhydene.2020.05.160.

[14] Arena, U.; Di Gregorio, F.; Santonastasi, M.: A techno-economic comparison between two design configurations for a small scale, biomass-to-energy gasification based system. Chemical Engineering Journal, 2010, 162, p. 580–590, DOI: https://doi.org/10.1016/j.cej.2010.05.067.

[15] Sharma, S.; Sheth, P.N.: Air–steam biomass gasification: Experiments, modeling and simulation. Energy Conversion and Management, 2016, 110, p. 307–318, DOI: https://doi.org/10.1016/j.enconman.2015.12.030.

[16] Kaltschmitt, M.; Hartmann, H.; Hofbauer, H.: Energie aus Biomasse. 3. Auflage. Berlin: Springer Berlin Heidelberg, ISBN: 978-3-662-47438-9, 2016.

[17] Lv, P.; Yuan, Z.; Ma, L.; Wu, C.; Chen, Y.; Zhu, J.: Hydrogen-rich gas production from biomass air and oxygen/steam gasification in a downdraft gasifier. Renewable Energy, 2007, 32, p. 2173–2185, DOI: https://doi.org/10.1016/j.renene.2006.11.010.

[18] Lehmann, A.K.; Stellwagen, K.; Plohberger, D.: Influence of the lubrications oil choice on the gas engine operation with biogases. 6. Dessauer Gasmotoren-Konferenz, Dessau, 2009, p. 144–154.

[19] Benedikt, F.; Schmid, J.C.; Fuchs, J.; Mauerhofer, A.M.; Müller, S.; Hofbauer, H.: Fuel flexible gasification with an advanced 100 kW dual fluidized bed steam gasification pilot plant. Energy, 2018, 164, p. 329–343, DOI: https://doi.org/10.1016/j.energy.2018.08.146.

[20] Bolhàr-Nordenkampf, M.; Rauch, R.; Bosch, K.; Aichernig, C.; Hofbauer, H.: Biomass CHP Plant Güssing – Using Gasification for Power Generation. 2nd Regional Conference on Energy Technology Towards a Clean Environment, 2003, Phuket, p. 566-572.

[21] Herdin, G.; Zankl, M.: The Use of H2 Rich Syngas in a Gas Engine – Thermodynamic Analyzes. 13. Tagung Der Arbeitsprozess des Verbrennungsmotors, Graz 2011, p. 568–582.

[22] Ahrenfeldt, J.; Jensen, T.; Henriksen, U.; and Schramm, J.: Experiments with Wood Gas Engines. SAE 2001-01-3681, DOI: https://doi.org/10.4271/2001-01-3681.

[23] Sridhar, G.; Yarasu, R.B.: Facts about Producer Gas Engine. 2010 – Paths to Sustainable Energy, 2010, p. 537–560, DOI: 10.5772/13030.

[24] Brandin, J.; Tunér, M.; Odenbrand, I.: Small Scale Gasifiction: Gas Engine CHP for Biofuels. Lund, Sweden: Lund University, ISBN: 978-91-86983-07-9, 2011.

[25] Konstantinoff, L.; Möltner, L.; Pillei, M.; Steiner, T.; Dornauer, T.; Herdin, G.; Mairegger, D.: Optimization of the Charge Motion in Internal Combustion Engines Driven by Sewage Gas for Combined Heat and Power Units. Journal of Engineering for Gas Turbines and Power, 2018, 140, p. 1–8, DOI: https://doi.org/10.1115/ICEF2017-3529.

[26] Vereinbarung gemäß Art 15a B-VG über das Inverkehrbringen von Kleinfeuerungen und die Überprüfung von Feuerungsanlagen und Blockheizkraftwerken (2011) gemäß Mitteilung der Verbindungsstelle der Bundesländer beim Amt der NÖ Landesregierung vom 28. Jänner 2011 and das Bundeskanzleramt (VSt-5451/69) (22.01.2013). [Online] Available: https://www.ris.bka.gv.at/GeltendeFassung.wxe?Abfrage=LrSbg&Gesetzesnummer=20000826, Accessed on 7th May, 2023.

[27] Baufeld, T.; Lustgarten, G.; Murakami, S.; Stoewe, C.: Combustion Concepts for Future Gas Engines. 13. Conference The Working Process, 2011, Graz, p. 305–323.

[28] Merker, G. P.; Teichmann, R.: Grundlagen Verbrennungsmotoren. 9. Auflage, Wiesbaden: Springer Vieweg, ISBN: 978-3-658-23557-4, 2019.

[29] Srinivasan, K. K.; Agarwal, A. K.; Krishnan, S. R.; Mulone, V.: Natural Gas Engines. Singapore: Springer Singapore, ISBN: 978-981-13-3307-1, 2019.

[30] van Basshuysen, R.; Bargende, M.: Erdgas und erneuerbares Methan für den Fahrzeugantrieb: Wege zur klimaneutralen Mobilität. Wiesbaden: Springer Vieweg, ISBN: 978-3-658-07159-2, 2015.

[31] Hofmann, P.; Hofherr, T.; Hoffmann, G.; Preuhs, J.-F.: Potenzial der CNG-Direkteinblasung für Downsizingmotoren. MTZ Motortechnische Zeitschrift, 2016, 77, p. 28–35, DOI: https://doi.org/10.1007/s35146-016-0064-x.

[32] Hofmann, P.; Hofherr, T.; Damböck, M.; Fritz, W.; Kampelmühler, F.: Der CULT Antrieb: Hocheffizienter CNG Motor mit Direkteinblasung. 34. Internationales Wiener Motorensymposium, Wien, 2013.

[33] Pflaum, H.; Hofmann, P.; Geringer, B.: Potenzial von unterschiedlichen Biogasqualitäten im Ottomotorischen Betrieb. 12. Conference The Working Process of the Internal combustion Engine, Graz, 2009, p. 397–412.

[34] Holly, W.: Numerische Brennverfahrensauslegung von Großgasmotoren für unterschiedliche Kraftstoffe. Dissertation on Institute of Powertrains and Automotive Technology (IFA) TU Wien, 2016.

[35] Schneßl, E.; Kogler. G: Großgasmotorenkonzepte für Gase mit extrem niedrigem Heizwert. 6. Dessauer Gasmotoren-Konferenz, Dessau, 2009, p. 271–293.

[36] Chmela, F.; Krenn, M.; Pirker, G.; Schlick, H.; Wimmer, A.: Simulation des Brennratenverlaufs beim Betrieb mit Sondergasen. 8. Dessauer Gasmotoren-Konferenz, Dessau, 2013, p. 197–210.

[37] Heywood, J.B.: Internal combustion engine fundamentals. 2nd Edition. USA: Mc Graw Hill, ISBN: 978-1-260-11610-6, 2018.

[38] Pischinger, R.; Klell, M.; Sams, T.: Thermodynamik der Verbrennungskraftmaschine. 3. Auflage. Wien: SpringerWienNewYork, ISBN: 9783211992760, 2009.

[39] Rabello de Castro, R.; Brequigny, P.; Dufitumukiza, J.P.; Mounaïm-Rousselle, C.: Laminar flame speed of different syngas compositions for varying thermodynamic conditions, Fuel, 2021, 301, p. 1-9, DOI: https://doi.org/10.1016/j.fuel.2021.121025.

[40] Tschöke, H.; Mollenhauer, K.; Maier, R.: Handbuch Dieselmotoren. 4. Auflage. Wiesbaden: Springer Fachmedien Wiesbaden, ISBN: 9783658076979, 2018.

[41] Warnatz, J.; Maas, U.; Dibble, R.W.: Combustion: Physical and Chemical Fundamentals, Modeling and Simulation, Experiments, Pollutant Formation. 4th Edition. Berlin: Springer Berlin Heidelberg, ISBN: 9783540453635, 2006.

[42] Okuda, K.; Momose, A.: Nissan's 100% electric motor-driven e-POWER technology reaches global milestone. Nissan Motor Corporation, [Online] Available: https://global.nissannews.com/en/releases/210226-01-e. Accesed on: 08. 05.2023.

[43] Wohlgemuth, S.: CO2-optimierter Antrieb eines Kleinfahrzeuges. Dissertation am Lehrstuhl für Verbrennungskraftmaschinen der Technischen Universität München, 2016.

[44] Bögl, A.; Hemminger, B.; Janssen, A. N.; Kerkau, M.; Kerner, J.; Kronich, A.; Schlüter, M.: Die neuen V6 Turbomotoren im Porsche Macan. 35. Internationales Wiener Motorensymposium, Wien, 2014.

[45] Eichler, F.; Middendorf, H.; Helbing, C.; Hentschel, J.; Scherf, J.; Wendt, W.: Der neue 1,0l 3-Zylinder TSI. 35. Internationales Wiener Motorensymposium, Wien, 2014.

[46] Sasaki, Y.; Adachi, S.; Nakata, K.; Tanei, K.; Shibuya, S.: The new Toyota 1.0L L3 ESTEC gasoline engine. 35. Internationales Wiener Motorensymposium, Wien, 2014.

[47] Golloch, R.: Downsizing bei Verbrennungsmotoren. Berlin: Springer, ISBN: 3540238832, 2005.

[48] Johansson, B.; Olsson, K.: Combustion Chambers for Natural Gas SI Engines Part I: Fluid Flow and Combustion. SAE 1995-02-01, DOI: https://doi.org/10.4271/950469.

[49] Olsson, K.; Johansson, B.: Combustion Chambers for Natural Gas SI Engines Part 2: Combustion and Emissions. SAE 1995-02-01, DOI: https://doi.org/10.4271/950517.

[50] Einewall, P.; Johansson, B.: Combustion Chambers for Supercharged Natural Gas Engines. SAE 1997-02-24, DOI: https://doi.org/10.4271/970221.

[51] Teruhiro, S.; Masanori, I.; Kazuhisa, O.; Fujio, S.: Basic Research on Combustion Chambers for Lean Burn Gas Engines. SAE 1993-10-01. DOI: https://doi.org/10.4271/932710.

[52] Yan, B.; Tong, L.; Wang, H.; Zheng, Z.; Qin, Y.; Yao, M.: Experimental and numerical investigation of the effects of combustion chamber reentrant level on combustion characteristics and thermal efficiency of stoichiometric operation natural gas engine with EGR. Applied Thermal Engineering, 2017, 123, pp. 1473–1483, DOI: https://doi.org/10.1016/j.applthermaleng.2017.05.139.

[53] Ulfvik, J.; Achilles, M.; Tuner, M.; Johansson, B.; Ahrenfeldt, J.; Schauer, F. X.; Henriksen, U.: SI Gas Engine: Evaluation of Engine Performance, Efficiency and Emissions Comparing Producer Gas and Natural Gas. SAE 2011-01-0916, DOI: https://doi.org/10.4271/2011-01-0916.

[54] Sita Rama Raju, A.V.; Ramesh, A.; Nagalingam, B.: Effect of Intensified Swirl and Squish on the Performance of a Lean Burn Engine Operated on LPG. SAE 2000-01-1951, DOI: https://doi.org/10.4271/2000-01-1951.

[55] Heuser, P.; Geiger, J.; Lauer, S.; Sankhla, H.; Dhongde, A.; Simm, P.: Der Erdgasmotor im Nutzfahrzeug als Dieselmotor-Derivat. 35. Internationales Wiener Motorensymposium. Wien, 2014.

[56] Gruber, F.: Fremdgezündete Brennkraftmaschine mit mindestens einer Zündeinrichtung pro Zylinder. Offenlegungsschrift EP1253304A2. 30.10.2002.

[57] Fuchs, J.; Leitner, A.; Tinschmann, G.; Trapp, C.: Konzept Für Direkt Gezündete Gross-Gasmotoren. MTZ Motortechnische Zeitschrift, 2013, 74, p. 386–391.

[58] Caris, D.F.; Nelson, E.E.: A new look at High Compression Engines. SAE 1959-01-01, DOI: https://doi.org/10.4271/590015.

[59] Duan, X.; Liu, Y.; Lai, M.-C.; Guo, G.; Liu, J.; Chen, Z.; Deng, B.: Effects of natural gas composition and compression ratio on the thermodynamic and combustion characteristics of a heavy-duty lean-burn SI engine fueled with liquefied natural gas. Fuel, 2019, 254, p. 1-13, DOI: https://doi.org/10.1016/j.fuel.2019.115733.

[60] Koga, H.; Kiura, T.: A Study of Controlled Auto-Ignition in Small Natural Gas Engines. SAE 2013-10-15, DOI: https://doi.org/10.4271/2013-32-9098.

[61] Sridhar, G.; Paul, P.J.; Mukunda, H.S.: Biomass derived producer gas as a reciprocating engine fuel—an experimental analysis. Biomass and Bioenergy, 2001, 21, p. 61–72, DOI: https://doi.org/10.1016/S0961-9534(01)00014-9.

[62] Homdoung, N.; Tippayawong, N.; Dussadee, N.: Performance and emissions of a modified small engine operated on producer gas. Energy Conversion and Management, 2015, 94, p. 286–292, DOI: https://doi.org/10.1016/j.enconman.2015.01.078.

[63] Porpatham, E.; Ramesh, A.; Nagalingam, B.: Effect of compression ratio on the performance and combustion of a biogas fuelled spark ignition engine. Fuel, 2012, 95, p. 247–256, DOI: https://doi.org/10.1016/j.fuel.2011.10.059.

[64] Fontana, G.; Galloni, E.: Variable valve timing for fuel economy improvement in a small spark-ignition engine. Applied Energy, 2009, 86, pp. 96–105, DOI: https://doi.org/10.1016/j.apenergy.2008.04.009.

[65] Capaldi, P.: A high efficiency 10 kWe microcogenerator based on an Atkinson cycle internal combustion engine. Applied Thermal Engineering, 2014, 71, pp. 913–920, DOI: https://doi.org/10.1016/j.applthermaleng.2014.02.035.

[66] Ahrenfeldt, J.; Foged, E. V.; Strand, R.; Henriksen, U. B.: Development and Test of a new Concept for Biomass Producer Gas Engines. Denmark: Danmarks Tekniske Universitet, Risø Nationallaboratoriet for Bæredygtig Energi,

Forskningscenter Risoe, Risoe-R No. 1728(EN), ISBN: 978-87-550-3811-0, 2010.

[67] Bhaduri, S.; Contino, F.; Jeanmart, H.; Breuer, E.: The effects of biomass syngas composition, moisture, tar loading and operating conditions on the combustion of a tar-tolerant HCCI (Homogeneous Charge Compression Ignition) engine. Energy, 2015, 87, p. 289–302 DOI: https://doi.org/10.1016/j.energy.2015.04.076.

[68] Shivapuji A.M.; Dasappa S.: Selection and thermodynamic analysis of a turbocharger for a producer gas-fuelled multi-cylinder engine. Journal of Power and Energy, 2014, 228, pp. 340–356, DOI: https://doi.org/10.1177/0957650913517677.

[69] Carlucci, A.; Benegiamo, M.; Saracino, R.; Gaballo, M.; Mannal, S.; Motz, S.: Cylinder Pressure-Based Closed Loop Combustion Control: A Valid Support to Fulfill Current and Future Requirements of Diesel Powertrain Systems. SAE 2015-24-2423, DOI: https://doi.org/10.4271/2015-24-2423.

[70] Willems, F.; Doosje, E.; Engels, F.; Seykens, X.: Cylinder Pressure-Based Control in Heavy-Duty EGR Diesel Engines Using a Virtual Heat Release and Emission Sensor.: SAE 2010-01-0564, DOI: https://doi.org/10.4271/2010-01-0564.

[71] Kopecek, H.; Spyra, N.; Birgel, A.; Spreitzer, K.; Trapp, C.: Cylinder Pressure Based Controls of Operation of Gas Engines of High Power Density. 9. Dessauer Gasmotoren-Konferenz, Dessau, 2015, p. 301–313.

[72] Portin, K.; Hellén, J: Gasmotorensteuerung basierend auf integrierter Zylinderdrucküberwachung. 6. Dessauer Gasmotoren-Konferenz, Dessau, 2009, p. 208–219.

[73] Henschen, P., Bauer, M., Hagl, P.: Development of a combustion control system for medium-speed gas engines based on cylinder pressure measurement. 8. Dessauer Gasmotoren-Konferenz, Dessau, 2013, p. 167–178.

[74] Choi, S.; Im, H.; Choi, K.; Kim, S-J.: In-Cylinder Pressure Based Gasoline Engine Combustion Control. 42. International Vienna Motor Symposium. 2021, Wien, pp. 1–21, ISBN: 978-3-9504969-0-1.

[75] Roubaud, A.; Röthlisberger, R.; Favrat, D.: Lean-Burn Cogeneration Biogas Engine with Unscavenged Combustion Prechamber: Comparison with Natural Gas. International Journal of Applied Thermodynamics, 2002, 5, p. 169–175, DOI: http://dx.doi.org/10.5541/ijot.99.

[76] Graf, J.; Lauer, T.: Innovative Zündung: Identifizierung technisch und wirtschaftlich umsetzbarer Zündsysteme und Demonstration der grundsätzlichen Potenziale an unterschiedlichen Ottomotorkonzepten. Frankfurt am Main: Forschungsvereinigung Verbrennungskraftmaschinen, Vorhaben Nr. 1008, Heft 959 – 2012, 2011.

[77] Hadl, K.; Luef, R.; Eichlseder, H.: Experimentelle Untersuchungen von CNG-Diesel und Wasserstoff-Diesel Dual-Fuel Brennverfahren für den mobilen Einsatz. 11. Tagung „Motorische Verbrennung - aktuelle Probleme und moderne Lösungsansätze", Ludwigsburg, 2013, p. 183–194, ISBN: 978-3-931901-87-5.

[78] Hepp, C.; Krenn, M.; Wasserbauer, J.; Eichlseder, H.: Dual Fuel Compression Ignition Combustion Concept for Gasoline and Diesel. SAE 2014-01-1319, DOI: https://doi.org/10.4271/2014-01-1319.

[79] Flierl, R.; Temp, A.; Wegmann, A.; Barrios, A.; Schmitt, S.: Simultane Verbrennung –Methan -Benzin- und Methan -Diesel -Mischbetrieb. MTZ - Motortechnische Zeitschrift, 2011, 72, pp. 806–814, DOI: https://doi.org/10.1365/s35146-011-0175-3.

[80] Redtenbacher, C., Kiesling, C.; Wimmer, A.; Sprenger, F.; Fasching, P.: Dual Fuel Brennverfahren. 37. Internationales Wiener Motorensymposium, Wien, 2016, p. 403–429.

[81] Burkhardt, H.: Wood Gasification – Technology of the future or of the past?. 8. Dessauer Gasmotoren-Konferenz, Dessau, 2013, p. 43–53.

[82] Folkson, R.: Alternative Fuels and Advanced Vehicle Technologies for Improved Environmental Performance: Towards Zero Carbon Transportation. 2nd Edition. San Diego: Elsevier Science & Technology, ISBN: 9780323900287, 2022.

[83] Yamasaki, Y.; Kaneko, S.: Prediction of Ignition and Combustion Development in an HCCI Engine Fueled by Syngas. SAE 2014-32-0002, DOI: https://doi.org/10.4271/2014-32-0002.

[84] Chiodi, M.; Kaechele, A.; Bargende, M.; Wichelhaus, D.; Poetsch, C: Development of an Innovative Combustion Process: Spark-Assisted Compression Ignition. SAE 2017-24-0147, DOI: https://doi.org/10.4271/2017-24-0147.

[85] Yamasaki, Y.; Kanno, M.; Taura, Y.; Kaneko, S.: Study on Biomass Gas HCCI Engine, SAE 2009-32-0066.

[86] Achilles, M.; Ulfvik, J.; Tuner, M.; Johansson, B.; Ahrenfeldt, J.; Henriksen, U.; Schauer, F. X.: HCCI Gas Engine: Evaluation of Engine Performance, Efficiency

and Emissions - Comparing Producer Gas and Natural Gas. SAE 2011-01-1196, DOI: https://doi.org/10.4271/2011-01-1196.

[87]   Chiodi, M.; Kächele, A.; Bargende, M.; Koch, D.; Wachtmeister, G.; Wichelhaus, D.: Development of an innovative combustion process: Spark-assisted compression ignition. 18. Internationales Stuttgarter Symposium, Stuttgart, 2018, p. 247–256, DOI: https://doi.org/10.1007/978-3-658-21194-3_22.

[88]   Persson, H.: Spark Assisted Compression Ignition, SACI. Doctoral Thesis on Division of Combustion Engines, Lund University, ISBN: ISBN 978-91-628-7578-7, 2008.

[89]   Lavoie, G. A.; Martz, J.; Wooldridge, M.; Assanis, D.: A multi-mode combustion diagram for spark assisted compression ignition. Combustion and Flame, 2010, 157, pp. 1106–1110, DOI: https://doi.org/10.1016/j.combustflame.2010.02.009.

[90]   Reitz, R.; Wickman, D.; Wright, C.; Kokjohn, S.; Andrie, M.; Shears, D.; Procknow, D.; Kamo, L.: Spark-assisted HCCI residential CHP. Advanced Research Projects Agency – Energy, USA: Gensets Annual Program Review Meeting,   [Online]   Available: https://arpa-e.energy.gov/sites/default/files/9_GENSETS%20-%20WERC-Final.pdf Accesed on 08.05.2023.

[91]   Mazda Motor Corporation: Next-generation technology Skyactiv-X Gasoline Engine.   [Online]   Available: https://www2.mazda.com/en/next-generation/technology/, Accessed on 08.05.2023.

[92]   Brettschneider, J.: Erweiterung der Gleichung zur Berechnung des Luftverhältnisses λ. Bosch Technische Berichte, 1994, 56, pp. 30–45, ISSN: 0006-789 X.

[93]   Lackner, M.; Palotá, Á.B.; Winter, F.: Combustion: From basics to applications. Weinheim: Wiley-VCH Verlag GmbH & Co. KGaA, ISBN: 978-3-527-66721-5, 2013.

[94]   Diem, S., Kohl, H., Popov, T.: Messbericht über die Messungen am BHKW GGV2.7 in Griffen der Fa. GLOCK Technology GmbH. Institut für Verfahrenstechnik, Umwelttechnik und Technische Biowissenschaften, TU Wien. 2021.

[95]   Gamma Technologies Inc.: GT-Suite - Engine Performance Application Manual. Westmont Illinois, 2018.

[96]   Richards,   K.J.;   Senecal,   P.K.;   Pomraning,   E.: CONVERGE_Studio_3.0_Manual. CONVERGE 3.0*, Convergent Science, Madison, 2023.

[97] Richards, K.J.; Senecal, P.K.; Pomraning, E.: CONVERGE (V3.0) Manual. CONVERGE 3.0*, Convergent Science, Madison, 2023.

[98] Wang, B.; Li, T.; Ge, L.; Ogawa, H.: Optimization of combustion chamber geometry for natural gas engines with diesel micro-pilot-induced ignition. Energy Conversion and Management, 2016, 122, p. 552–563, DOI: https://doi.org/10.1016/j.enconman.2016.06.027.

[99] Han, Z.; Reitz, R.D.: Turbulence Modelling of Internal Combustion Engines Using RNG κ-ε Models. Combustion Science and Technology, 1995, 106, p. 267–295, DOI: https://doi.org/10.1080/00102209508907782.

[100] Sjöberg, M.; Zeng, W.: Combined Effects of Fuel and Dilution Type on Efficiency Gains of Lean Well-Mixed DISI Engine Operation with Enhanced Ignition and Intake Heating for Enabling Mixed-Mode Combustion. SAE 2016-01-0689, DOI: https://doi.org/10.4271/2016-01-0689.

[101] Quader, A.: Why Intake Charge Dilution Decreases Nitric Oxide Emission from Spark Ignition Engines. SAE 1971-02-01, DOI: https://doi.org/10.4271/710009.

[102] Pucher, H.; Zinner, K.: Aufladung von Verbrennungsmotoren: Grundlagen, Berechnungen, Ausführungen. 4. Auflage. Berlin: Springer Vieweg, Berlin, Heidelberg, ISBN: 978-3-642-28989-7, 2012.

APPENDIX I

During the doctoral research work, the following publications were released:

- Galović, J.; Hofmann, P.; Popov, T.; Müller, S.; Weinländer, C.; Frieling, D.: Application of Wood Gas in Internal Combustion Engines – Efficiency and Emissions. *13th International Colloquium Fuels, Conventional and Future Energy for Automobiles*, Essling, 15.09.2021, ISBN 978-3-8169-8539-6, 2021.
- Galović, J.; Konrad, J.; Hofmann, P.: Combustion Process Development for a Wood Gas ICE of Biomass Power Plants. *31st Aachen Colloquium Sustainable Mobility*, Aachen, 2022, GbR. Paper No.47. ISBN: 978-3-00-072524-1.
- Galović, J.; Konrad, J.; Hofmann, P.: Combustion Process Optimization for Wood Gas Engine of a Biomass Power Plant. *30th CIMAC World Congress*, Busan, 2023.

APPENDIX II

Curriculum Vitae

Jure GALOVIĆ

Birth date and place: ▮▮▮▮▮▮▮▮▮▮
Nationality: ▮▮▮▮▮▮

_____

ACADEMIC CAREER

4/2019 – present	**TU Wien, Austria** Doctoral programme in Engineering Sciences: *Mechanical Engineering* Dissertation: *"Combustion Process Improvement for a Wood Gas Internal Combustion Engine of a Biomass Power Plant"*
4/2014 – 4/2018	**TU Wien, Austria** Master's programme *Mechanical Engineering* Diploma Thesis: *"Thermochemical Heat Storage for Motor Vehicles – System Optimization of Heat Storage Based on Salt Hydrate"*
11/2013 – 4/2014	**TU Wien, Austria** German classes
9/2010 – 9/2013	**University of Technology Rijeka, Croatia** Bachelor's degree in *Mechanical Engineering* Bachelor thesis*: "Zero energy house – power system"*

PROFESSIONAL EXPERIENCE

6/2018 – present	**Institute of Powertrains and Automotive Technology at TU Wien, Austria** Project Assistant: Thermal management for vehicles; Internal combustion engines: Wood gas ICE, H_2-ICE
12/2017 – 05/2018	**Institute for Powertrains and Automotive Technology at TU Wien, Austria** Project co-worker
2/2013 – 5/2013	**Coal power plant Plomin HEP, Croatia** *Internship*

LANGUAGES

Croatian:	*native*
German:	*fluent*
English:	*fluent*

TU Bibliothek
Your knowledge hub
WIEN